Insertion depth effect and blockage effect for vane and cup anemometers

EURAMET pilot study no. F1565
Final report

J. Geršl[1], J. Sluše[1], D. Pachinger[2], J. Hornig[3], J. Kampe[3], I. Care[4], A. Bertašienė[5], J. E. Vind[6], A. Roß[7], D. Westermann[7], H. Westermann[7], G. Bobovnik[8], P. Sambol[8], J. Kutin[8], R. Filo[9], M. Jurča[9], R. Riho[9], A. Piccato[10], M. de Huu[11]

[1]Czech Metrology Institute, Okružní 31, 63800, Brno, Czech Republic
[2]BEV/E+E, Engerwitzdorf, Austria
[3]Physikalisch-Technische Bundesanstalt, Braunschweig, Germany
[4]CETIAT, Villeurbanne, France
[5]Lithuanian Energy Institute, Kaunas, Lithuania
[6]Danish Technological Institute, Aarhus, Denmark
[7]Deutsche WindGuard Wind Tunnel Services GmbH, Varel, Germany
[8]University of Ljubljana, Faculty of Mechanical Engineering, Laboratory for Measurements in Process Engineering, Ljubljana, Slovenia
[9]Slovak Hydrometeorological Institute, Bratislava, Slovakia
[10]INRiM, Torino, Italy
[11]METAS, Bern, Switzerland
E-mail (corresponding author): jgersl@cmi.cz

10th April 2026

Contents

Abstract

Two effects influencing accuracy of anemometer calibrations have been investigated – the insertion depth effect and blockage effect.

Four types of vane anemometers and several configurations of cup anemometers were tested for the insertion depth effect in nine European wind tunnels. Besides the significant sensitivity of the anemometers reading to their insertion depth in the wind tunnels, which was known already before, a new finding was achieved that the anemometers reading is sensitive also to a presence or absence of a wall at a test section boundary even if the anemometer sensor is far enough from the boundary not to be affected by a boundary or mixing layer. This effect is probably caused by a flow pattern behind the anemometers' mounting rods which is different for different boundary conditions.

The blockage effect was investigated by means of velocity field measurement upstream three types of large size anemometers (2 vane anemometers and 1 cup anemometer) in four wind tunnels of different dimensions and types and by comparison to a calibration in a very large wind tunnel with negligible blockage effect. Findings on optimal LDA positioning were obtained which can be used as a guidance for mitigation of the blockage effect for all wind tunnels and anemometers with similar construction, geometry and dimensions as used in this project. Also, conclusions on wind tunnel size which is large enough for particular anemometer types were drawn.

1. Introduction

In this study we investigate two types of installation effects which influence calibration results of anemometers in wind tunnels and which can lead to significantly different measurement errors obtained in wind tunnels of different type or size.

The first of the effects, so called insertion depth effect, affects anemometers consisting of a straight mounting rod with an air speed sensor at the tip of the rod (e.g., most common types of thermal, vane or cup anemometers). When these types of anemometers are gradually inserted deeper into the wind tunnel test section their air speed indication may vary by several percent even if the velocity field in the wind tunnel is homogeneous. For a thermal anemometer this behaviour was reported in [1, 2], for cup anemometers in [3] and for various types of vane anemometers in [4, 5]. The effect is probably caused by a flow pattern in the vicinity of the anemometers' mounting rod which evolves with changing length of the mounting rod exposed to air flow (changing insertion depth). This evolving flow pattern influences a sensor at the tip of the mounting rod leading to observed variations of the air speed indication of up to about 10 %. This makes comparability of anemometer calibrations problematic because different insertion depths are usually used in wind tunnels with different dimensions and typical calibration uncertainties are an order of magnitude smaller than the variations caused by the insertion depth effect.

The goal of this study is to find out how the insertion depth effect depends on type (open/closed) and size of a wind tunnel test section and whether consistent calibration results can be obtained when anemometers are installed with the same insertion depth in different wind tunnels. Four vane anemometers with propeller diameters from 16 mm to 107 mm were tested in 9 wind tunnels with test section diameters from 17.5 cm to 100 cm including both open and closed types of the test section. Air speed range from 0.5 m/s to 20 m/s was investigated. On top of that, several types of cup and vane anemometers were tested in the largest wind tunnel at 8 m/s in test section bounded or unbounded by a wall. In each wind tunnel a dependence of a measurement error of the anemometers on their insertion depth was measured, the resulting curves were compared and conclusions on systematic deviations between calibrations using the same insertion depth in different wind tunnels were drawn.

The second of the effects is the blockage effect. When a large size cup or vane anemometer is calibrated in a wind tunnel the velocity field surrounding the anemometer for given velocity indication of the instrument depends on geometry (size and shape) of the test section and on conditions at the test section boundary (open or closed). A reference anemometer, e.g. LDA, is then placed to certain position usually upstream the meter under test and a measurement error is obtained which is sensitive to both – selection of the wind tunnel and selection of the position for the reference anemometer. As ideal calibration we may consider a calibration in an infinite unbounded asymptotically homogeneous flow with a reference air speed measured far upstream of the meter under test. A question then is what is the deviation of the measurement error obtained in a real wind tunnel from the ideal conditions, how this measurement error depends on position of the reference anemometer and if the deviation from the ideal conditions can be mitigated by a suitable selection of the reference position.

In order to address these questions, air velocity fields upstream three anemometers were measured: cup anemometer with propeller diameter of 18 cm, vane anemometer with propeller diameter of 10.7 cm surrounded by a solid frame and vane anemometer with propeller diameter of 20 cm without any frame. The velocity fields were measured for two nominal velocities 5 m/s and 20 m/s (or 12 m/s in case of the smaller vane anemometer) in 4 wind tunnels – 3 of them with open circular test section with diameters 25.5 cm, 32 cm and 45 cm and one of them with closed square test section 54 cm x 54 cm. For the open test sections, the corresponding blockage ratios cover values below, close to and above the recommended maximum of 10 % and for the closed test section the corresponding blockage ratios are below or close to the recommended maximum of 5 % [6, 7]. All the velocity fields were measured using an LDA system placed on a positioning device. On top of that, all the anemometers were calibrated in a large wind tunnel with square cross section 100 cm x 100 cm which we consider as an approximate realization of the ideal conditions.

Based on the measured velocity fields in different wind tunnels we discuss the sensitivity of the calibration results to the position of the reference LDA and we investigate the optimal LDA positioning which leads to minimal difference between the measurement error obtained in a "small size" wind tunnel and in the "large size" wind tunnel approximating the ideal conditions.

References

[1] M. Rohm, H. Müller, J. Kampe, 2007: Geometrical influence calibrating flow velocity sensors in wind tunnels, http://www.gala-ev.org/images/Beitraege/Beitraege%202007/pdf/42.pdf

[2] M. Rohm, Y. Cordier-Duperray, 2009: Influence of the Insertion Depth on the Response of a Hot Film Anemometer in Different Wind Tunnels, https://doi.org/10.1002/9780470611371.ch8

[3] D. Westermann; N. Balaresque and P.Busche, *Systematic deviation of the anemometer calibration due to geometrical interference*, Report of Deutsche WindGuard Wind Tunnel Services GmbH, 2011

[4] Euramet project no. F1431 – final report, https://www.euramet.org/technical-committees/tc-projects/details/project/experimental-study-of-blockage-effect-in-wind-tunnels-for-calibrations-of-anemometers

[5] J. Geršl, J. Sluše, D. Pachinger, J. Kampe, A. Roß and P. Kouba, Effect of the insertion depth on calibration results of vane anemometers, Measurement 222 (2023) 113630, https://doi.org/10.1016/j.measurement.2023.113630

[6] IEC 61400-12-1:2005 Wind turbines – Part 12-1: Power performance measurements of electricity producing wind turbines

[7] ISO 17713-1:2007 Meteorology. Wind measurements. Part 1: Wind tunnel test methods for rotating anemometer performance

2. Participants and test schedule

There were 9 laboratories from 8 countries participating in the project. An overview of the laboratories ordered chronologically according to the time of the first measurement can be found in Tab. 2.1 below. Geometrical parameters of the wind tunnels are summarised in Tab. 2.2 including references to photos of the wind tunnels in appendix A.

Organisation	**Short name**	**Country**	**Date of measurement**
Czech Metrology Institute	CMI	Czech Republic	1.8.-25.9.2022 13.5.-30.6.2023 28.6.-12.12.2024 14.3.-31.8.2025
BEV/E+E Elektronik GesmbH	BEV/E+E	Austria	26.9.-20.11.2022
Physikalisch-Technische Bundesanstalt	PTB	Germany	21.11.2022-29.1.2023
CETIAT	CETIAT	France	30.1.-12.5.2023
Lithuanian Energy Institute	LEI	Lithuania	1.7.-6.8.2023
Danish Technological Institute	DTI	Denmark	7.8.-10.9.2023 16.12.2024-24.1.2025
Deutsche WindGuard Wind Tunnel Services GmbH	DWG	Germany	11.9.2023-15.10.2023 9.2024 23.6.-4.7.2025
University of Ljubljana, Laboratory for Measurements in Process Engineering	UL-LMPS	Slovenia	5.6.-27.6.2024
Slovak Hydrometeorological Institute	SHMU	Slovakia	25.1.-13.3. 2025

Tab. 2.1 Participants and test schedule

wind tunnel no.	**lab**	**wind tunnel type**	**test section type**	**nozzle shape**	**nozzle diameter /width (cm)**	**test section length (cm)**	**reference anemometer**	**Fig. no.**
1	DWG	closed	open/closed*	square	100	180	Pitot tubes	A.1
2	CMI	closed	open	circular	45	63	LDA	A.2
3	LEI	closed	open	circular	40	100	LDA/US	A.3
4	PTB	closed	open	circular	32	46.8	LDA	A.4
5	BEV/E+E	closed	open	circular	25.5	35	LDA	A.5
6	UL-LMPS	open	box	circular	17.5	21	LDA	A.6
7	SHMU	open	closed	circular	65	>200	Pitot tube, Thermo-anemometer	A.7
8	CETIAT	closed	closed	square	51[#]	105	LDA	A.8
9	DTI	open	closed	square	50	200	LDA	A.9

* Bottom and top walls of the test section are present and sides are open for the DWG wind tunnel.
[#] The side walls of the CETIAT test section are diverging starting with distance of 51 cm and ending with 57 cm after the test section length of 105 cm

Tab. 2.2 Overview of the participating wind tunnels (ordered according to the nozzle diameter/width; first for open/box test sections and then for closed test sections)

3. Tests of the insertion depth effect for vane anemometers in wind tunnels of various types and sizes

In this section we describe measurements of the insertion depth dependencies for four vane anemometers in the nine wind tunnels with various test section diameters and types (open/closed) and we discuss the results.

3.1 Tested vane anemometers

Four vane anemometer probes were tested for the insertion depth dependencies, namely:

a) Testo 0635 9540 (Fig. 3.1),
b) Schiltknecht MINI (Fig. 3.2),
c) Schiltknecht MACRO (Fig. 3.3)
d) Testo 0635 9340 (Fig. 3.4).

The selected anemometers differ in the propeller diameter, in shape of a frame where the propeller is mounted, in shape and thickness of the support tube (handrail) of the propeller frame and in diameter of the mounting rod which is connected to the handrail and fixed to a construction of a wind tunnel. Basic dimensions of the selected probes are summarised in Tab. 3.1. Here, the propeller frame diameter is the outer diameter of the frame where the propeller is mounted, propeller frame depth is the length of the frame in direction of the air flow, handrail diameter is a diameter or range of diameters of the support tube of the propeller frame and probe length is a length from the top of the propeller frame to bottom of the handrail.

type of the probe	Testo 0635 9540	Schiltknecht MINI	Schiltknecht MACRO	Testo 0635 9340
propeller frame diam. (mm)	16	22	85	107
propeller frame depth (mm)	16	28	80	43
handrail diam. (mm)	8-16	15	15	12-24
probe length (mm)	170	170	235	263
mounting rod diam. (mm)	see Tab. 3.2	12	12	see Tab. 3.2
measuring range (m/s)	0.6-60	0.5-40	0.3-40	0.1-15
resolution (m/s)	0.01	0.01	0.01	0.01
serial number probe	10256787/204	77634	C-72268	709
serial number meas. unit	02355145	75792	75792	61054935

Tab. 3.1 Parameters of the anemometers and their mounting

lab	**Testo 16 mm**	**Testo 107 mm**
DWG	10 mm	13 mm
CMI	10 mm	10 mm
LEI	10 mm	20.6 mm
PTB	16 mm	16 mm
BEV/E+E	10 mm	10 mm
UL-LMPS	10 mm	-
SHMU	10 mm	-
CETIAT	10 mm	10 mm

Tab. 3.2 Diameters of the segment slid out from the telescopic mounting rod used for the Testo anemometers, keeping all the narrower segments inserted in completely

The Schiltknecht probes were installed using an aluminium pipe with 12 mm diameter connected to the bottom screw of the probe (Fig. 3.6). The Testo probes were installed using an original telescopic mounting rod from Testo composed from four segments with diameters 10 mm, 13 mm, 16 mm and 20.6 mm

(Fig. 3.5). Usage of the telescopic mounting rod was not clearly defined in the technical protocol, therefore, different segments were used by different laboratories, especially for the larger Testo probe. Diameters of the segment slid out (keeping all the narrower segments inserted in completely) are summarised in Tab. 3.2. For the smaller Testo probe just one laboratory (PTB) didn't use the 10 mm segment. The differences in the segments used can only be relevant for insertion depths larger than 207 mm for the small probe and larger than 260 mm for the large probe. For smaller insertion depths the different segments are outside the air stream in the test section.

Measuring unit MiniAir20 was used for the Schiltknecht probes and Testo 445 for the Testo probes.

Fig. 3.1 Testo 0635 9540 probe

Fig. 3.2 Schiltknecht MINI probe

Fig. 3.3 Schiltknecht MACRO probe

Fig. 3.4 Testo 0635 9340 probe

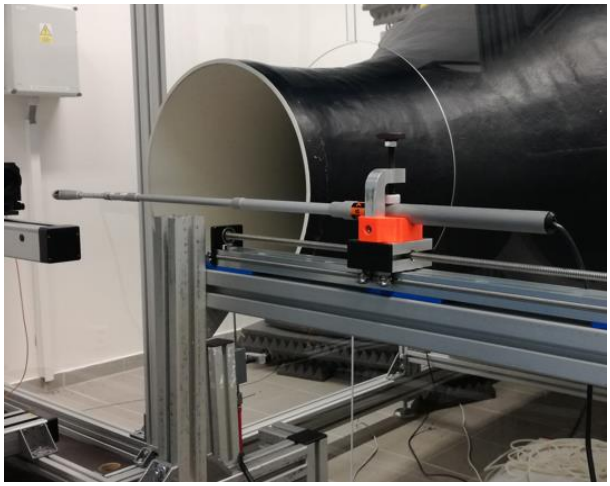

Fig. 3.5 Telescopic mounting rod used for the Testo anemometers

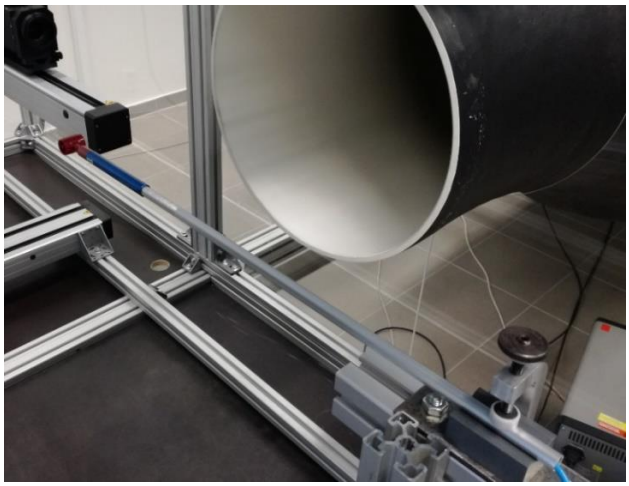

Fig. 3.6 Mounting rod used for the Schiltknecht anemometers

3.2 Measurement procedure

The purpose of the procedure described below is to obtain a measurement error of the anemometers as a function of their insertion depth in test sections of the participating wind tunnels.

3.2.1 Insertion depth definition

We define the insertion depth *d* of an anemometer probe as the distance of the centre of the anemometer probe (rotation axis of the anemometer propeller) from intersection of the anemometer's mounting rod with a prolonged inner wall of the wind tunnel nozzle (in case of an open test section or test section covered by a box) or with the test section wall (in case of a closed test section) - see Fig. 3.7.

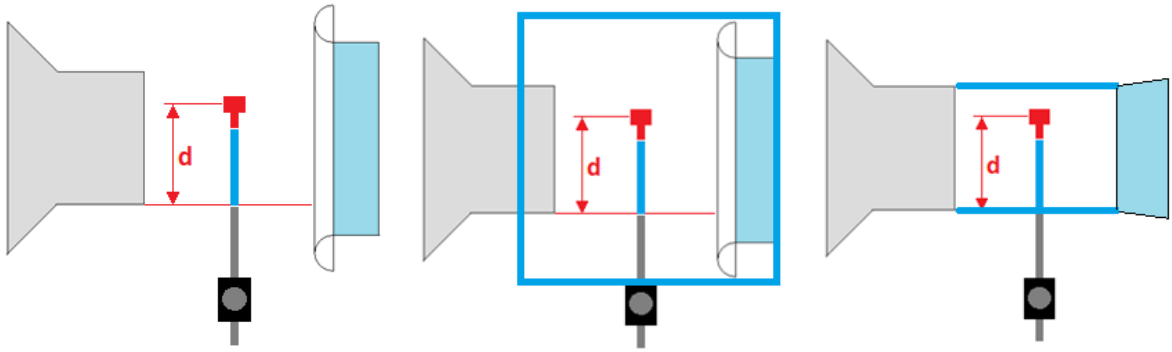

Fig. 3.7 Definition of the insertion depth *d* in an open test section (left), a test section covered by a box (middle) and a closed test section (right)

3.2.2 Anemometer installation

The anemometers were mounted to an automatic shifting device with positioning range of 485 mm which enables to change the anemometer's insertion depth by setting the required value in a computer software (Fig. 3.8). The anemometers were installed to a distance from the wind tunnel nozzle which is normally used for calibrations. Careful angular alignment of the probes with respect to the air stream direction was done.

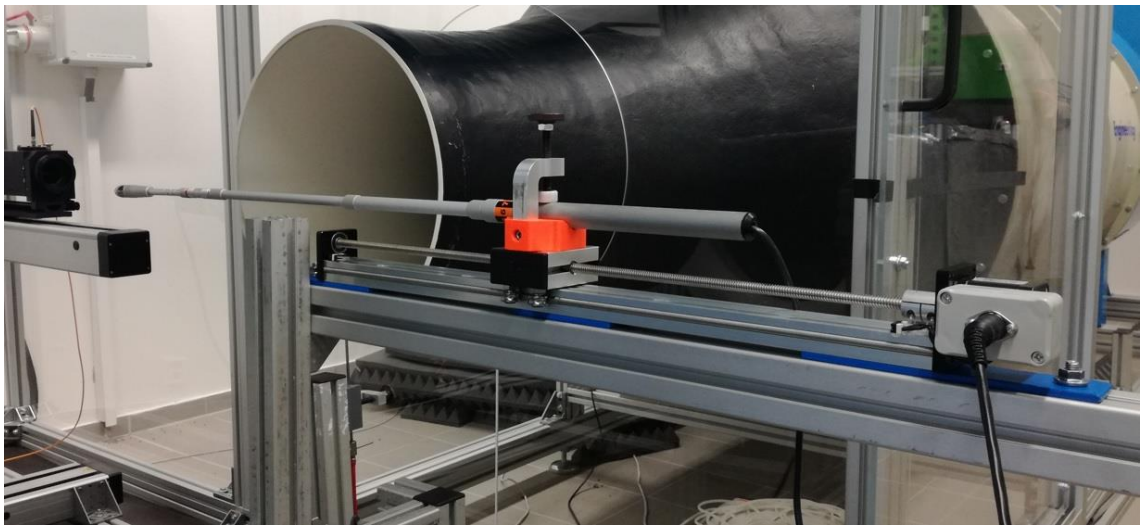

Fig. 3.8 The shifting device to which the anemometers are mounted

3.2.3 Tested air speeds

The measurements were performed for reference air speeds in wind tunnels which are given in Tab. 3.3 below. Each speed in a wind tunnel was set by a fixed fan frequency, i.e., no air speed feedback from the test section was used to adjust the fan frequency during the test.

Meter under test	Tested reference air speeds (m/s)
Testo 0635 9540 (small probe)	0.6, 2, 5, 8, 12, 20
Testo 0635 9340 (large probe)	0.5, 2, 5, 8, 12
Schiltknecht MINI	0.5, 2, 5, 8, 12, 20
Schiltknecht MACRO	0.5, 2, 5, 8, 12, 20

Tab. 3.3 Tested reference air speeds for each of the anemometers.

3.2.4 Range and step of the insertion depths

Participants determined a measurement range of the insertion depth d according to their technical possibilities, taking into account that the air speed near the test section boundary is affected by a turbulent mixing layer or boundary layer.
The insertion depth of the anemometers was increased with a step of 15 mm in this range by all the laboratories.
The positions of the anemometers for the insertion depth test include a position where the anemometer would be placed in case of an ordinary calibration (e.g., test section centre). The corresponding insertion depth is denoted d_C.

3.2.5 Inhomogeneity of the velocity field in empty test section

In order to exclude possible variations of the anemometer indication caused by slight inhomogeneities of the air velocity field in the wind tunnel, the air velocity in the empty test section was measured, using LDA or L-type Pitot tube, in all the positions where the anemometer sensors (centres of propellers) occurred during the insertion depth test. Denoting $v_E(d)$ the air speed in empty test section, i.e. with no meter under test (MUT) installed, in a position corresponding to the insertion depth d, we define a correction

$$\Delta v(d) = v_E(d) - v_E(d_C). \quad (1)$$

This correction was determined for all the tested air speeds.

3.2.6 Measurement of the insertion depth dependencies

The measurement for each anemometer and each velocity set in the wind tunnel consists of the following steps:

a) shift the MUT to a position for ordinary calibrations ($d = d_C$) and record a reference velocity in the wind tunnel $v_{REF\,1}$
b) shift the MUT to a position with minimal value of d and record the MUT reading $v_{MUT}(d)$; the MUT reading is an average of at least 20 single readings taken during a 1-minute period (or longer)
c) shift the MUT with the increment of 15 mm and record the MUT readings $v_{MUT}(d)$ for each value of d (again average from at least 20 readings during a 1-minute period)
d) as soon as $d = d_C$ is reached again, record both the MUT reading $v_{MUT}(d)$ and the reference velocity in the wind tunnel $v_{REF\,2}$
e) continue with the shifts of the MUT with the increment of 15 mm and record the MUT readings $v_{MUT}(d)$ for each value of d until you reach the maximum value of d
f) return the MUT to the position $d = d_C$ and record the reference velocity in the wind tunnel $v_{REF\,3}$

The reference velocity in the wind tunnel $v_{REF\,i}$ is the reference velocity which would be used for an ordinary calibration and it includes, if appliable, also a correction for the velocity difference between a position of a reference anemometer and position of MUT during an ordinary calibration. The velocity $v_{REF\,i}$ is measured as an average during the same time period as is used for the MUT reading.

The purpose of getting the 3 values of $v_{REF\,i}$ – at the beginning, in the middle and at the end – is to check the flow stability during the insertion depth test. The stability is considered satisfactory if the maximal difference between the values $v_{REF\,1}$, $v_{REF\,2}$ and $v_{REF\,3}$ is below 0.8 % for 0.5 m/s, below 0.3 % for 2 m/s and below 0.2 % for 5 m/s and higher.

The reason why the MUT is shifted to the $d = d_C$ position always when the $v_{REF\,i}$ record is taken is that the MUT position itself influences the velocity field in the test section and therefore also the reference anemometer reading. This holds especially for the large size anemometers. Therefore, to avoid the $v_{REF\,i}$ variation due to this effect, the MUT is placed always to the same position when $v_{REF\,i}$ is measured.

Besides the average MUT reading $v_{MUT}(d)$ calculated from at least 20 single readings also a standard deviation $\sigma_{MUT}(d)$ of the single MUT readings was calculated and reported for each tested value of the insertion depth d. This could indicate possible changes in the MUT vibrations or in a turbulence of the flow in the vicinity of the anemometer sensor.

3.2.7 Data evaluation

We denote v_{REF} an average of the $v_{REF\,i}$ measurements, i.e.

$$v_{REF} = \frac{1}{3}(v_{REF\,1} + v_{REF\,2} + v_{REF\,3}). \tag{2}$$

A reference velocity $v'_{REF}(d)$ for each position of a tested anemometer is then defined as

$$v'_{REF}(d) = v_{REF} + \Delta v(d), \tag{3}$$

i.e., it takes the air speed non-uniformity in the test section into account. As v_{REF} already includes a correction of direct reference anemometer reading for the air speed difference (in empty test section) between the reference position and the central MUT position ($d = d_C$) the velocity $v'_{REF}(d)$ can be understood as the direct reference anemometer reading corrected for the air speed difference between the reference position and the actual MUT position (actual value of d). Relative percentual error of a MUT is then defined as

$$E(d) = \frac{v_{MUT}(d) - v'_{REF}(d)}{v'_{REF}(d)} \times 100. \tag{4}$$

This definition gives a measurement error of a MUT in a particular wind tunnel when the MUT is installed with the insertion depth d. Therefore, this quantity is suitable for comparisons of the calibration results between various labs and between various insertion depths. It should be noted, however, that the direct reference anemometer reading in (2) is always taken with MUT in the $d = d_C$ position in order to avoid a disturbance of the reference reading by MUT which can, for certain positions, occur too near downstream the reference anemometer.

The measurement error (4) is constructed in a way that isolates the insertion depth effect from several other sources of possible insertion depth dependencies. Namely, the dependence of the measurement error (4) on the insertion depth is not affected by slight variations of the velocity field in the (empty) test section thanks to the correction (3). Also, it is not affected by changing velocity field in front of the shifted MUT and by its influence on the reference anemometer reading because this reading is always taken with MUT in the $d = d_C$ position (as already discussed above). However, it may be affected by a decrease in the wind tunnel flow rate due to increasing resistance in the test section as the insertion depth of a MUT is increased and the obstacle volume is growing. This effect influences $v_{MUT}(d)$ but not $v'_{REF}(d)$ and therefore it is not compensated in (4). As a result, the reported insertion depth dependencies $E(d)$ are combinations of the insertion depth effect and the effect of changing test section resistance. The magnitude of the latter effect grows with decreasing test section size, however, it is still expected to be much smaller than the insertion depth effect due to the small diameters of the mounting rods.

Next, expanded uncertainty $U(E(d))$ of the error $E(d)$ was determined and the following table of results was submitted to the pilot laboratory for each tested anemometer and each tested air speed.

	MUT: ABC, nominal air speed: X m/s					
d	v_{REF}	$v'_{REF}(d)$	$v_{MUT}(d)$	$\sigma_{MUT}(d)$	$E(d)$	$U(E(d))$
(mm)	(m/s)	(m/s)	(m/s)	(m/s)	(%)	(%)

Tab. 3.4 Data format submitted to the pilot laboratory

3.3 Boundary conditions in test sections of participating wind tunnels

In wind tunnels with open test section (BEV/E+E, PTB, CMI) or test section enclosed in a larger box (LEI, UL-LMPS) there is no solid wall between the air stream moving out from the nozzle and the air in the surroundings. In the wind tunnel of DWG, installation of the anemometers from side was used for the tests described in this section 3, therefore, also in this case no wall was present at the boundary. The wind tunnel of CETIAT (Fig. A.8) has a closed test section, i.e. the wind tunnel nozzle smoothly continues with a duct bounded by a wall, however, the tested anemometers were installed through a wider gap in the wall as shown in Fig. 3.9 below. The wind tunnel of DTI (Fig. A.9) has a closed test section too, however, the wind tunnel itself is open circuit (on contrary to CETIAT which is closed circuit). The first tests in DTI were carried out with anemometers installed through a wide opening in the test section wall (Fig. 3.10a). Due to the open circuit construction of the wind tunnel, the pressure in the test section is lower than the ambient pressure, leading to suction of air through the opening in the wall. This probably led to measurement results which highly deviated from the other laboratories. The tests in DTI were repeated for some of the anemometers with the opening tightly closed around the mounting rods by a tape (Fig. 3.10b). In this report we present the data of DTI from the second measurement with tight opening only. Another wind tunnel with closed test section is the one of SHMU (Fig. A.7). Here a tight entrance port was used for installation of the anemometers (Fig. 3.11).

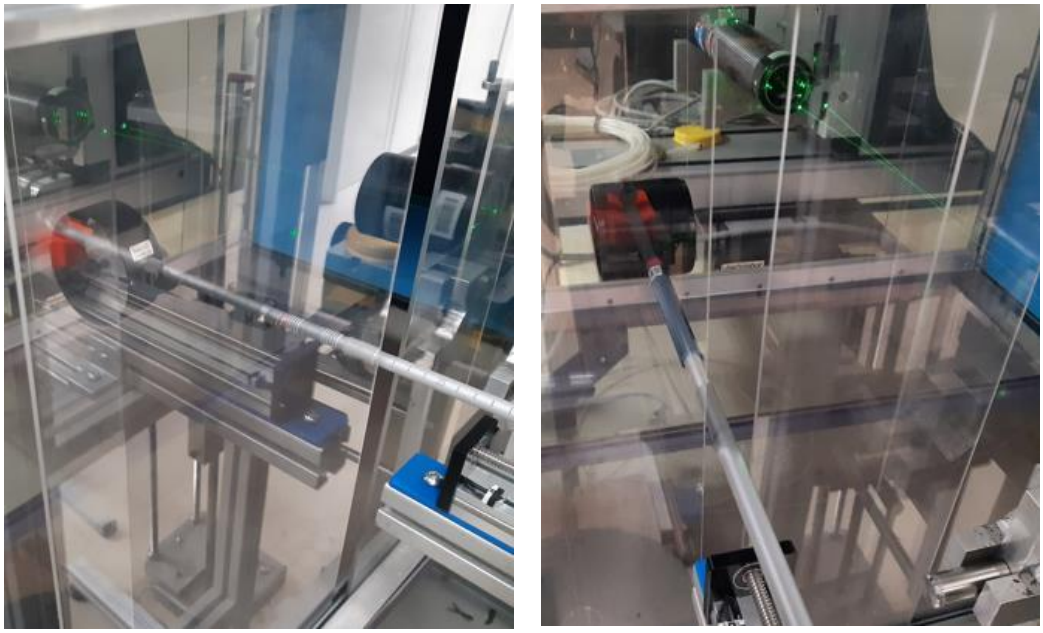

Fig. 3.9 Gap in test section wall used for installation of anemometers in CETIAT.

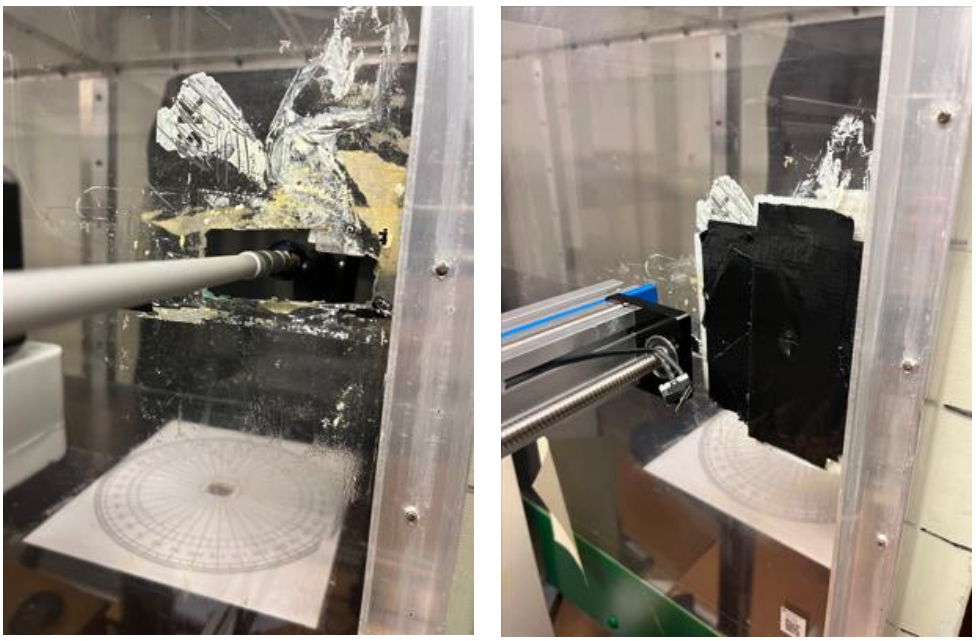

(a) (b)

Fig. 3.10 Openings in test section wall used for installation of anemometers in DTI: (a) non-tight opening (data not used in this report), (b) tight opening (data used in this report)

Fig. 3.11 Tight entrance port in test section wall of the SHMU wind tunnel.

3.4 Results

3.4.1 Measured insertion depth dependencies of the anemometers' errors

Complete data sets are included in the supplementary material Sup1. Plots of the anemometers' errors (4) as functions of the insertion depth are shown in Figs. 3.12a to 3.15e. Circles in the plots show central positions in particular wind tunnels ($d = d_C$) where anemometers are placed for ordinary calibrations.

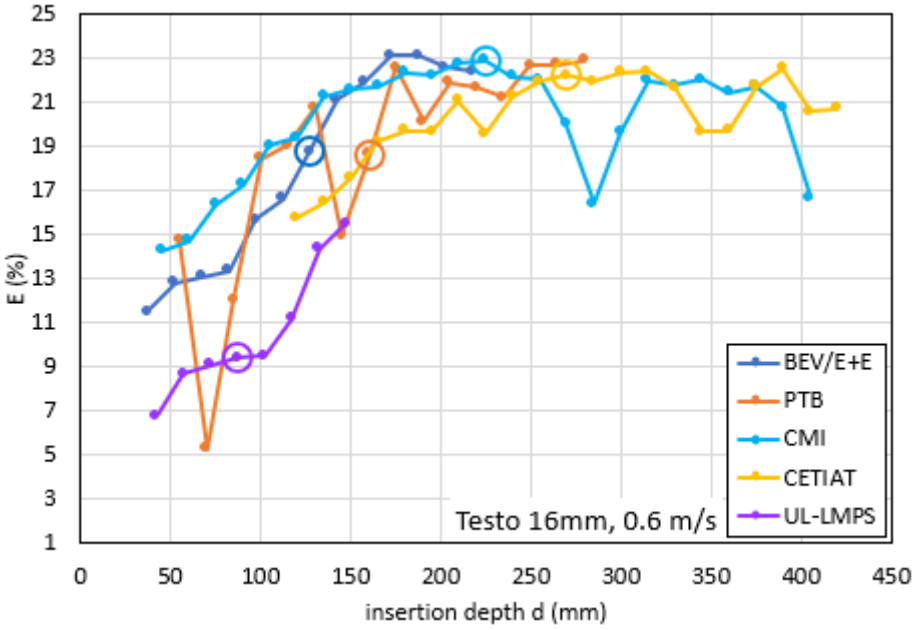

Fig. 3.12a
E(*d*) curves for Testo 0635 9540 (16 mm probe), 0.6 m/s

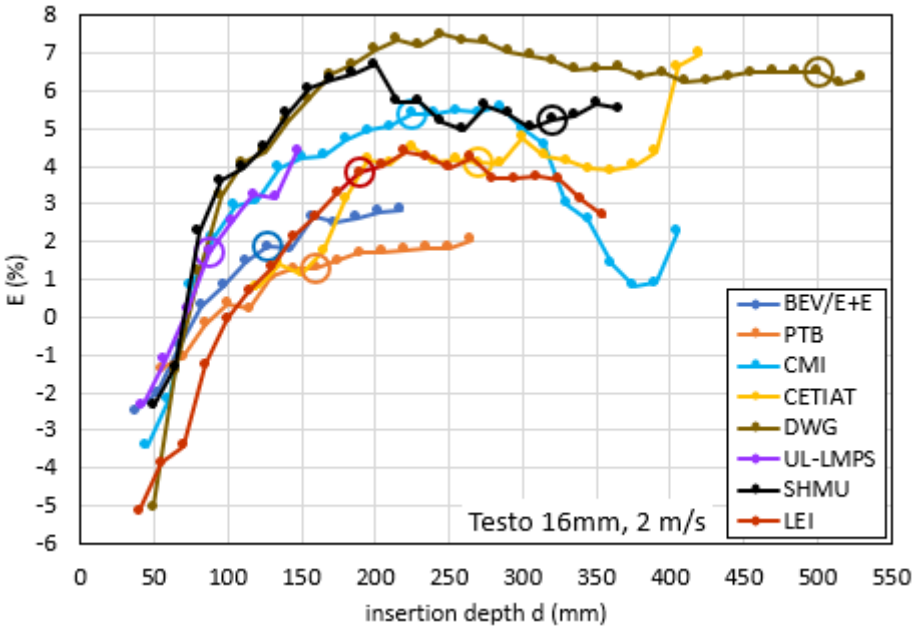

Fig. 3.12b
E(*d*) curves for Testo 0635 9540 (16 mm probe), 2 m/s

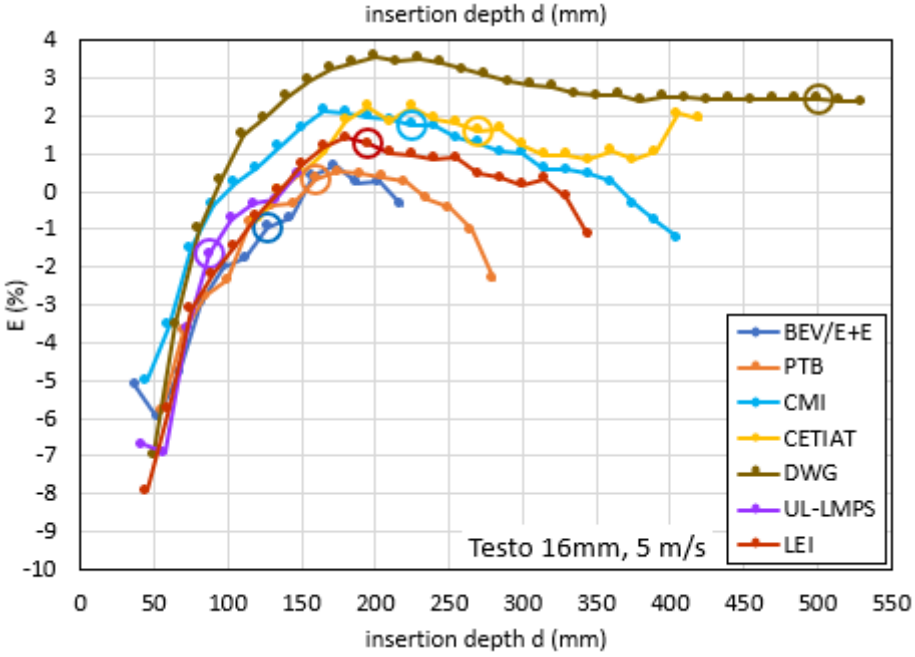

Fig. 3.12c
E(*d*) curves for Testo 0635 9540 (16 mm probe), 5 m/s

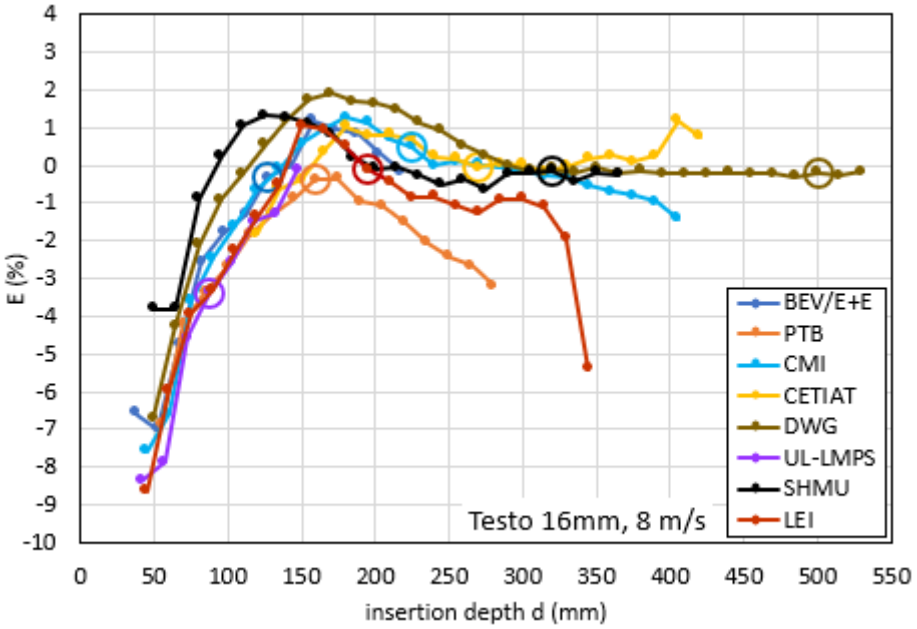

Fig. 3.12d
$E(d)$ curves for Testo 0635 9540 (16 mm probe), 8 m/s

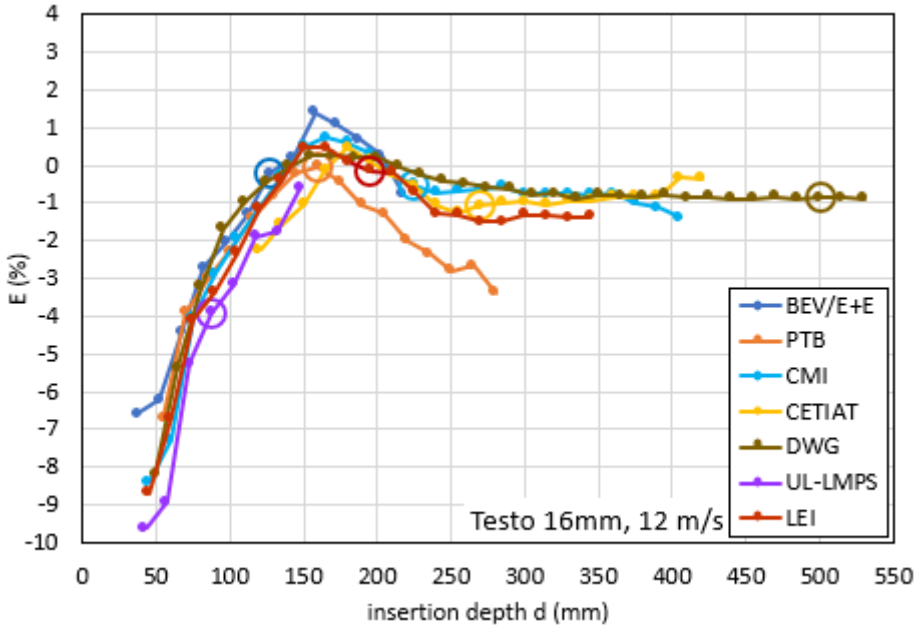

Fig. 3.12e
$E(d)$ curves for Testo 0635 9540 (16 mm probe), 12 m/s

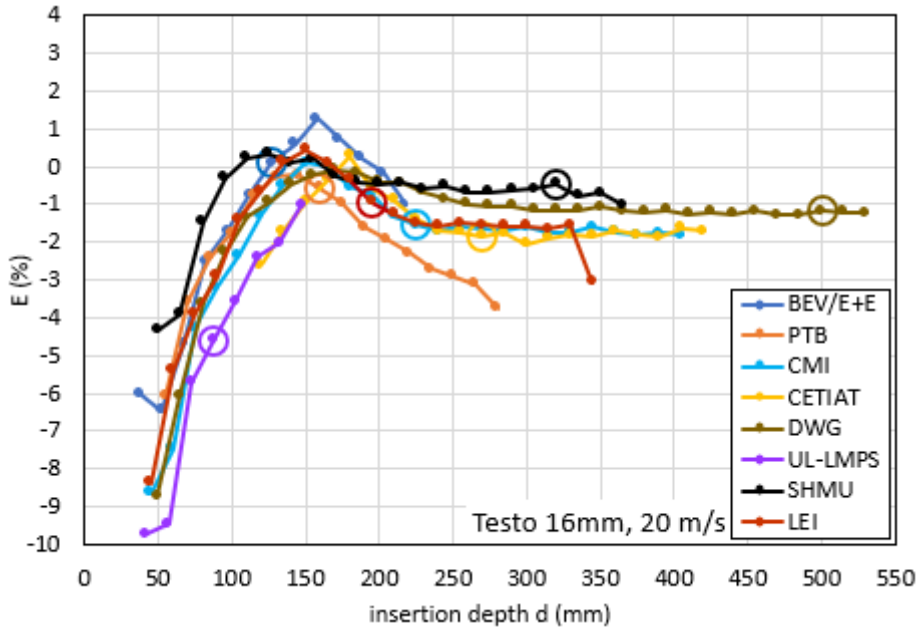

Fig. 3.12f
$E(d)$ curves for Testo 0635 9540 (16 mm probe), 20 m/s

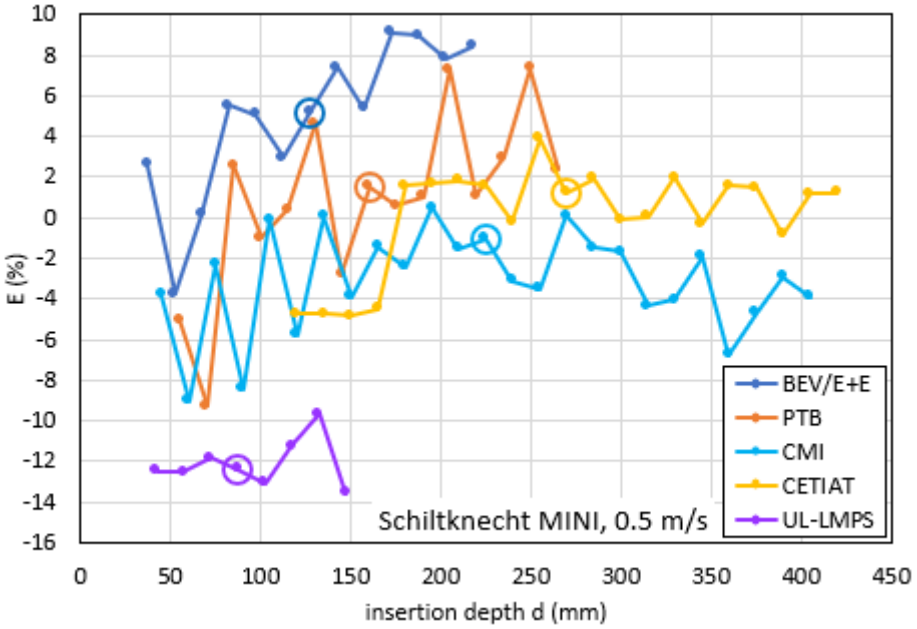

Fig. 3.13a
E(*d*) curves for Schiltknecht MINI, 0.5 m/s

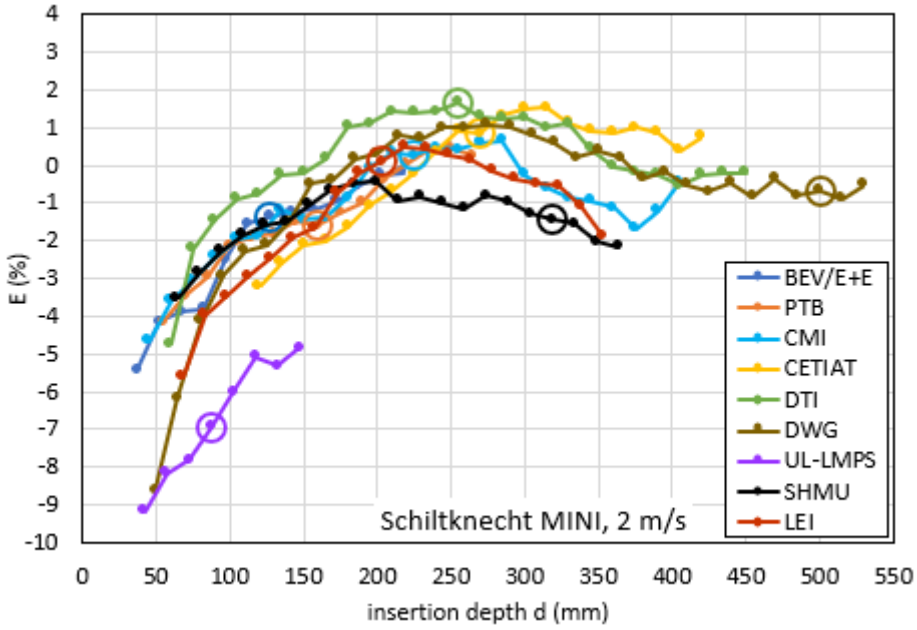

Fig. 3.13b
E(*d*) curves for Schiltknecht MINI, 2 m/s

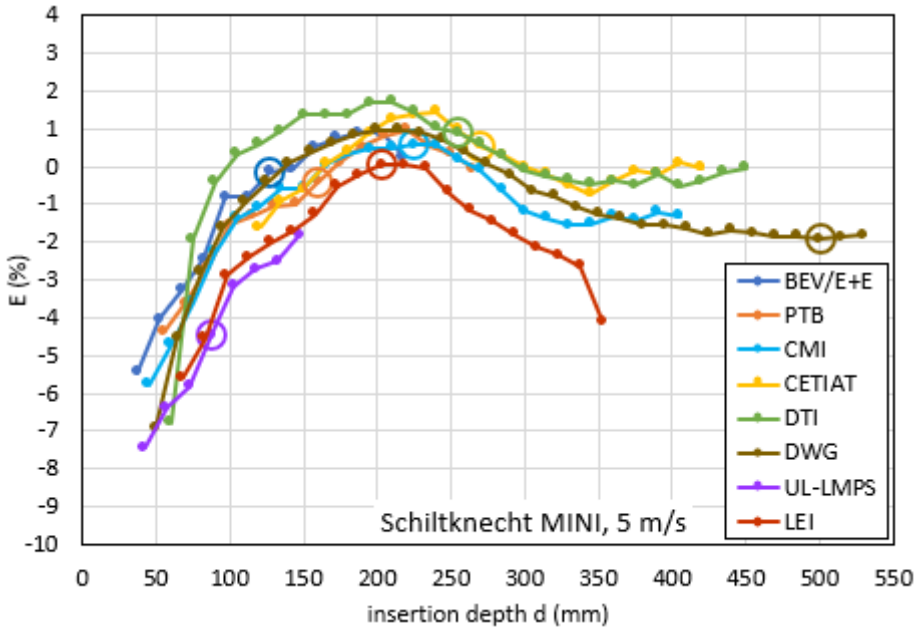

Fig. 3.13c
E(*d*) curves for Schiltknecht MINI, 5 m/s

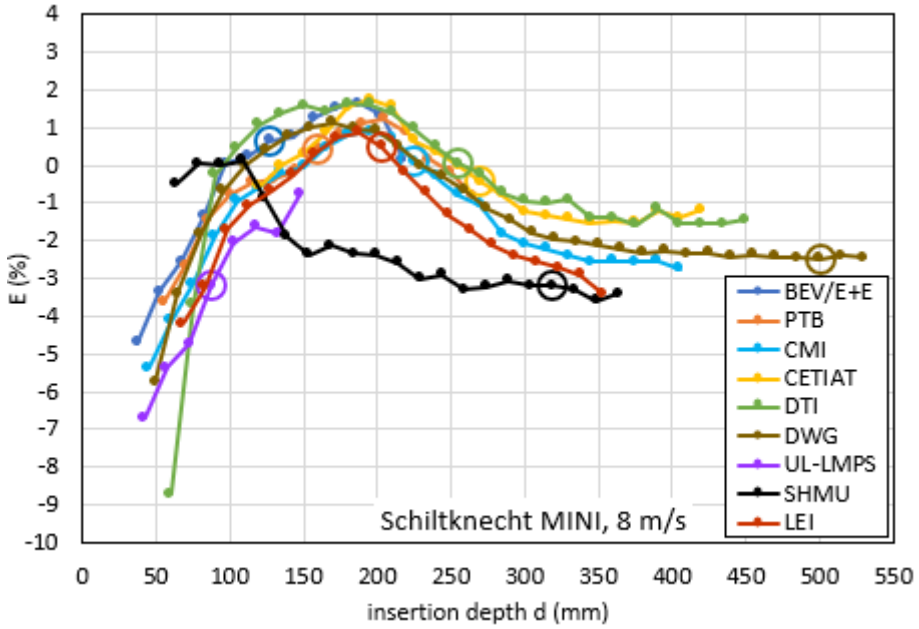

Fig. 3.13d
$E(d)$ curves for Schiltknecht MINI, 8 m/s

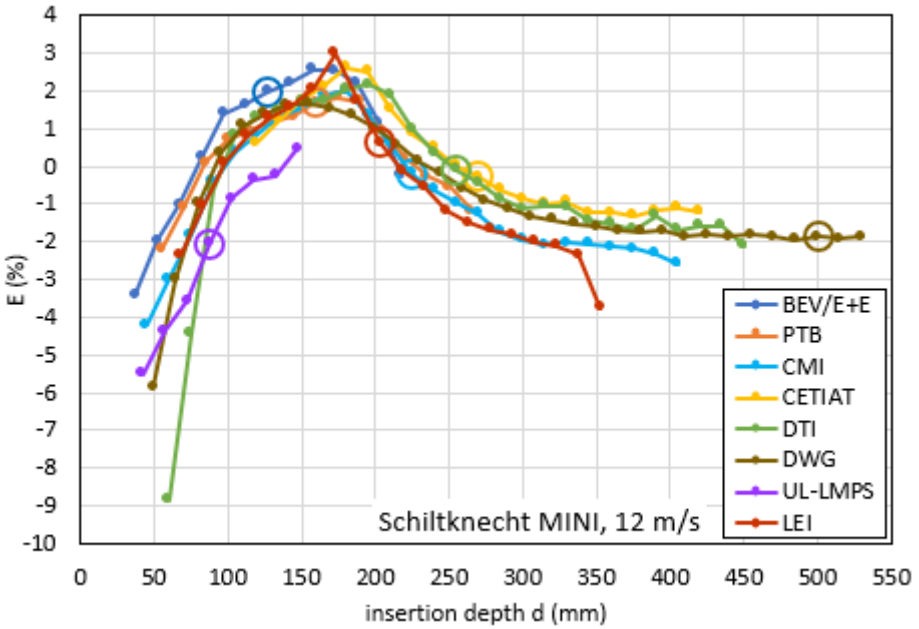

Fig. 3.13e
$E(d)$ curves for Schiltknecht MINI, 12 m/s

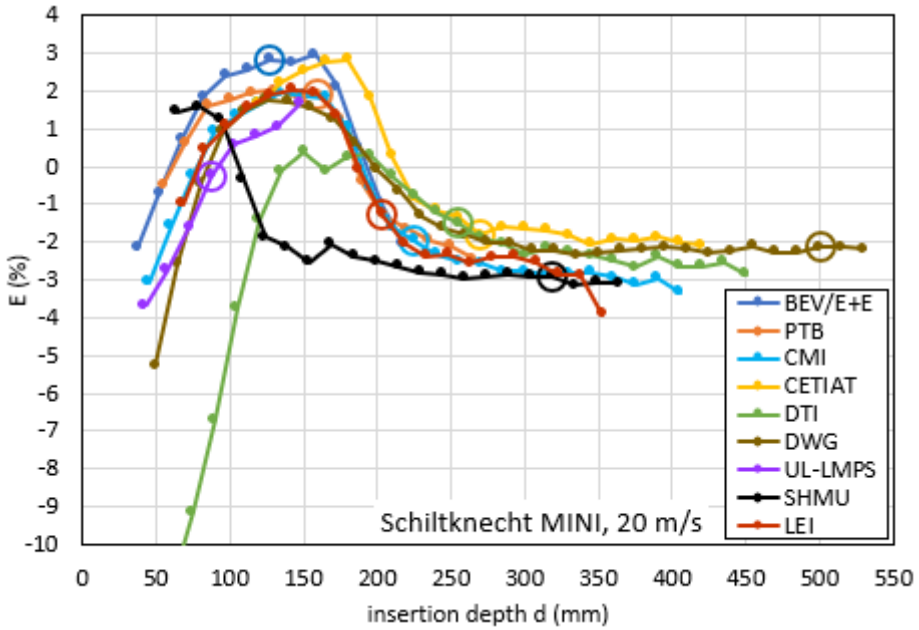

Fig. 3.13f
$E(d)$ curves for Schiltknecht MINI, 20 m/s

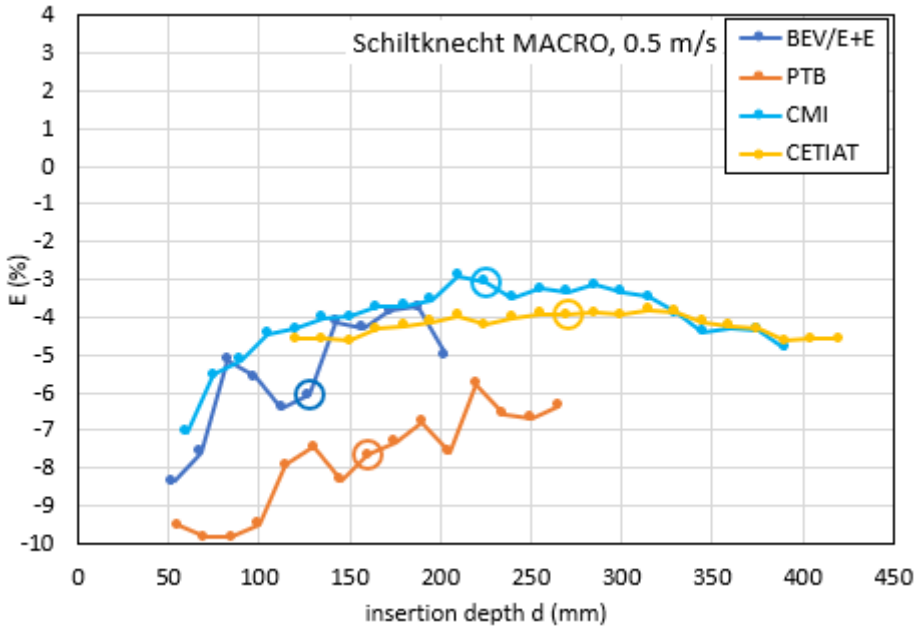

Fig. 3.14a
$E(d)$ curves for Schiltknecht MACRO, 0.5 m/s

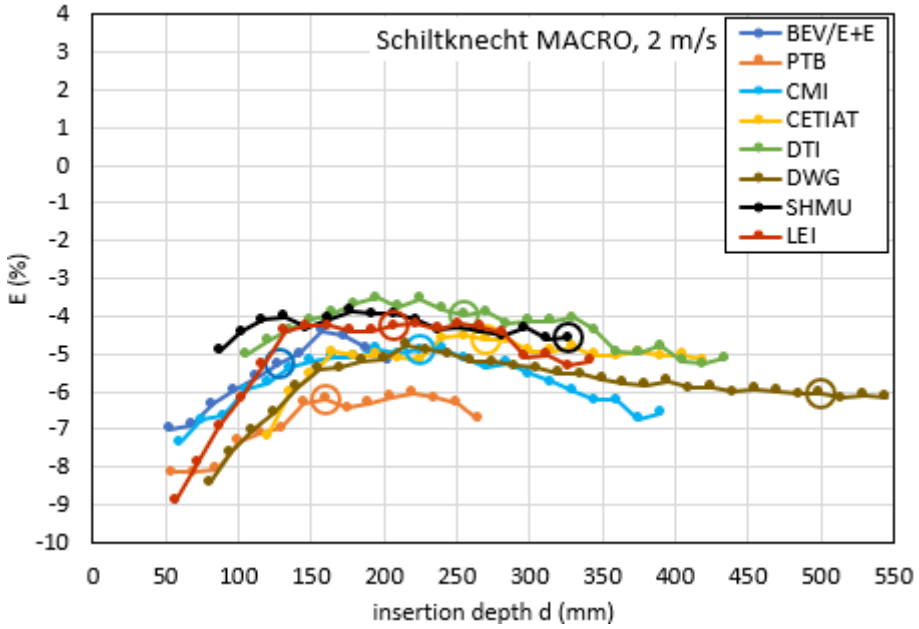

Fig. 3.14b
$E(d)$ curves for Schiltknecht MACRO, 2 m/s

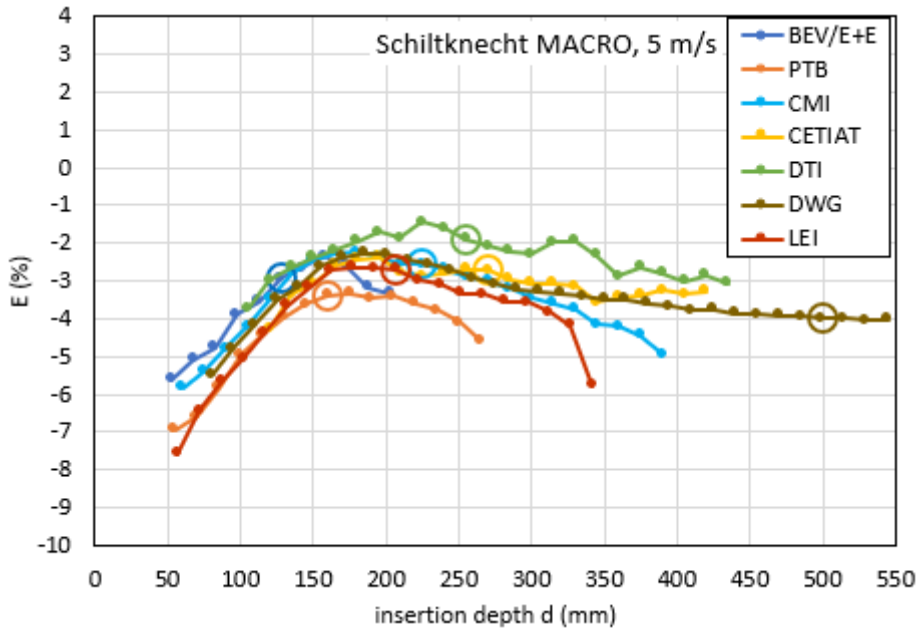

Fig. 3.14c
$E(d)$ curves for Schiltknecht MACRO, 5 m/s

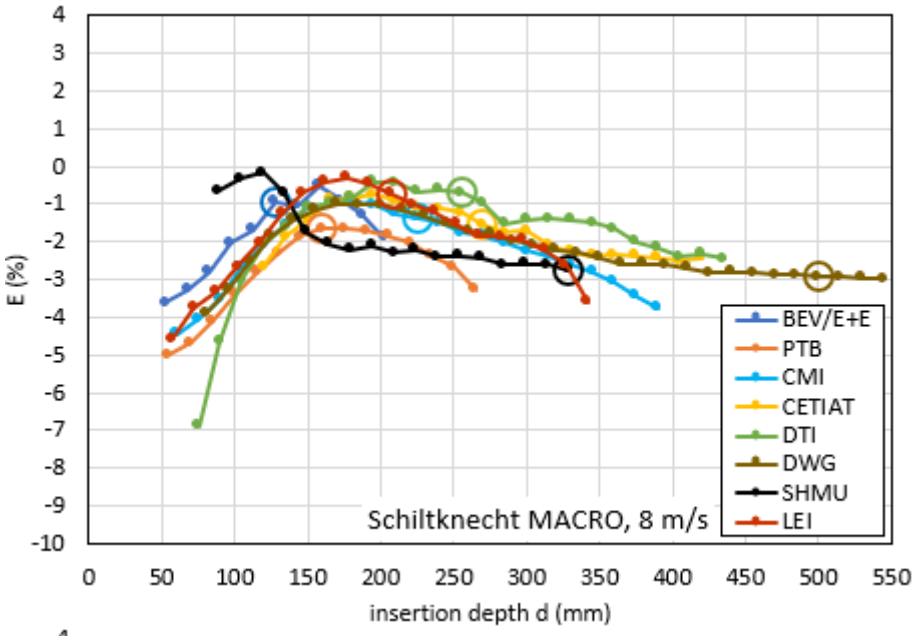

Fig. 3.14d
$E(d)$ curves for Schiltknecht MACRO, 8 m/s

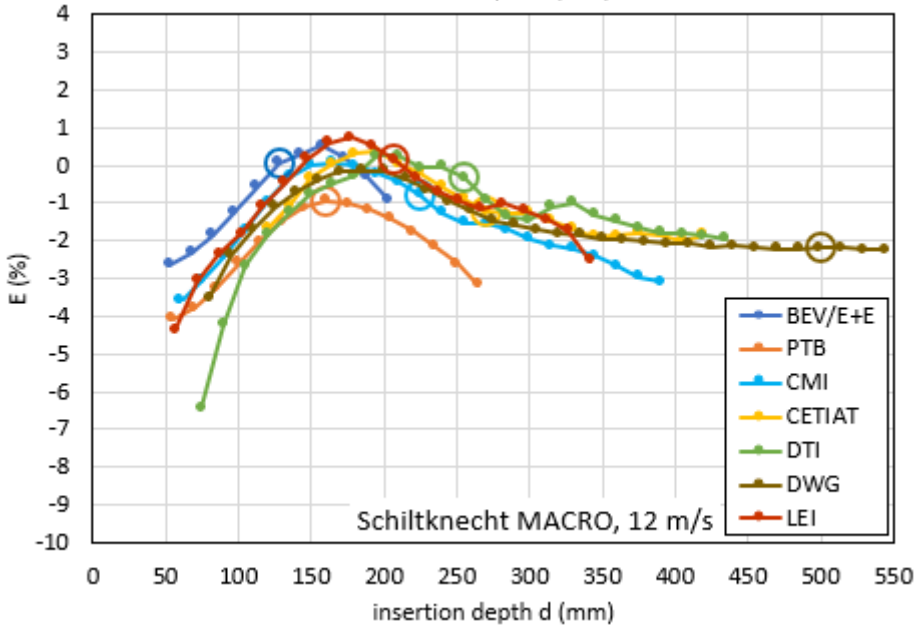

Fig. 3.14e
$E(d)$ curves for Schiltknecht MACRO, 12 m/s

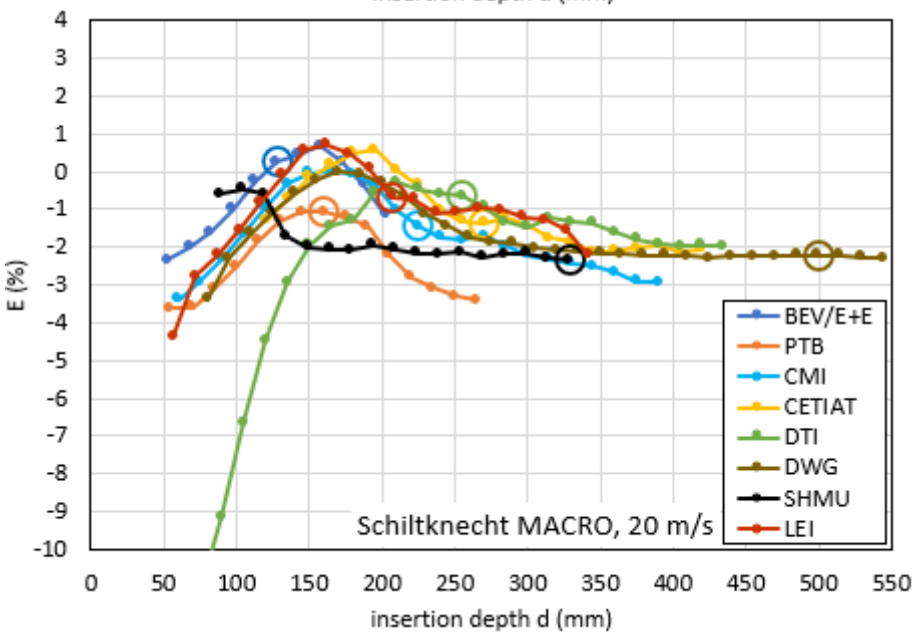

Fig. 3.14f
$E(d)$ curves for Schiltknecht MACRO, 20 m/s

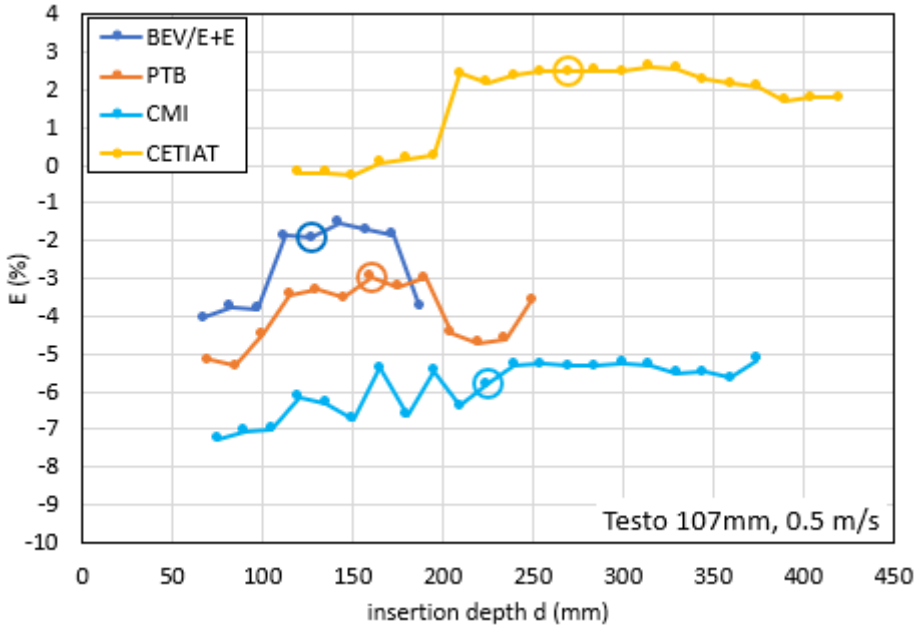

Fig. 3.15a
$E(d)$ curves for Testo 0635 9340 (107 mm probe), 0.5 m/s

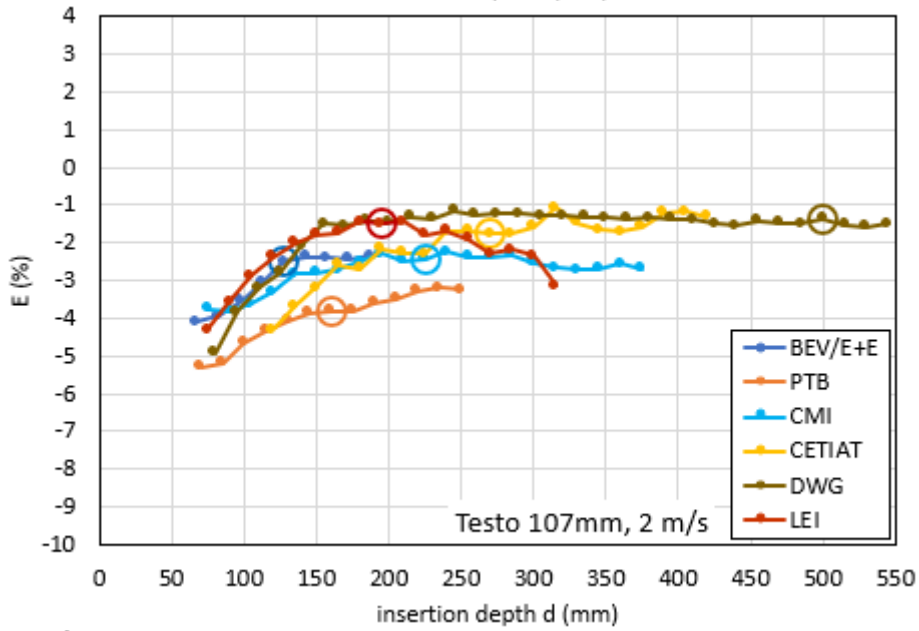

Fig. 3.15b
$E(d)$ curves for Testo 0635 9340 (107 mm probe), 2 m/s

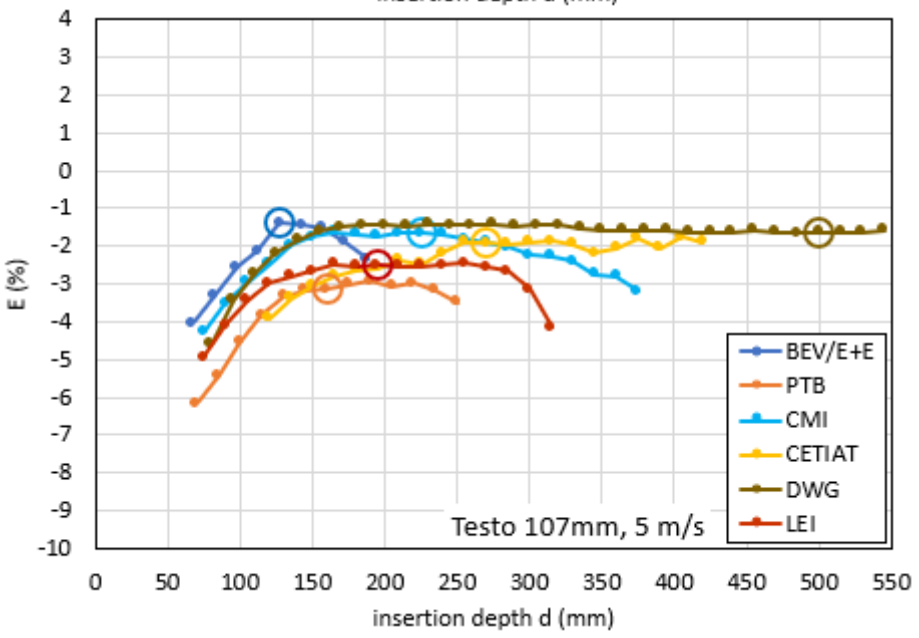

Fig. 3.15c
$E(d)$ curves for Testo 0635 9340 (107 mm probe), 5 m/s

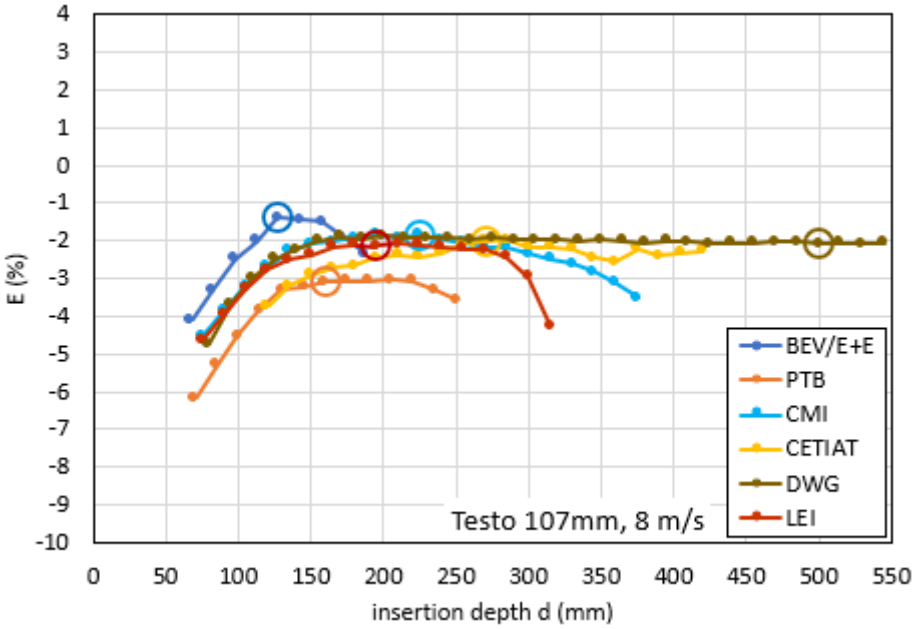

Fig. 3.15d
$E(d)$ curves for Testo 0635 9340 (107 mm probe), 8 m/s

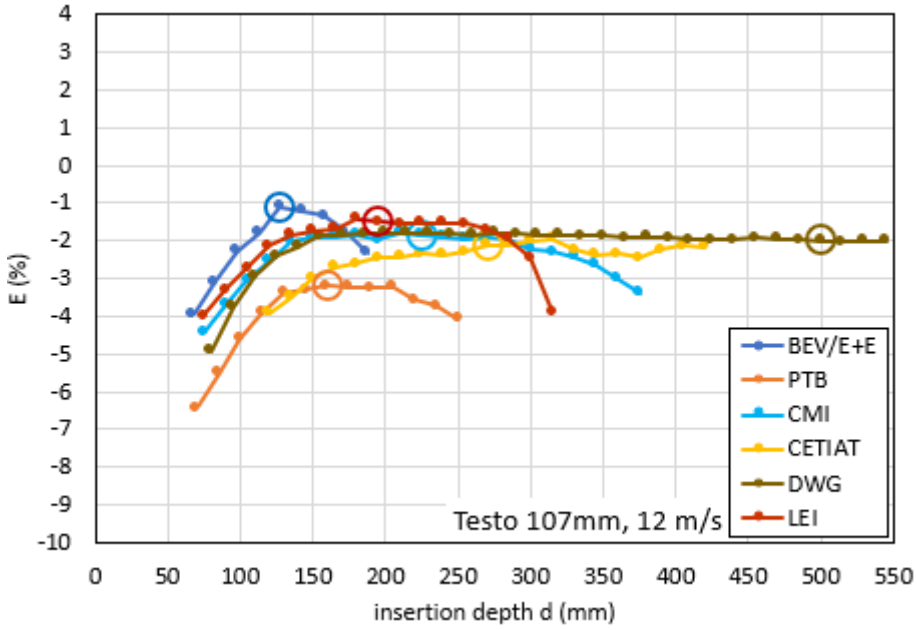

Fig. 3.15e
$E(d)$ curves for Testo 0635 9340 (107 mm probe), 12 m/s

3.4.2 Long-term stability of the anemometers under test

During the lifetime of the project the tested anemometers were calibrated several times at CMI in order to evaluate their long-term stability. Complete calibration data are included in the supplementary material Sup1. The measurement error curves from the repeated calibrations are shown in Figs. 3.16 to 3.19 below. The uncertainty component related to the anemometers' instability (drift) is calculated as is usual in interlaboratory comparisons

$$u_{\text{drift}} = \frac{E_{max} - E_{min}}{2\sqrt{3}} \tag{5}$$

where E_{max} is the largest and E_{min} the smallest measurement error obtained during the repeated calibrations. The calculated values of u_{drift} are shown in Tab. 3.5. Large scatter of the errors is observed especially for the smallest air speed 0.5 m/s or 0.6 m/s for the Testo 16mm probe and for the Schiltknecht MACRO probe. Significant scatter occurs also for the Testo 16mm probe at 2 m/s and Testo 107mm probe at 0.5 m/s. Otherwise, the results are satisfactory.

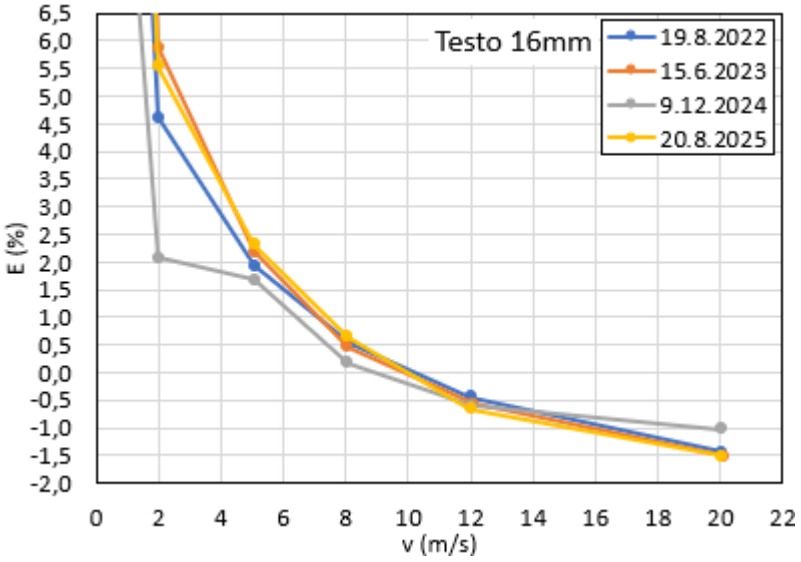

Fig. 3.16 Error curves from repeated calibrations of Testo 0635 9540 (16 mm probe). The undisplayed values for 0.6 m/s are 20.4%, 23.7%, 12.5% and 21.7%.

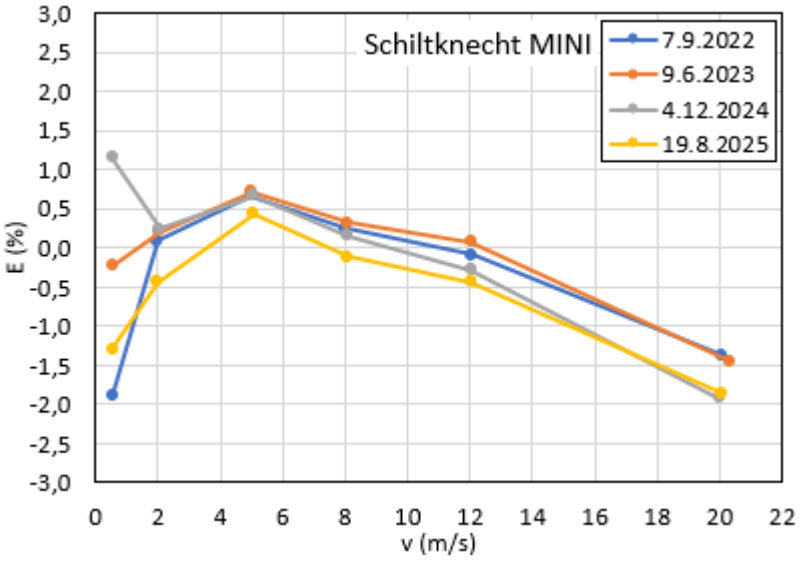

Fig. 3.17 Error curves from repeated calibrations of Schilknecht MINI.

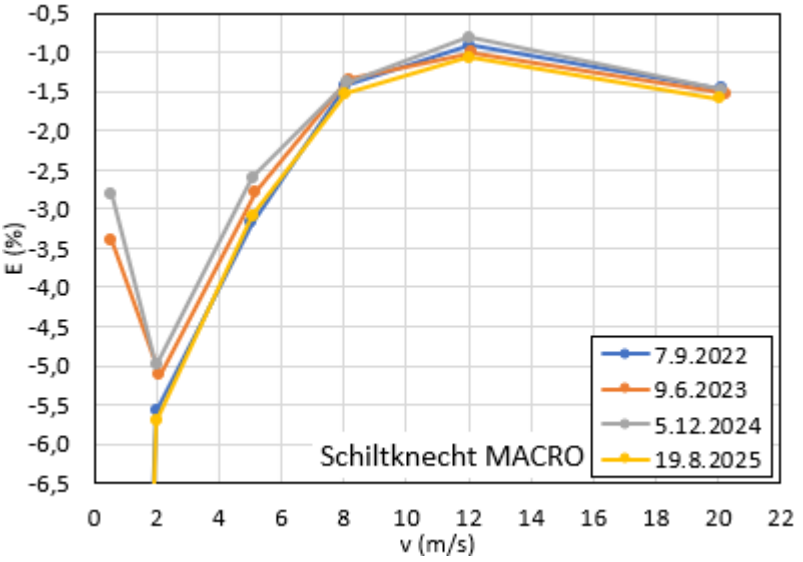

Fig. 3.18 Error curves from repeated calibrations of Schiltknecht MACRO. The undisplayed values for 0.5 m/s are -21.7% and -22.8%.

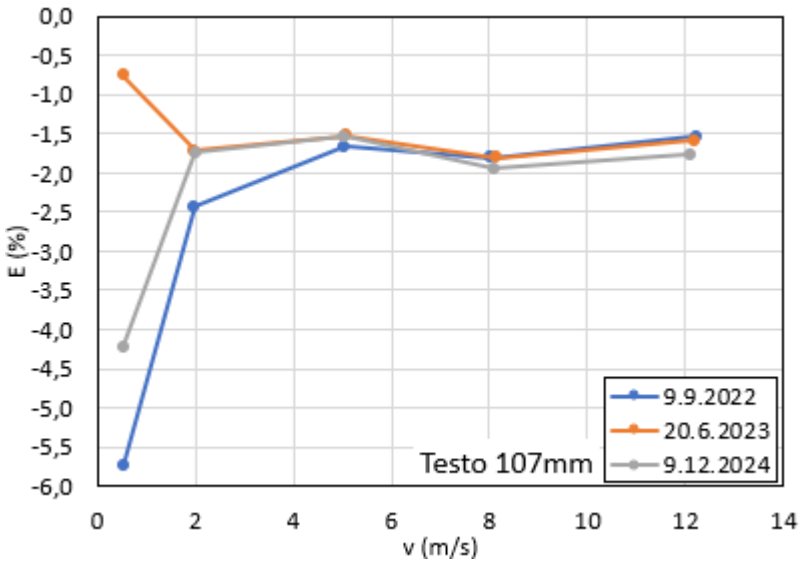

Fig. 3.19 Error curves from repeated calibrations of Testo 0635 9340 (107 mm probe).

	u_{drift} (%)			
v_{nom} (m/s)	Testo 16 mm	Schiltknecht MINI	Schiltknecht MACRO	Testo 107 mm
0.5 – 0.6	3.23	0.88	5.78	1.44
2	1.10	0.19	0.21	0.21
5	0.19	0.08	0.16	0.04
8	0.13	0.12	0.05	0.04
12	0.06	0.15	0.08	0.07
20	0.14	0.16	0.04	

Tab. 3.5 Values of u_{drift} calculated from the repeated calibrations

3.4.3 Comparing results of the participating laboratories

In order to quantify the agreement between the calibration results of various laboratories at given insertion depth we evaluated lab-to-lab equivalence degrees for each pair of the laboratories and for each insertion depth. The lab-to-lab equivalence degree is defined as

$$E_n = \frac{|E_{lab1} - E_{lab2}|}{\sqrt{U_{lab1}^2 + U_{lab2}^2 + 2(2u_{\mathrm{drift}})^2}} \tag{6}$$

where E_{lab1} and E_{lab2} are the measurement errors of a pair of the laboratories, U_{lab1} and U_{lab2} are their expanded uncertainties as reported by the laboratories (not including the component related to the long-term instability of the calibrated anemometer) and u_{drift} is the uncertainty related to the anemometer drift which is expanded by the factor 2 and added to uncertainties of both of the laboratories, therefore, the square of $2u_{\mathrm{drift}}$ is counted twice.

We chose this simple comparison analysis, instead of evaluating a comparison reference value with outlier identification, since the latter might not be appropriate for our measurements where possible systematic deviations due to the different installations are expected.

Complete tables and plots of the lab-to-lab equivalence degrees for each anemometer and each air speed are included in the supplementary material Sup1. There are 3 plots of the E_n values for each case – the first comparing open test sections to open test sections, the second comparing closed test sections to closed test sections (if appliable) and the third comparing closed test sections to open test sections. Due to the high number of tables and plots we keep them in the supplementary material only. In Fig. 3.20 below, one example of the E_n plot is shown.

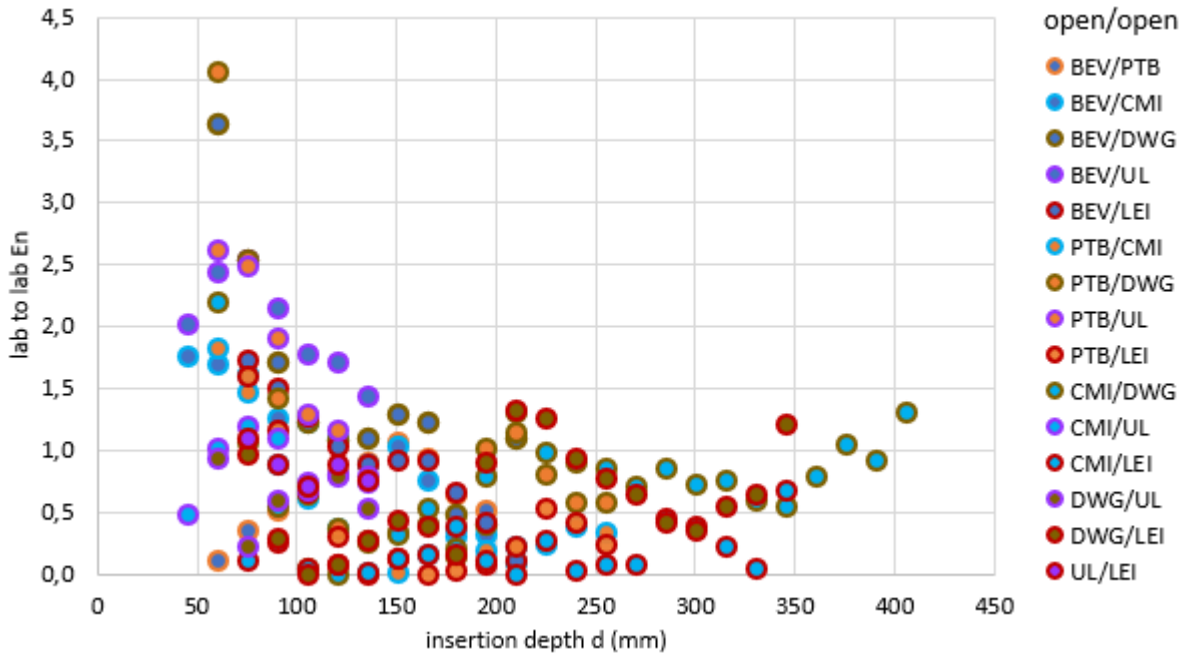

Fig. 3.20 Example of a plot of the lab-to-lab equivalence degrees E_n for the Schiltknecht MINI anemometer at 20 m/s, open test sections only.

3.5 Discussion of the results

Patterns typical for all probes and test section types

For the vane anemometers tested within this project we can observe certain typical characteristics of their measurement errors as functions of the insertion depth $E(d)$. When increasing the insertion depth the $E(d)$ curve initially grows by several percent, then a maximum is reached and the curve starts to decrease. Then, if the test section of the wind tunnel is large enough, the $E(d)$ curve approaches certain stabilised value. Other characteristics like slope of the initial ramp, position of the maximum, depth of the drop after the maximum or region of stabilisation then depend on the anemometer type and air speed used.

For the small probes Testo 16mm and Schiltknecht MINI a shift of the maximum of the $E(d)$ curve towards smaller insertion depths was observed for growing air speed.

Comparison of closed test sections to open test sections or to another closed test sections

There are three wind tunnels with closed test section participating in the project – CETIAT, DTI and SHMU. Their installations are described in section 3.3. CETIAT uses a closed circuit wind tunnel and the anemometers are inserted through a wide opening in the test section wall which is not tightly enclosing the mounting rod of the anemometers. In case of CETIAT, no general systematic difference of the measurement error as function of the insertion depth was observed compared to the wind tunnels with open test section.

On the other hand, SHMU uses an open circuit (Eiffel type) wind tunnel and the anemometers are inserted through an opening tightly enclosing the anemometers' mounting rod. In this case, a clear systematic difference compared to wind tunnels with open test section is observed (see Figs. 3.12d,f; 3.13d,f; 3.14d,f). The $E(d)$ curves of SHMU have a maximum, decrease region and beginning of the stabilisation region shifted to lower values of the insertion depth by 50 mm to 90 mm depending on the probe and air speed used. This behaviour was confirmed by an independent test in DWG (described in the next section) where insertion depth dependencies for the Schiltknecht probes (different probes with the same construction) were measured for two configurations – with and without a wall at the test section boundary. Due to this

systematic shift of the $E(d)$ curves of SHMU a difference of up to 4 % from the curves measured in open test sections was observed.

DTI uses a similar setup as SHMU – an open circuit wind tunnel with anemometers inserted through an opening in the test section wall which is tightly enclosing the anemometers' mounting rod. In this case, however, similar behaviour as for SHMU was not observed. For larger insertion depths above 200 mm the DTI curves fit well with the CETIAT curves, in most cases, leading to lab-to-lab equivalence degrees below 1. However, for smaller insertion depths various patterns are observed with the initial ramp of the $E(d)$ curve shifted either to lower or to higher values of the insertion depth or fitting well with the CETIAT data (see Figs. 3.13b-f, 3.14b-f).

Comparison within the open test sections - small probes

For the small Testo 16mm probe for 2 m/s, 5 m/s and 8 m/s, a systematic grow of the measurement error with growing test section size can be observed for the larger wind tunnels with open test section (PTB, LEI, CMI, DWG) at insertion depths above 100 mm (see Figs. 3.12b-d). The percentual difference between the error curves decreases with growing air speed and for 12 m/s and 20 m/s it is nearly eliminated, except the curve of PTB which remains deviated (see Figs. 3.12e,f). In terms of the lab-to-lab equivalence degrees E_n – for 2 m/s (and 0.5 m/s) the results are inconclusive because of the significant instability of the meter during the project lifetime (see Tab. 3.5). For 5 m/s and 8 m/s, the E_n reach values of up to 3.8 and for 12 m/s and 20 m/s up to about 3.

Several possible causes of the deviations have been considered and tested. As the most probable cause an angular misalignment of the probe was identified. The probe has a rounded design lacking planar surfaces and therefore its angular alignment in a wind tunnel is less accurate. On top of that the probe is highly sensitive to its rotation around the mounting rod axis and the sensitivity is increasing with decreasing air speed. For 2 m/s, rotation of 2° may lead to 5 % deviation in velocity reading. For 5 m/s it is 3 % per 3°. For details see Appendix B.
Other possible influences, as an effect of different mixing layer thickness at boundaries of different wind tunnels and an effect of different telescopic mounting rod segment used by PTB, were also tested. The former was tested by comparing the anemometer reading in various distances from an outlet nozzle of the wind tunnel of CMI. The letter was tested by comparing the anemometer reading with 10 mm vs. 16 mm segments of the mounting rod used. In both cases, no significant impact on the velocity reading was observed.

For Schiltknecht MINI, comparison of the error curves of wind tunnels with open test section shows a better agreement than for the Testo 16mm anemometer, except the lowest air speed 0.5 m/s (see Figs. 3.13a-f). For several air speeds, the curve of the smallest wind tunnel of UL-LMPS is deviated to low error values, however, if we exclude this wind tunnel, lab-to-lab equivalence degrees are obtained which do not exceed 1.5 for vast majority of the cases if the insertion depth is larger than 100 mm. For insertion depths below 100 mm larger deviations occur. This is probably related to the fact that a steep ramp of the error curve is present in this region and, therefore, the anemometer indication is more sensitive to the insertion depth. For the lowest speed of 0.5 m/s the agreement is not so good and the E_n values exceed 3 in some cases.

Comparison within the open test sections - large probes

For the large probes Schiltknecht MACRO and Testo 107mm we observe smaller variations of the measurement error with insertion depth compared to the small probes Schiltknecht MINI and Testo 16mm (see Figs. 3.14a-f, 3.15a-e). Possible explanation is that the changing flow pattern in surroundings of the mounting rod influences only a limited region in the vicinity of the tip of the rod and, therefore, small probes which are completely immersed in this region are affected more than the large probes which are immersed only partially.

For the large probes we also observe a drop of the measurement error for higher insertion depths where the probe approaches the opposite side of the test section boundary. In a region where the probe is not entering the boundary layer yet a possible cause of the drop could be a varying blockage effect. Position of the probe itself influences the flow field in its surroundings and can affect the anemometer reading, especially when it approaches the test section boundary. On top of that, in extreme values of the insertion depth the large probes already enter the boundary layer (mixing layer) for some wind tunnels where the air speed drops and turbulence intensity grows. This can cause an additional drop in the anemometer reading.

Comparing the $E(d)$ curves of the large vane anemometers in the wind tunnels with open test section we observe that the PTB curve is systematically deviated to lower error values (see Figs. 3.14a-f, 3.15b-e). If PTB is excluded the lab-to-lab equivalence degrees E_n do not exceed 1.5 in vast majority of cases. So, only small systematic deviations are observed. The deviation of PTB remains unexplained, however. With PTB the E_n values increase to about 3 in some cases. Possible sources of a shift of the $E(d)$ curves to lower or higher error values are, for example, disturbance of flow in the reference LDA position by the tested anemometer (especially for the large probes and smaller wind tunnels) or angular misalignment of the tested probes.

3.6 Conclusions to section 3

We have shown that the velocity indication and, therefore, also the resulting measurement error of the tested anemometers depends on both – the insertion depth in a test section of a wind tunnel and the conditions at the test section boundary. The latter was demonstrated especially for test sections with or without a wall at their boundary (closed vs. open test sections).
Quantitatively, variations of the measurement error of up to 10 % were observed for different insertion depths in a single wind tunnel (see, e.g., Figs. 3.12c,d for the small Testo probe) and differences in the measurement error of up to 5 % were observed between open and closed test sections for the same insertion depth (see, e.g., Fig. 3.13f for Schiltknecht MINI at d = 150 mm). Between open test sections, differences in the measurement error of up to 4 % were observed for the same insertion depth (see, e.g., Fig. 3.12c for the small Testo probe at d = 265 mm), however, in this case the differences are probably caused by angular misalignment of the probe, rather than by different conditions at the test section boundary.
Therefore, calibrations in different wind tunnels using the same insertion depth may still lead to systematic deviations between the calibration results, especially when a different type of the test section is used (open or closed). Also, deviations in air speed measurement can appear when an anemometer is used for boundary conditions which differ from the conditions of calibration. For example, when a small vane anemometer which is used as a reference in a wind tunnel with closed test section is calibrated in a wind tunnel with open test section a deviation of several percent can be introduced even if the same insertion depth is used.

4. Tests of the insertion depth effect for vane and cup anemometers in the wind tunnel of DWG

In this section tests of the insertion depth effect conducted in Deutsche WindGuard Wind Tunnel Services are described. The wind tunnel of DWG has an option of changeable boundary conditions – either open boundary or boundary with a wall can be used. Deviations of the $E(d)$ curves for different boundary types were tested for several vane and cup anemometers. Also, effect of thickness of the cup anemometer mounting to the $E(d)$ curves was investigated as well as an effect of their rotor size.

4.1 Tested anemometers

Vane anemometers TSR MiniAir60 with the probes MINI and MACRO were used for the tests. These probes are identical in construction with the probes Schiltknecht MINI and MACRO which were used in section 3. The TSR probes were, however, used with the original mounting rod with a diameter of 15 mm (same as the diameter of the handrail). On top of that a vane anemometer RM Young Gill Propeller 27106DT was tested. All the three vane anemometers are equipped with a frequency output. Parameters of the tested vane anemometers are summarised in Tab. 4.1 below and they are depicted in Fig. 4.1.

type of the probe	TSR MINI	TSR MACRO	RM Young Gill Propeller
propeller frame diam. (mm)	22	85	200*
propeller frame depth (mm)	28	80	30*
handrail diam. (mm)	15	15	-
mounting rod diam. (mm)	15	15	27
conversion, v (m/s) =	0.0111 x f(Hz)	0.0208 x f(Hz)	0.03 x f(Hz)
serial number probe	S51239	S53220	10077

Tab. 4.1 Parameters of the tested vane anemometers; *propeller of the anemometer RM Young is not enclosed in a frame – the values relate to the propeller itself

(a) (b) (c)

Fig. 4.1 Tested vane anemometers: (a) TSR MINI, (b) TSR MACRO, (c) RM Young Gill Propeller 27106DT

Next, several configurations of cup anemometers were tested. Namely, two cup anemometer bodies with different dimensions, Thies First Class Advanced and Thies Classic, were used and both of them were equipped with several rotors of different diameters and different sizes of the cups. Six configurations were tested in total which are described in Tab. 4.2 below and depicted in Figs. 4.2 and 4.3.

Body type	Thies First Class Advanced	Thies Classic
Body outer diameter (mm)	18 (upper part), 50 (lower part)	70
Mounting outer diameter (mm)	33.7	48.3
Rotors tested	#1 (d_C = 55 mm, d_P = 150 mm) #2 (d_C = 80 mm, d_P = 240 mm)* #3 (d_C = 80 mm, d_P = 320 mm)	#1 (d_C = 55 mm, d_P = 150 mm) #3 (d_C = 80 mm, d_P = 320 mm)* #4 (d_C = 140 mm, d_P = 350 mm)

Tab. 4.2 Parameters of the tested cup anemometers; rotors marked by asterisk are standard for the particular body type; d_C denotes diameter of the cups and d_P denotes diameter of the entire rotor.

(a) (b) (c)

Fig. 4.2 Tested cup anemometers with Thies First Class Advanced body: (a) rotor #1, (b) rotor #2, (c) rotor #3

(a) (b) (c)

Fig. 4.3 Tested cup anemometers with Thies Classic body: (a) rotor #1, (b) rotor #3, (c) rotor #4

4.2 Measurement procedure

The procedure described in paragraphs 3.2.4 to 3.2.7 was used. Inhomogeneity of the velocity field in empty test section was measured using a Pitot tube. Negligible variations of the velocity field were found and therefore $\Delta v(d) = 0$ is assumed. The reference air speed was recorded for each position of the tested anemometer and it is denoted $v_{ref\_ac}(d)$ in the supplementary material Sup1. The remaining reported quantities are defined in the same way as in the section 3. Namely, $v'_{REF}(d) = v_{REF}$ (eq. (3) with $\Delta v(d) = 0$) with v_{REF} being calculated according to eq. (2) as average from the reference values obtained when the tested anemometer occurs in the test section centre ($d = d_C$).

The tests have been performed for air speed of 8 m/s only. In all cases, the anemometers were installed from the bottom. The vane anemometers (Fig. 4.1) and the cup anemometers with the Thies First Class Advanced mounting (Fig. 4.2) were tested for both – test section bounded by a wall with tight opening for the anemometer mounting pipe (as shown in the Figs. 4.1 and 4.2) and open test section (examples in Fig. 4.4). The cup anemometers with the Thies Classic mounting (Fig. 4.3) were tested with the wall at the boundary and the tight opening only.

All the tested anemometers have a frequency output. A calibration factor a converting the frequency output f to a MUT velocity reading v_{MUT} by a linear equation $v_{MUT} = a.f$ was determined when the tested anemometers were placed in the test section centre (d = 500 mm) and when a solid wall was present at the test section boundary. Therefore, the measurement error curves presented below pass near zero error for the configuration with wall at d = 500 mm. For all the other insertion depths and for the configurations with open boundary the same conversion factor a was used for a given MUT.

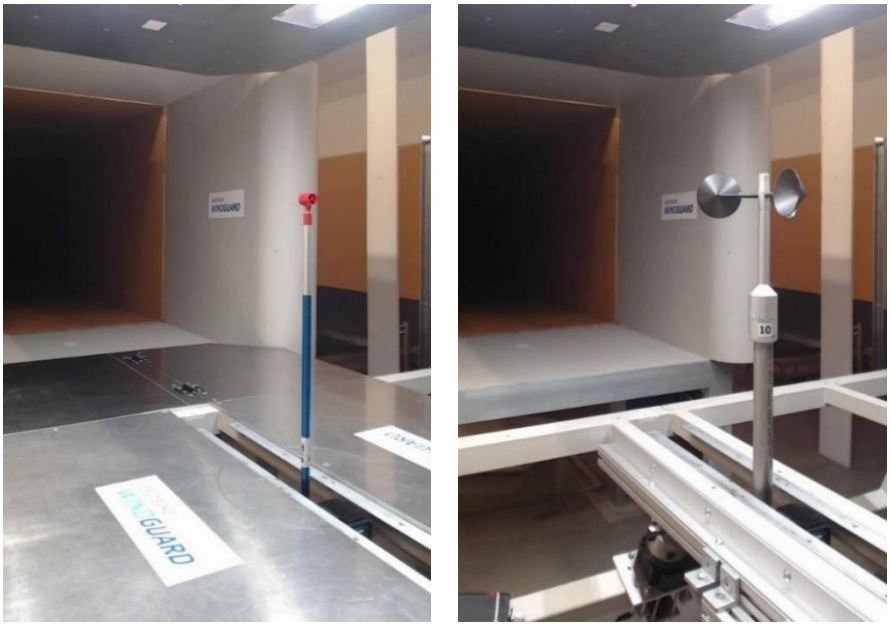

Fig. 4.4 Examples of the installations with open test section boundary. The installation on the left is used for TSR MINI and TSR MACRO anemometers. The installation on the right (larger surface uncovered) is used for the RM Young Gill Propeller and all the cup anemometers with Thies FCA mounting.

4.3 Results and discussion

Vane anemometers

Complete tables and plots with the measurement results for the vane anemometers are included in the supplementary material Sup1. Plots of the $E(d)$ curves for each of the tested cases are shown also in Figs. 4.5 to 4.7 below.

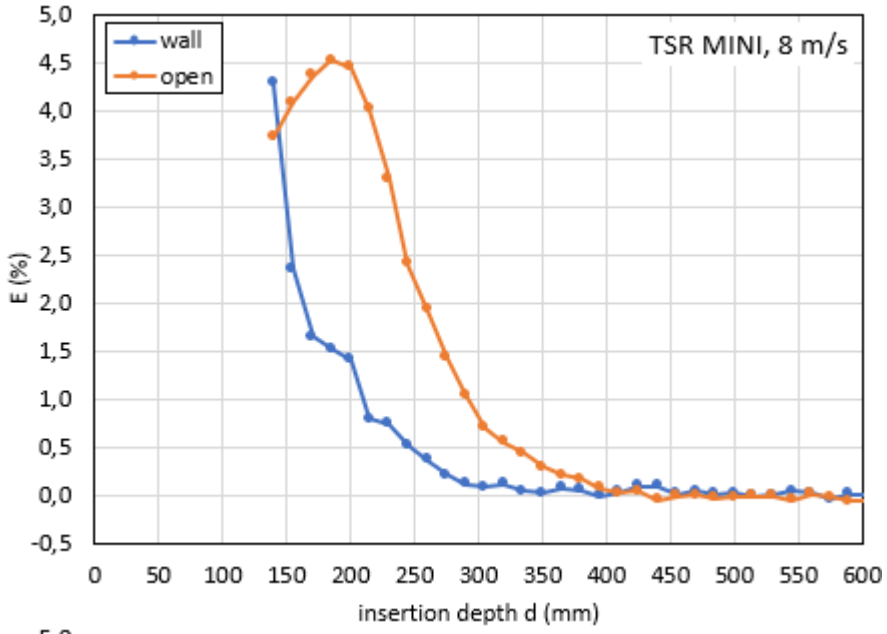

Fig. 4.5 $E(d)$ curves for TSR MINI, 8 m/s, test section boundary with wall or open

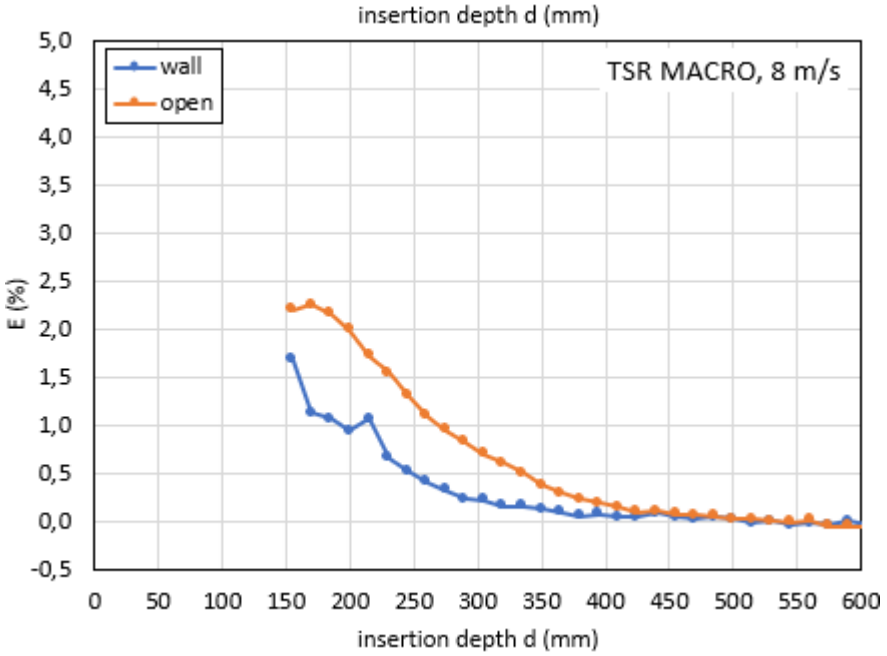

Fig. 4.6 $E(d)$ curves for TSR MACRO, 8 m/s, test section boundary with wall or open

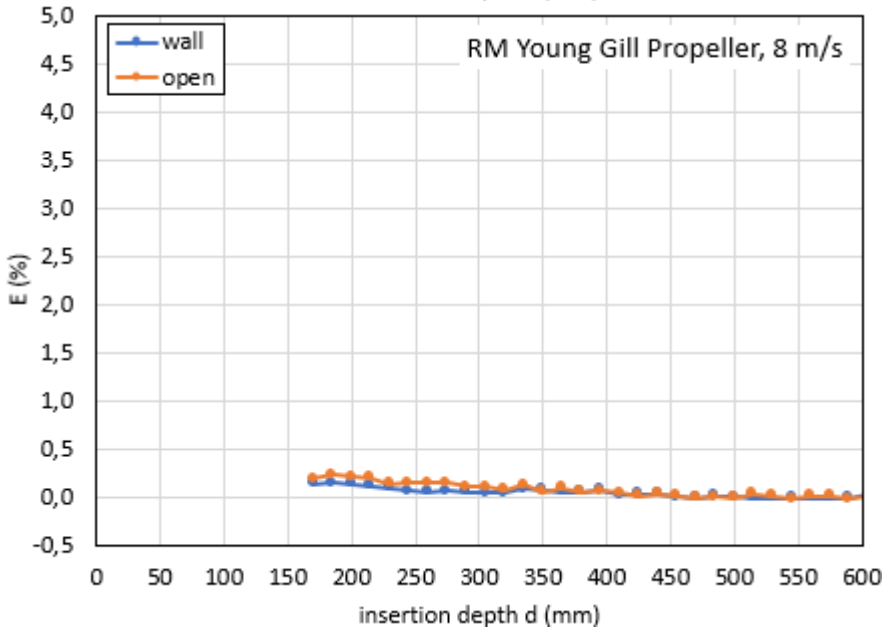

Fig. 4.7 $E(d)$ curves for RM Young Gill Propeller, 8 m/s, test section boundary with wall or open

As we can see in Figs. 4.5 and 4.6, the $E(d)$ curves of the TSR MINI and TSR MACRO anemometers for the setup with wall at the test section boundary are shifted by approximately 80 mm to lower values of the insertion depth compared to the setup with open test section boundary. Similar behaviour has been observed in section 3 for the curves obtained in the closed test section of SHMU. In order to compare the effect of wall observed for the SHMU data with the effect reported in this section we plot the SHMU data and DWG data from Figs. 3.13d and 3.14d (Schiltknecht MINI and Schiltknecht MACRO; 8 m/s; SHMU with closed test section, DWG with open test section) together with the data from Figs. 4.5 and 4.6 (TSR MINI and TSR MACRO; 8 m/s; DWG with and without the wall). The results are shown in Figs. 4.14 and 4.15 below. Note that the $E(d)$ curves of SHMU and DWG from section 3 are shifted in the measurement error axis such that all the error curves tend to the same value for large insertion depths. Also note that different mounting rod was used in section 3 (home made tube with 12 mm diameter) and section 4 (original tube with 15 mm diameter) and the open boundary installation in DWG was not exactly the same in section 3 (installation from side with complete surface uncovered) and in section 4 (installation from bottom with a part of the surface uncovered as shown in Fig. 4.4 left).

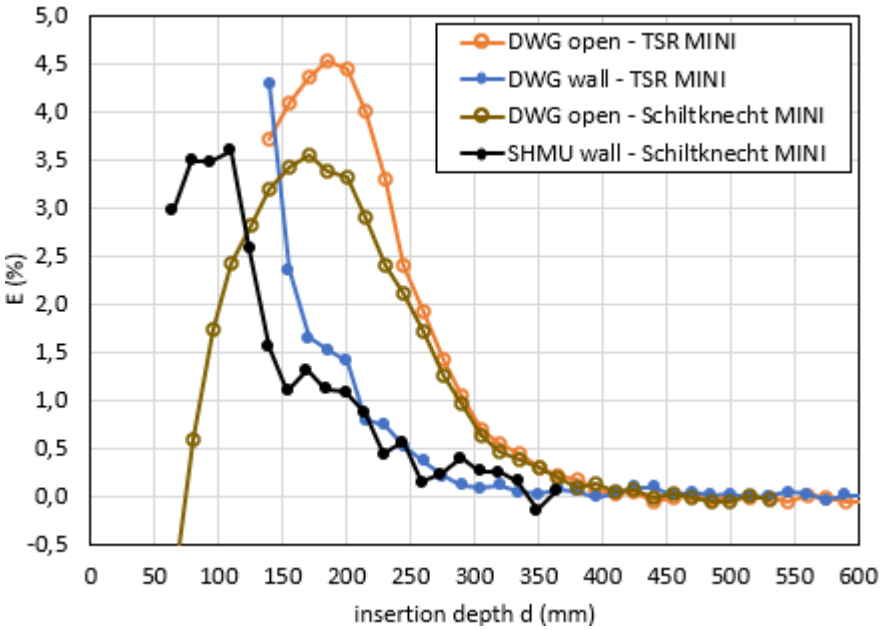

Fig. 4.14 Comparison of $E(d)$ curves for test sections with open or closed (wall) boundaries; TSR MINI / Schiltknecht MINI; 8 m/s

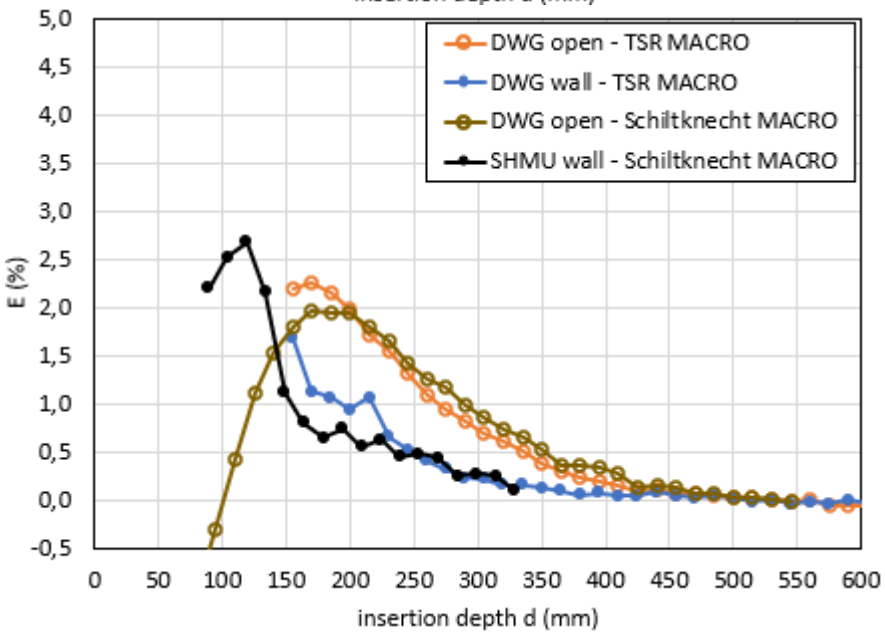

Fig. 4.15 Comparison of $E(d)$ curves for test sections with open or closed (wall) boundaries; TSR MACRO / Schiltknecht MACRO; 8 m/s

In spite of these differences, a clear qualitative correspondence between the effect of wall observed in section 3 and section 4 can be seen, confirming that the presence of wall at a test section boundary has a

systematic influence to the insertion depth dependencies of the measurement error and, therefore, it may cause significant differences between calibration results obtained in wind tunnels with open or closed test section, even if the calibrations are performed with the same insertion depth.

On the other hand, the data for the RM Young Gill Propeller anemometer in Fig. 4.7 show negligible effect of both – the insertion depth and the presence of the wall at the test section boundary. This is enabled by the construction of the meter with its mounting pipe roughly 45 cm downstream the propeller. In this case, the propeller is not affected by the evolving flow pattern in the vicinity of the mounting pipe.

Cup anemometers

Complete tables and plots with the measurement results for the cup anemometers are included in the supplementary material Sup1. Plots of the $E(d)$ curves for each of the tested cases are shown also in Figs. 4.8 to 4.13 below.

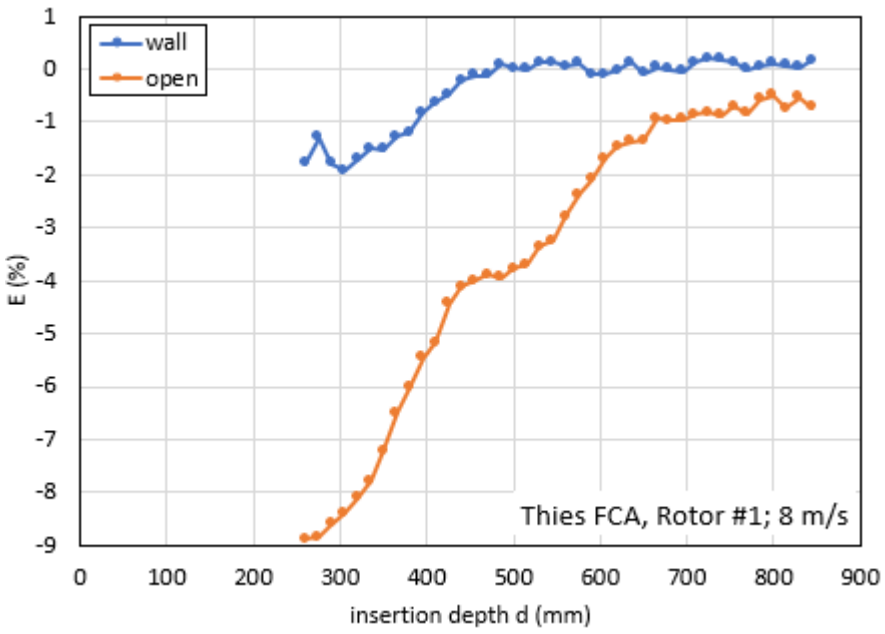

Fig. 4.8 $E(d)$ curves for Thies FCA mounting with rotor #1, 8 m/s, test section boundary with wall or open

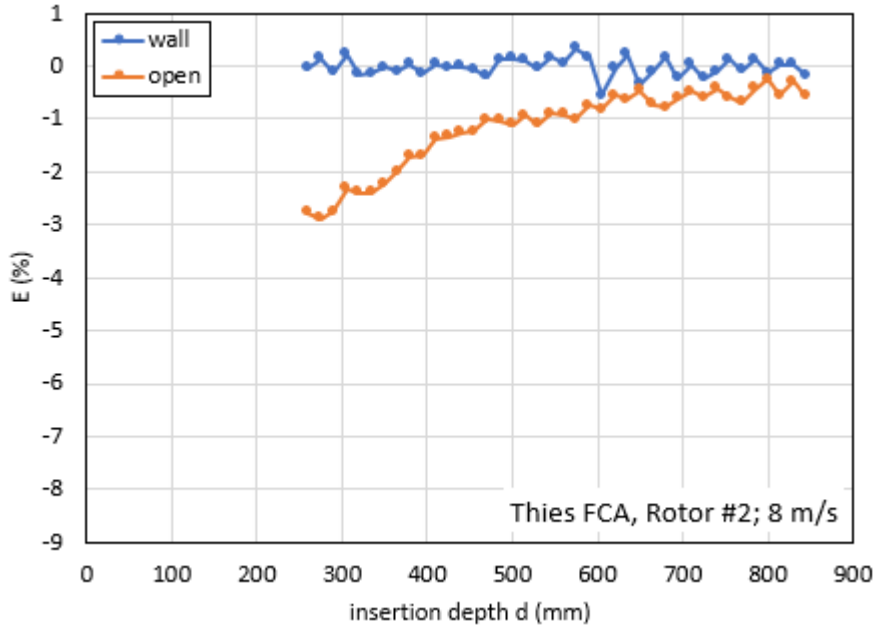

Fig. 4.9 $E(d)$ curves for Thies FCA mounting with rotor #2, 8 m/s, test section boundary with wall or open

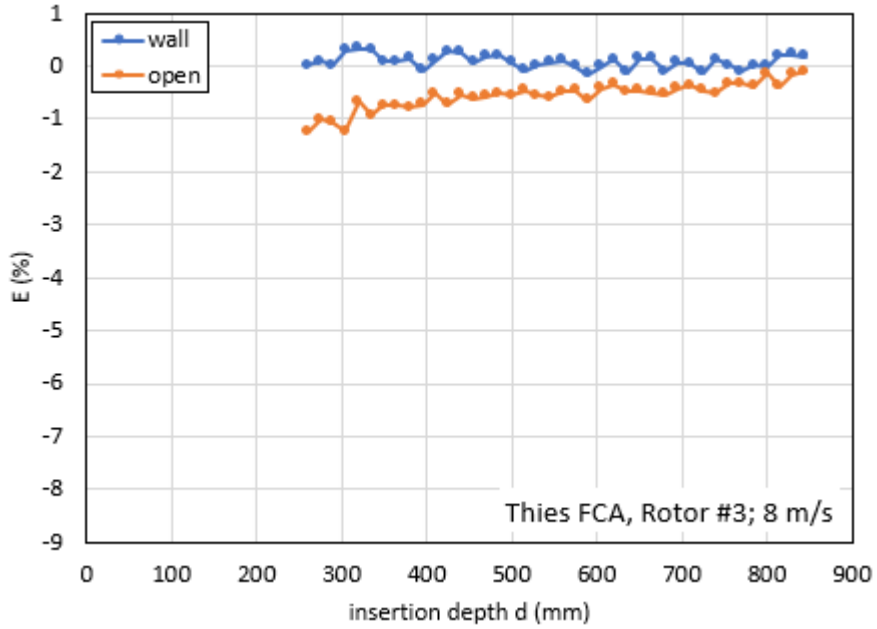

Fig. 4.10 $E(d)$ curves for Thies FCA mounting with rotor #3, 8 m/s, test section boundary with wall or open

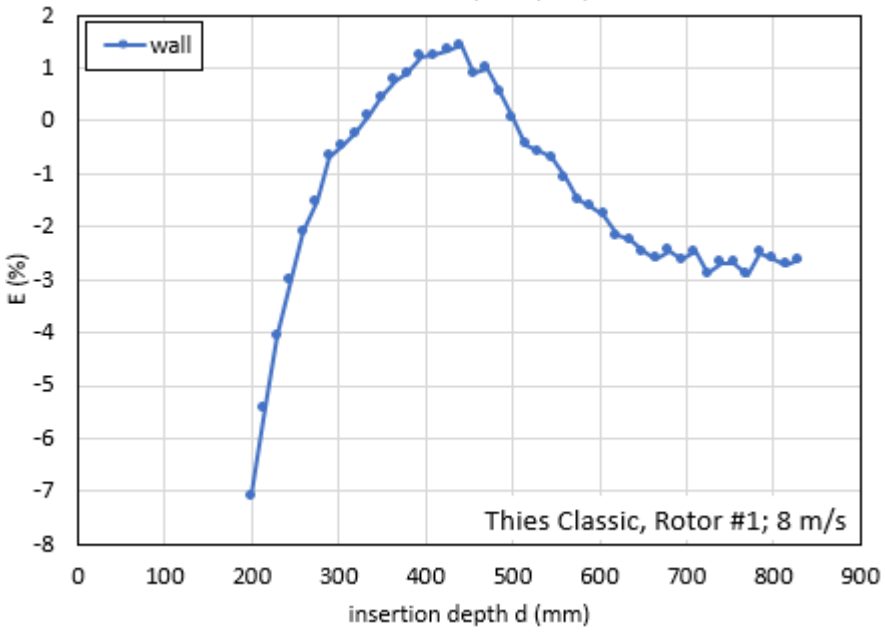

Fig. 4.11 $E(d)$ curves for Thies Classic mounting with rotor #1, 8 m/s, test section boundary with wall

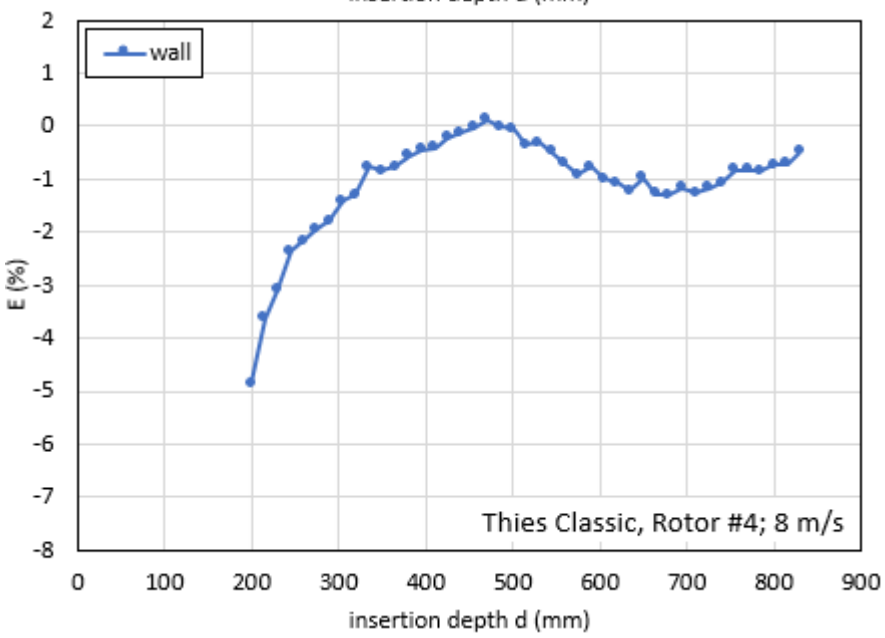

Fig. 4.12 $E(d)$ curves for Thies Classic mounting with rotor #4, 8 m/s, test section boundary with wall

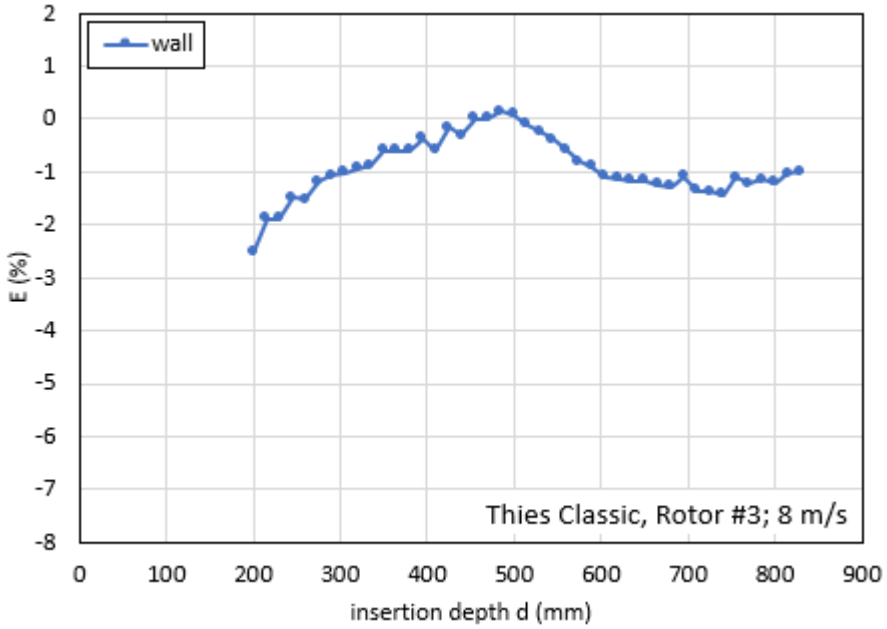

Fig. 4.13 $E(d)$ curves for Thies Classic mounting with rotor #3, 8 m/s, test section boundary with wall

Effect of the rotor size

The larger is the distance of the inner edge of the cups from the rotation axis the smaller are the variations of the $E(d)$ curve. The largest variations are observed for the smallest rotor #1 with inner edge of the cups 20 mm from the rotation axis (maximum to minimum: 8.7% for Thies FCA, open; 2.1% for Thies FCA, wall; 8.5 % for Thies Classic, wall) and the smallest variations are observed for the rotor #3 with inner edge of the cups 80 mm from the rotation axis (maximum to minimum: 1.2 % for Thies FCA, open; 0.47 % for Thies FCA, wall; 2.7 % for Thies Classic, wall).
This confirms that the insertion depth effect is caused by a changing flow pattern near the tip of the mounting construction (top of the anemometer body in this case).

Effect of thickness of the mounting pipe and the anemometer body

Using the Thies Classic installation with thicker anemometer body and thicker mounting pipe leads to significant increase in the $E(d)$ curve variations compared to the Thies FCA installation with slim anemometer body and thinner mounting pipe. When the installation is changed from Thies FCA to Thies Classic the variation of the $E(d)$ curve (maximum to minimum difference) increases from 2.1 % to 8.5 % for rotor #1 and from 0.47 % to 2.7 % for rotor #3. In this case, only data with wall at the test section boundary are available.

Effect of the wall at the test section boundary

In Figs. 4.8 to 4.10 we can see a clear effect of the wall at the test section boundary. Calibrating the anemometers with the wall at the boundary leads to a significant reduction of the $E(d)$ curve variation compared to the open test section. When the wall is installed the variation of the $E(d)$ curve (maximum to minimum difference) decreases from 8.7 % to 2.1 % for rotor #1, from 2.7 % to 0.9 % for rotor #2 and from 1.2 % to 0.47 % for rotor #3 (tests with Thies FCA mounting only). For the larger rotors #2 and #3 statistical variations of the $E(d)$ curves are observed rather than systematic trends for the setup with the wall. A characteristic common with the effect of wall observed for the vane anemometers is that the error stabilisation region for the setups with wall starts for lower values of the insertion depth compared to the setups with open boundary. The largest differences between the measurement errors obtained with or without the wall at the boundary are observed for the lowest tested insertion depths near 260 mm. They reach values about 7 % for rotor #1, 3 % for rotor #2 and 1 % for rotor #3.

4.4 Conclusions to section 4

Tests of the vane anemometers TSR MINI and TSR MACRO in the wind tunnel of DWG confirmed the results obtained in section 3, namely, that the insertion depth dependency of the measurement error of the anemometers differs for cases with and without a wall at a test section boundary. If the wall is present the curve is shifted to lower insertion depths and the region where the measurement error does not change any more starts from lower insertion depths. Therefore, significant differences of several percent in the measurement error can occur when an anemometer is calibrated in wind tunnels with open or closed test section even if the same insertion depth is used.

Tests of the cup anemometers also showed the sensitivity to the presence of a wall at the test section boundary. If the wall is present, variation of the measurement error with the insertion depth is significantly reduced and the error stabilises starting from lower insertion depths similarly as for the vane anemometers. For the cup anemometers sensitivity to a rotor size and mounting pipe diameter was investigated too. It was shown that smaller rotor or thicker mounting pipe leads to larger variations of the measurement error with changing insertion depth.

5. Measurement of velocity fields in front of large size vane and cup anemometers

In this section we describe the measurements of the velocity fields upstream three large size anemometers in four wind tunnels of different types and dimensions: E+E/BEV, PTB, CMI (open test sections) and CETIAT (closed test section). We then discuss a sensitivity of the calibration results to positioning of the reference LDA and we look for an optimal LDA position leading to minimal deviation of the calibration results from a result obtained in the large size wind tunnel of DWG.

5.1 Tested anemometers

The velocity fields were measured in front of the following three anemometers:

a) vane anemometer Testo 0635 9340 (the same one as in section 3.1)
b) cup anemometer Vaisala WAA151
c) vane anemometer RM Young Gill Propeller MODEL 27106D

Parameters of the last two anemometers are summarised in Tab. 5.1 below (the first one is described in section 3.1). Estimated blockage ratios of the anemometers in the participating wind tunnels are summarised in Tab. 5.2. The blockage ratios are calculated in the same way as in the Euramet project no. F1431 [4].

	Vaisala WAA151	RM Young Gill Propeller
rotor/propeller diameter (mm)	182	200
cup diameter (mm)	53	-
height from bottom to the top of the cups (mm)	245	-
propeller depth (mm)	-	30
length from the tip to the mounting elbow (mm)	-	480
mounting pipe diameter (mm)	27	27
measuring range (m/s)	0.4-75	0.2-30
frequency to velocity conversion, v (m/s) =	0.1007 x f (Hz) + 0.3278	0.03 x f (Hz)
serial number	N3749498	06249

Tab. 5.1 Parameters of the tested anemometers

	Testo 0635 9340	Vaisala WAA151	RM Young Gill Propeller
BEV/E+E	18 %	18 %	25 %
PTB	11 %	11 %	15.6 %
CMI	5.7 %	8.9 %	7.9 %
CETIAT	3.5 %	5.4 %	4.8 %
DWG	0.9 %	1.4 %	1.3 %

Tab. 5.2 Estimated blockage ratios of the tested anemometers in the participating wind tunnels

The bottom side of the cup anemometer Vaisala is connected to an aluminium flange where a ¾" mounting pipe (outer diameter 27 mm) is screwed. The body of the vane anemometer RM Young ends with a 90° elbow where, again, a ¾" mounting pipe is fixed. An example of installation of the anemometers in the wind tunnel of CMI is shown in Fig. 5.1.

5.2 Measurement procedure

5.2.1 Anemometer installation

Each of the MUTs was installed with its propeller/rotor centre on the central longitudinal axis of the wind tunnel's test section. In case of the open test sections (BEV/E+E, PTB, CMI) the distance of the MUT from

the wind tunnel nozzle was set such that the geometric centre of the MUT's propeller/rotor was approximately in the middle of the test section, i.e., in half distance from the nozzle to the diffuser. Namely, distances of 175 mm (BEV/E+E), 225 mm (PTB) and 315 mm (CMI) were used. In case of CETIAT, the meters were installed with their most upstream point at a distance of 520 mm from the nozzle.

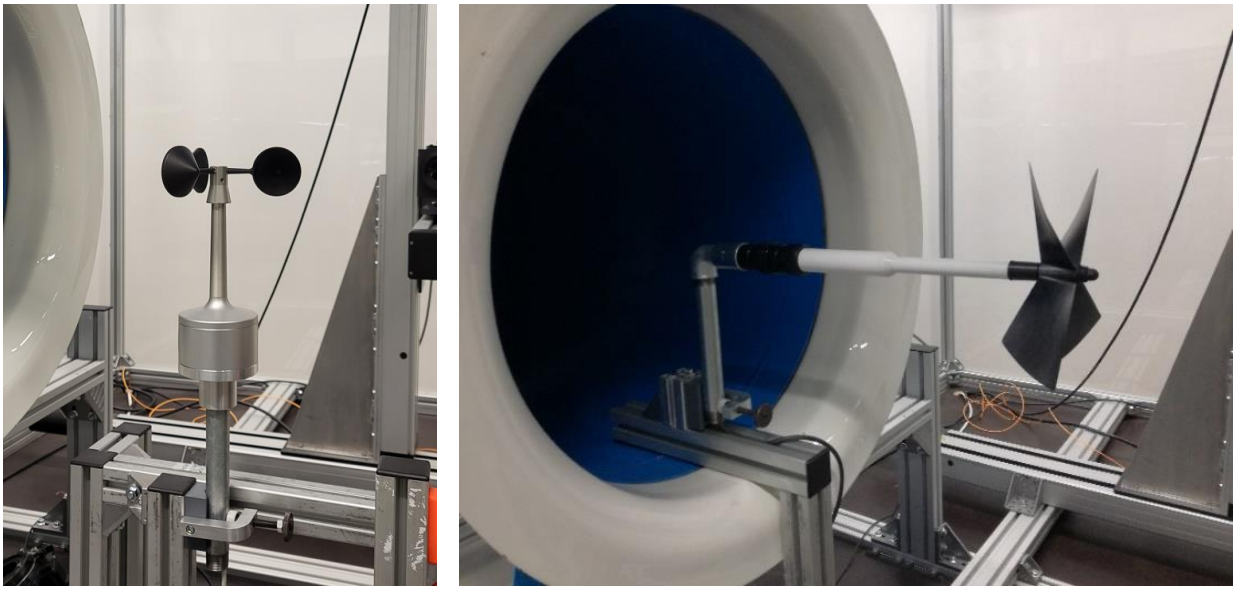

Fig. 5.1 Anemometers Vaisala WAA151 (left) and RM Young Gill Propeller (right)

5.2.2 Tested air speeds

For each of the anemometers the field of the longitudinal air velocity component was measured for two air speeds set in the wind tunnel. The air speed was set such that the velocity indication of the tested anemometer was as near as possible to the values prescribed in Tab. 5.3 below.

meter under test (MUT)	**MUT velocity indication (m/s)**
Testo 0635 9340	5, 12
Vaisala WAA151	5, 20
RM Young Gill Propeller MODEL 27106D	5, 20

Tab. 5.3 Air speeds for which the velocity fields in front of the anemometers are measured

5.2.3 Measurement planes and grids

The velocity fields were measured in one or two planes upstream the anemometers (see Figs. 5.2 to 5.4) which always contain the central longitudinal axis of the wind tunnel test section (axis z in the figures). In case of the Testo and Vaisala anemometers, two planes were used – one perpendicular and one parallel to the mounting rod of the anemometers (Figs. 5.2a,b for Testo and 5.3a,b for Vaisala). The half-plane just in front of the mounting rod was omitted. In case of the RM Young anemometer, one half-plane was used for the measurement (Fig. 5.4). Orientation of this half-plane (of the x axis in the figure) was not specified and it was selected by each laboratory. This should be sufficient because of the rotational symmetry of the RM Young anemometer. Velocity field asymmetry can be induced, however, when the wind tunnel nozzle is not circular (the case of CETIAT).

The Figs. 5.2 to 5.4 also show definition of the coordinates x, y, z which is then used in plots of the velocity fields. The origin of the coordinate system is always in the centre of the outlet of the wind tunnel nozzle. So, z is a distance from the nozzle outlet and x, y are transversal coordinates with zero on the central axis, x going in direction of a mounting rod (for Testo and Vaisala) and y going perpendicularly to a mounting rod.

The velocity field measurements in the prescribed planes were made pointwise in a grid of points (see Figs. 5.2 to 5.4 for a schematic sketch). The grid cells are squares with a constant size. For decreasing test section size the cell size also decreases because larger velocity gradients are expected. The cell size (grid step) and number of cells in transversal direction used in each wind tunnel are given in Tab. 5.4. In longitudinal direction, the grids cover most of the area between the wind tunnel nozzle and the installed anemometer (except the case of CETIAT).

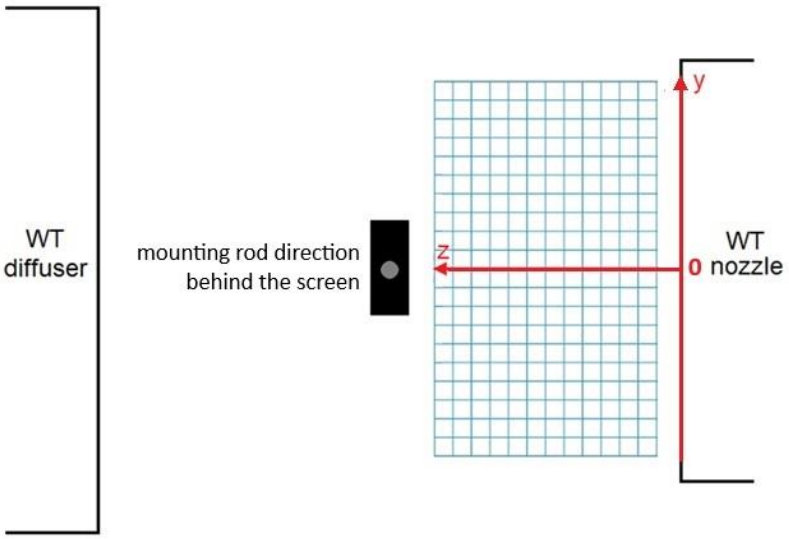

Fig. 5.2a Measurement grid and definition of coordinates for the anemometer Testo in a plane perpendicular to its mounting rod.

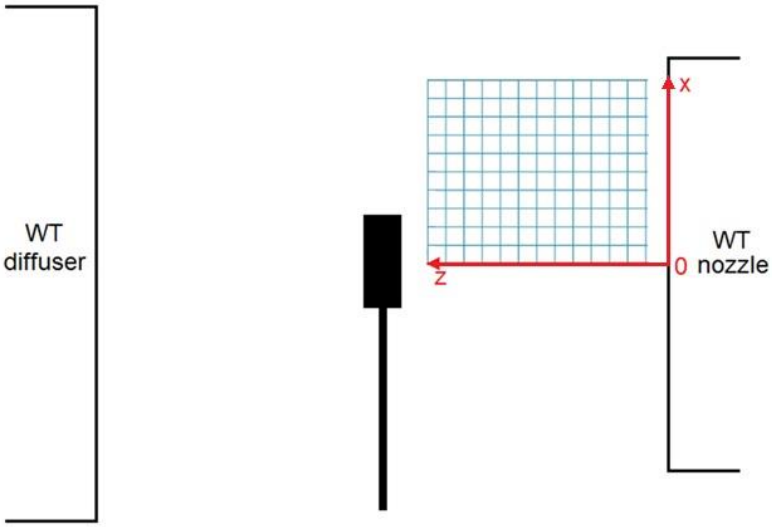

Fig. 5.2b Measurement grid and definition of coordinates for the anemometer Testo in a plane parallel to its mounting rod.

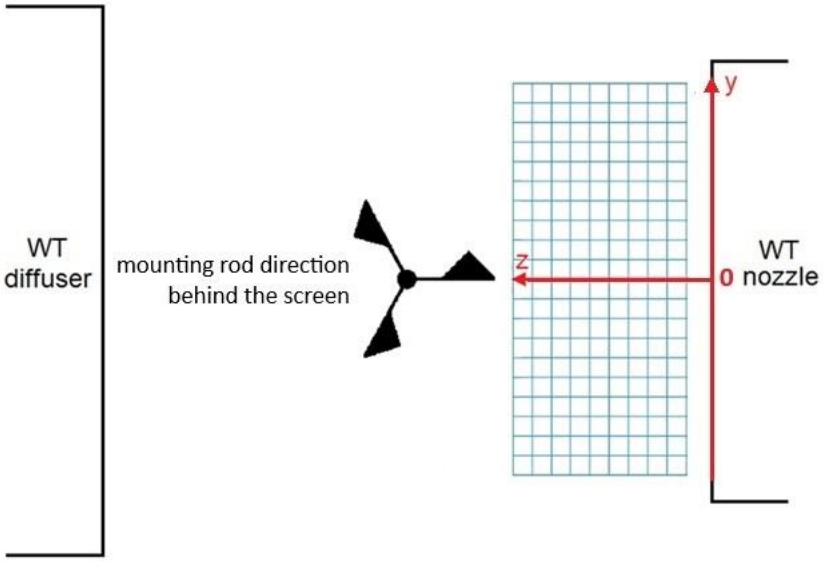

Fig. 5.3a Measurement grid and definition of coordinates for the anemometer Vaisala in horizontal plane.

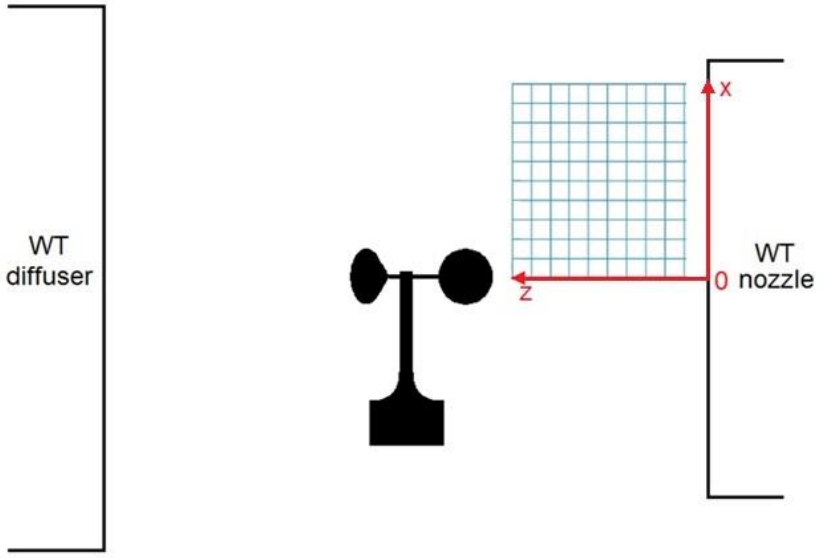

Fig. 5.3b Measurement grid and definition of coordinates for the anemometer Vaisala in vertical plane.

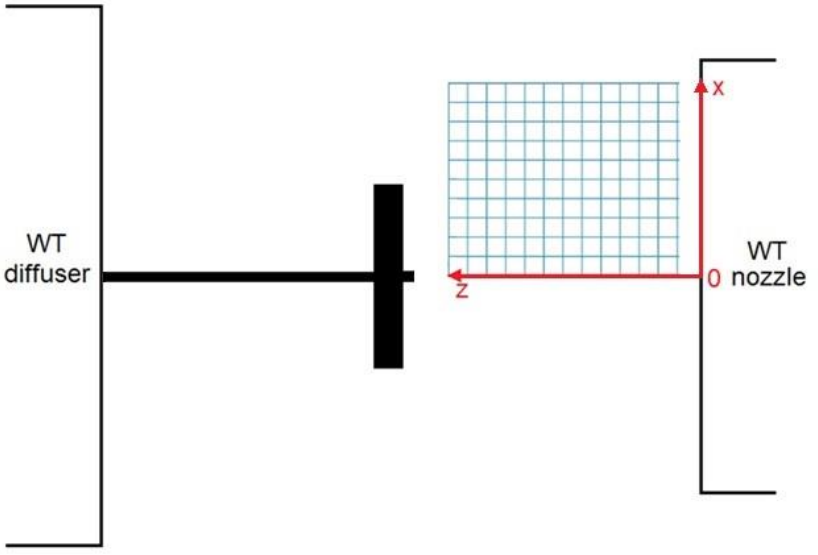

Fig. 5.4 Measurement grid and definition of coordinates for the anemometer RM Young.

lab	test section	grid step	no. cells from the test section axis in transversal direction	distance of the outermost grid points from the test section boundary
E+E/BEV	circular ø 25.5 cm	11 mm	8	39.5 mm
PTB	circular ø 32 cm	14 mm	10	20 mm
CMI	circular ø 45 cm	20 mm	10	25 mm
CETIAT	square 51 x 51 cm	20 mm	up to 12	up to 15 mm

Tab. 5.4 Parameters of the measurement grids for velocity fields

In each grid point the longitudinal velocity component (z-component) was measured by LDA. The velocity field measurement can be affected by a) non-homogeneity of the flow field in empty test section, b) fluctuations of the measured velocities due to a turbulence and c) fluctuations of the measured velocities due to a wind tunnel instability – either stochastic or systematic (drift). The following measurement and data evaluation procedure was used in order to correct or eliminate the above-mentioned effects.

5.2.4 Test procedure

1) Install an anemometer and set the wind tunnel air speed such that the anemometer indicates approximately the velocity prescribed in Tab. 5.3. Record the velocity value indicated by the MUT.
2) Select a *reference position* in a region near to the wind tunnel nozzle. The LDA used for the grid measurement repeatedly returns to this position to measure the velocity for a stability check. Or, if a second LDA is available it can be permanently installed in this position.
3) Determine a minimal number of particles N which should be detected by LDA in each grid point and in the reference position. The condition

$$\frac{Tu}{\sqrt{N}} < 0.025\ \%$$

should be satisfied where Tu is a turbulence intensity in a region near to the wind tunnel nozzle. (A few hundreds of particles were typically used in each grid point.)
4) Measure the velocity in the reference position by LDA and record it.
5) Continue with measurement of the z-component (longitudinal) of air speed in the grid points.
6) During the velocity measurements in the grid points the velocity value in the reference position should be measured by LDA at least 10 times and the measurements should be equally distributed over the time period needed for the complete measurement in the grid, one of the measurements being at the beginning (point 4) and one at the end. For example, after each row of the grid the measurement in the reference position can be done. The number of particles detected in the reference position should be approximately the same as the number of particles in the grid points.
7) When the measurement in the reference position is done by the LDA a reading of the MUT should be recorded too. In this way at least 10 MUT readings equally distributed during the test period are obtained. Each of the MUT readings should be at least 1 minute average.
8) The time sequence of the velocity measurements in the reference position should be checked during the test or after it. If a systematic drift of the velocities appears the flow stability in the wind tunnel should be ensured and the complete test should be repeated. Stochastic fluctuations of the values are acceptable but their standard deviation σ should not exceed 0.05 %.
9) The above-mentioned points should be followed for all the 3 tested anemometers and also for measurement in an *empty test section* (except the points 1 and 7 considering a MUT reading).
10) The velocity fields in the empty test section are used to correct the resulting fields in front of the MUTs. Therefore, the velocity fields in the empty test section should be measured for all the velocities and all the grid points as used for the measurements with the MUTs installed.
For these measurements the velocity in the wind tunnel should be set such that the LDA reading in the reference position is approximately 5 m/s, 12 m/s or 20 m/s.
Instead of the MUT reading in the point 7 an additional LDA measurement is done in the position where the MUT's propeller/rotor centre occurs (if the MUT would be installed). In this way at

least 10 LDA measurements equally distributed during the test period are obtained in the position of the MUT's propeller/rotor centre. The number of particles detected in the MUT's propeller/ rotor centre position should be approximately the same as the number of particles in the grid points and in the reference position.

5.2.5 Evaluation of the velocity field measurements

Notation and calculated quantities

We use the following notation:

$\boldsymbol{x}$ … position vector with components (*x, z*) or (*y, z*) in a wind tunnel test section
$v_{withMUT}(\boldsymbol{x})$ … air speed (*z*-component) in a point $\boldsymbol{x}$ as measured by LDA when a MUT is installed
v_{MUT} … MUT reading during measurement of the air speed field (average of the repeated measurements as described in point 7 of the test procedure)
$v_{empty}(\boldsymbol{x})$ … air speed (*z*-component) in a point $\boldsymbol{x}$ as measured by LDA in empty test section (with no MUT installed)
$v_{empty}(MUT)$ … air speed (*z*-component) measured by LDA in an empty test section in a position where MUT's propeller/rotor centre occurs when it is installed (average of the repeated measurements)

We define a field

$$v(\boldsymbol{x}) = v_{withMUT}(\boldsymbol{x}) + v_{empty}(MUT) - v_{empty}(\boldsymbol{x}) \tag{7}$$

which represents a calibration reference velocity value with the reference LDA placed in the position $\boldsymbol{x}$ and corrected for a velocity difference in empty test section between the position $\boldsymbol{x}$ and the position where MUT's propeller/rotor centre is installed.
Finally, a difference of the field $v(\boldsymbol{x})$ and the MUT reading v_{MUT} is calculated which, up to a minus sign, represents a measurement error of the MUT as it would be determined with the reference LDA placed in the position $\boldsymbol{x}$

$$-E(\boldsymbol{x}) = v(\boldsymbol{x}) - v_{MUT} = v_{withMUT}(\boldsymbol{x}) - v_{MUT} + v_{empty}(MUT) - v_{empty}(\boldsymbol{x}). \tag{8}$$

It is convenient to use this "negative error field" for visualising the flow upstream the tested anemometers and for comparison of the results from different wind tunnels due to the following properties:
(a) The negative error field -$E(\boldsymbol{x})$ is composed from the differences $v_{withMUT}(\boldsymbol{x}) - v_{MUT}$ and $v_{empty}(MUT) - v_{empty}(\boldsymbol{x})$ which are insensitive to small changes of the air speed setting in the wind tunnels. Therefore, small differences in the air speed setting either between the measurements with MUT installed and with an empty test section or between the measurements in different wind tunnels do not affect the resulting quantity -$E(\boldsymbol{x})$.
(b) The negative error field -$E(\boldsymbol{x})$ equals to the velocity perturbation field $v_{withMUT}(\boldsymbol{x}) - v_{empty}(\boldsymbol{x})$ up to a small constant offset $v_{empty}(MUT) - v_{MUT}$. Therefore, up to the offset, the effect of the MUT installation to the velocity field in a test section can be seen.
(c) Using the negative error field -$E(\boldsymbol{x})$ is suitable for metrology purposes because we directly see what the measurement error will be depending on the position of the reference LDA. Therefore, we can determine where the reference LDA should be placed in order to obtain comparable calibration results in different wind tunnels. Also, the reference LDA positions where the measurement error match the error obtained in the large wind tunnel of DWG can be visualised.

Smoothing the stochastic flow instability

Consider a field $F(\boldsymbol{x})$ obtained by a short time averaging of a quantity F in the grid of points such that $F(\boldsymbol{x})$ is affected by stochastic fluctuations of F and consider a related field $\bar{F}(\boldsymbol{x})$ obtained by a long time averaging of the quantity F in the grid points such that $\bar{F}(\boldsymbol{x})$ is nearly not affected by the fluctuations.

Assume that in a neighbourhood of a grid point $\boldsymbol{x}_0$ given by the 4 adjacent grid cells a linear (planar) approximation of the function $\bar{F}(\boldsymbol{x})$ is good enough, meaning that the deviations of $\bar{F}(\boldsymbol{x})$ from its linear approximation are much smaller than deviations of $\bar{F}(\boldsymbol{x})$ from $F(\boldsymbol{x})$ (i.e., the fluctuations of F).
In this case, $\bar{F}(\boldsymbol{x}_0)$ can be well approximated by average from values $\bar{F}(\boldsymbol{x}_i)$ in the 9 neighbour grid points including $\boldsymbol{x}_0$. This approximation would be exact equality in case of exact linearity of $\bar{F}(\boldsymbol{x})$ in the neighbourhood.
Therefore, also average from the really measured values $F(\boldsymbol{x}_i)$ in the 9 neighbour grid points of $\boldsymbol{x}_0$ (including $\boldsymbol{x}_0$) gives better estimate of $\bar{F}(\boldsymbol{x}_0)$ than the value $F(\boldsymbol{x}_0)$ alone, compensating the short averaging time by averaging of the 9 values. This kind of averaging gives a field which is less affected by the fluctuations and therefore is smoother. It can be applied to the measured velocity fields directly or to the derived quantities. Further in this report we present data where the smoothing procedure is applied to the negative error field $-E(\boldsymbol{x})$.
The smoothing can be applied only in the regions where the assumption of approximate linearity is satisfied, e.g. in the areas with small velocity gradients far enough from the tested anemometers.

5.3 Results

5.3.1 Calibrations in Deutsche WindGuard Wind Tunnel Services

Calibrations of the three tested anemometers have been performed in the large wind tunnel of Deutsche WindGuard Wind Tunnel Services (Fig. A.1). This wind tunnel has a square nozzle 100 cm x 100 cm and negligible blockage effect. Knowing the measurement errors obtained in DWG, which are not significantly affected by the blockage effect, we can look for suitable positions of a reference LDA in the smaller wind tunnels which give a measurement error comparable with that of DWG. The calibration results obtained in DWG are summarised in Tab. 5.5 below.

	nominal air speed:	5 m/s		12 m/s		20 m/s	
	date	E (m/s)	U (m/s)	E (m/s)	U (m/s)	E (m/s)	U (m/s)
Testo 0635 9340	27.6.2025	-0.086	0.040	-0.200	0.048		
Vaisala WAA151 (1)	27.6.2025	0.148	0.041			0.255	0.083
Vaisala WAA151 (2)	13.3.2026	0.110	0.040			0.299	0.082
RM Young Gill Prop.	5.7.2025	-0.055	0.040			-0.033	0.081

Tab. 5.5 Calibration results obtained in the large wind tunnel of DWG

Because of a larger shift of the measurement error of the Vaisala anemometer compared to a calibration in DWG within another Euramet project in 2018, this anemometer was calibrated twice in order to exclude possible reproducibility issues. Both calibrations are included in Tab. 5.5 (denoted (1) and (2)). The calibration (1), which was performed sooner after the velocity field measurements in the other laboratories, is used for further data evaluation in the next section. The measurement error (2) is deviated by -0.76 % for 5 m/s and by 0.22 % for 20 m/s.

5.3.2 The negative error fields

Complete measurement data including the calculated and smoothed field of the negative error $-E(\boldsymbol{x})$ can be found in the supplementary material Sup2. In the Figs. 5.5 to 5.44 below we present plots of the negative error field. The plots are ordered in a way which enables an easy comparison of the results from different wind tunnels – for each case (anemometer, test plane orientation, air speed) four plots of BEV/E+E, PTB, CMI and CETIAT are shown. For each plot a step of 0.25 % of the nominal velocity (5 m/s, 12 m/s or 20 m/s) is used in the colour scale of the negative error field. The full white line in the plots represents the reference LDA positions where the same measurement error would be obtained as in the large wind tunnel of DWG with negligible blockage effect. The two dashed white lines bound a region of the reference LDA positions where the obtained measurement error lies within the expanded uncertainty interval of the calibration in DWG. Therefore, the region between the dashed white lines can be interpreted as a region suitable for the reference LDA placement where a calibration result corresponding to a negligible blockage effect is obtained.

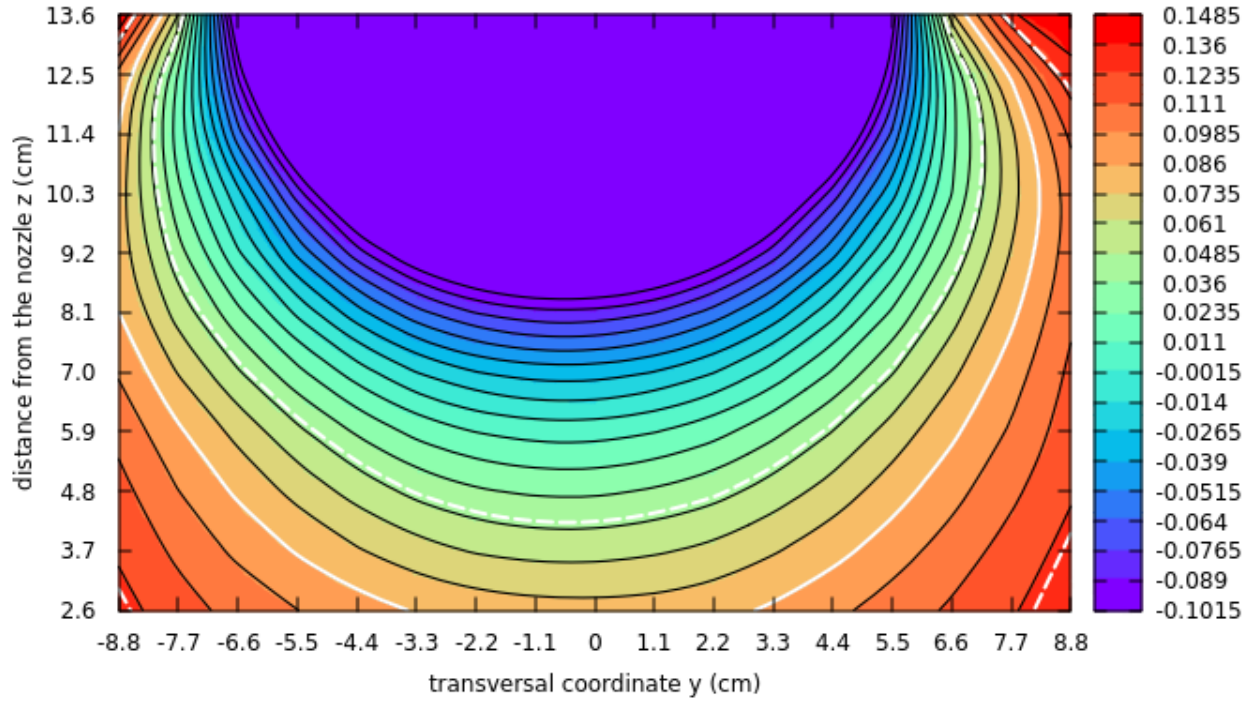

Fig. 5.5 Negative error field (scale in m/s) for Testo vane anemometer (propeller frame diameter 10.7 cm) in the wind tunnel of BEV/E+E, y-z plane, 5 m/s (Sup2 code: EE-T-5y). Test section open boundary (prolonged nozzle wall) at y = ±12.75 cm; the most upstream point of the anemometer at z = 15.3 cm.

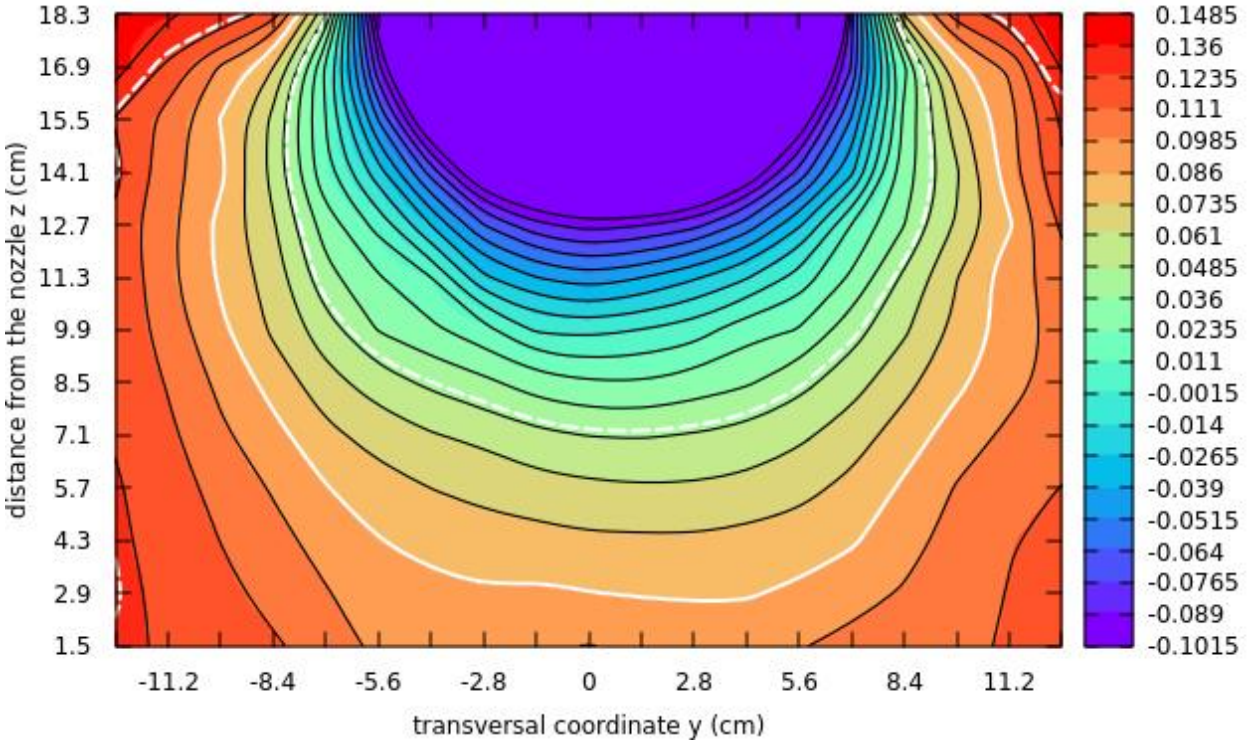

Fig. 5.6 Negative error field (scale in m/s) for Testo vane anemometer (propeller frame diameter 10.7 cm) in the wind tunnel of PTB, y-z plane, 5 m/s (Sup2 code: PT-T-5y). Test section open boundary (prolonged nozzle wall) at y = ±16 cm; the most upstream point of the anemometer at z = 20.3 cm.

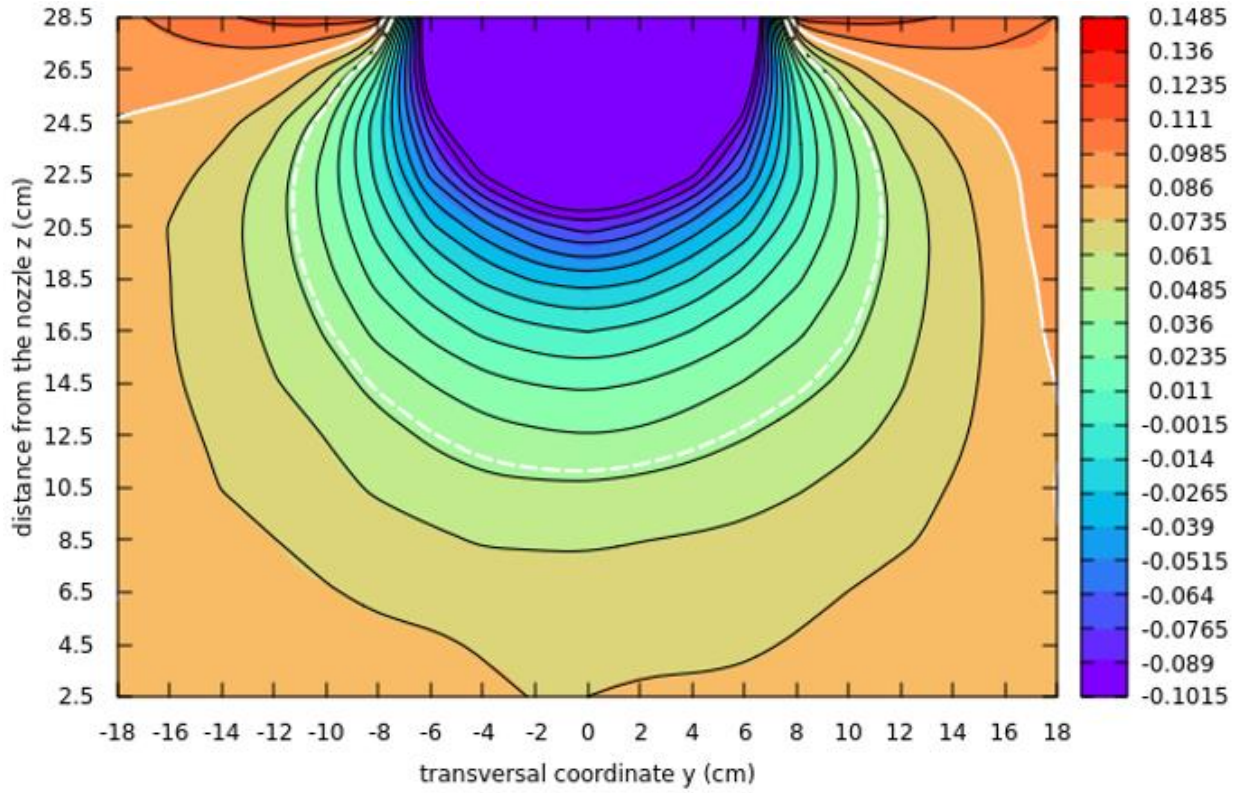

Fig. 5.7 Negative error field (scale in m/s) for Testo vane anemometer (propeller frame diameter 10.7 cm) in the wind tunnel of CMI, y-z plane, 5 m/s (Sup2 code: CM-T-5y). Test section open boundary (prolonged nozzle wall) at y = ±22.5 cm; the most upstream point of the anemometer at z = 29.3 cm.

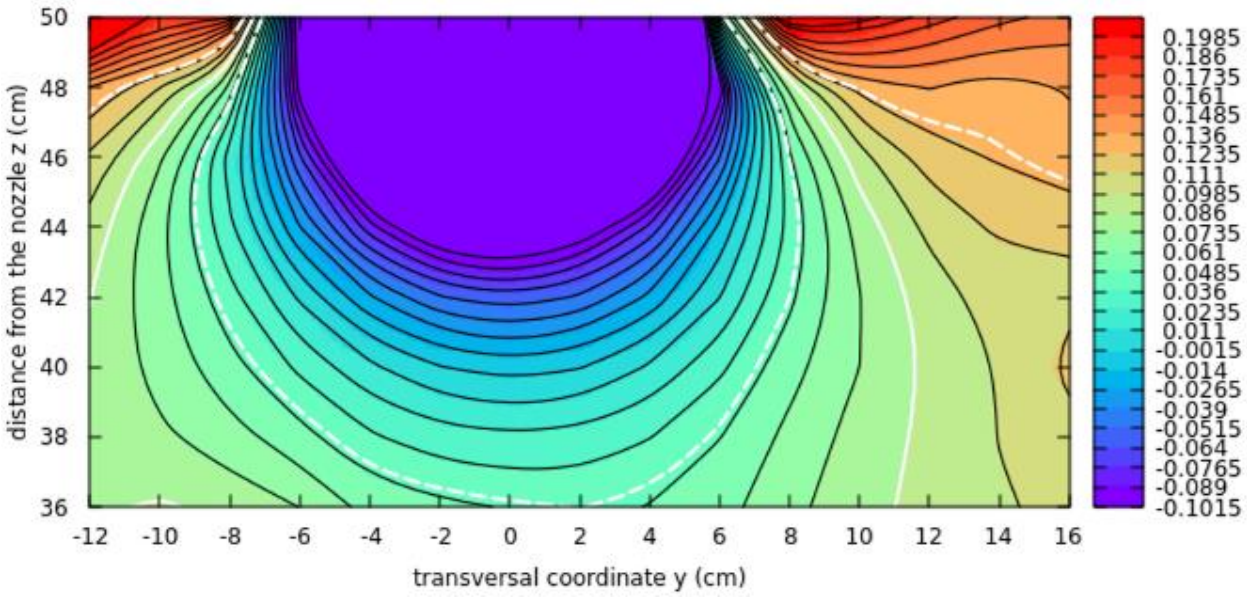

Fig. 5.8 Negative error field (scale in m/s) for Testo vane anemometer (propeller frame diameter 10.7 cm) in the wind tunnel of CETIAT, y-z plane, 5 m/s (Sup2 code: CE-T-5y). Test section boundary (solid wall) at y = ±25.5 cm; the most upstream point of the anemometer at z = 52 cm.

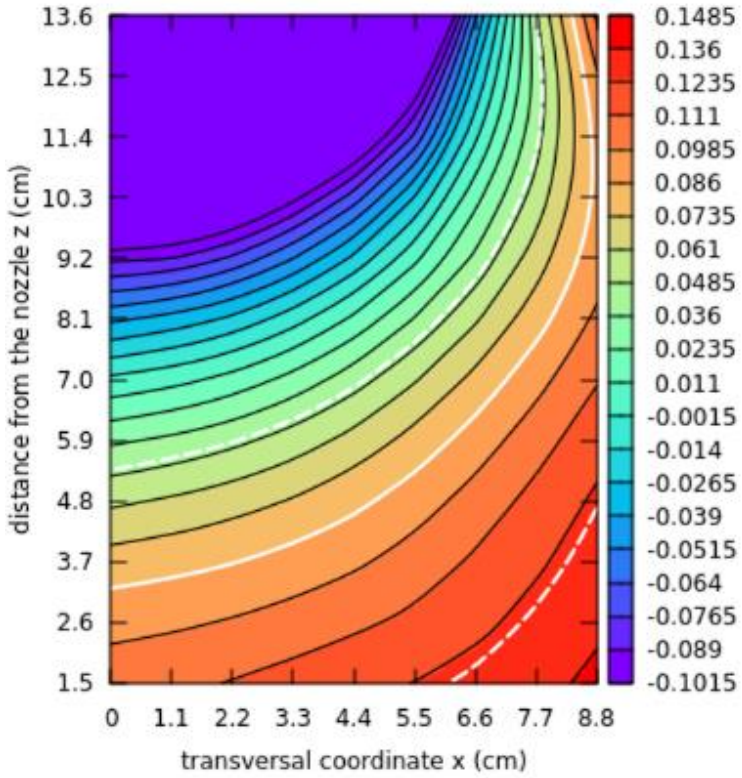

Fig. 5.9 Negative error field (scale in m/s) for Testo vane anemometer (propeller frame diameter 10.7 cm) in the wind tunnel of BEV/E+E, x-z plane, 5 m/s (Sup2 code: EE-T-5x). Test section open boundary (prolonged nozzle wall) at x = 12.75 cm; the most upstream point of the anemometer at z = 15.3 cm.

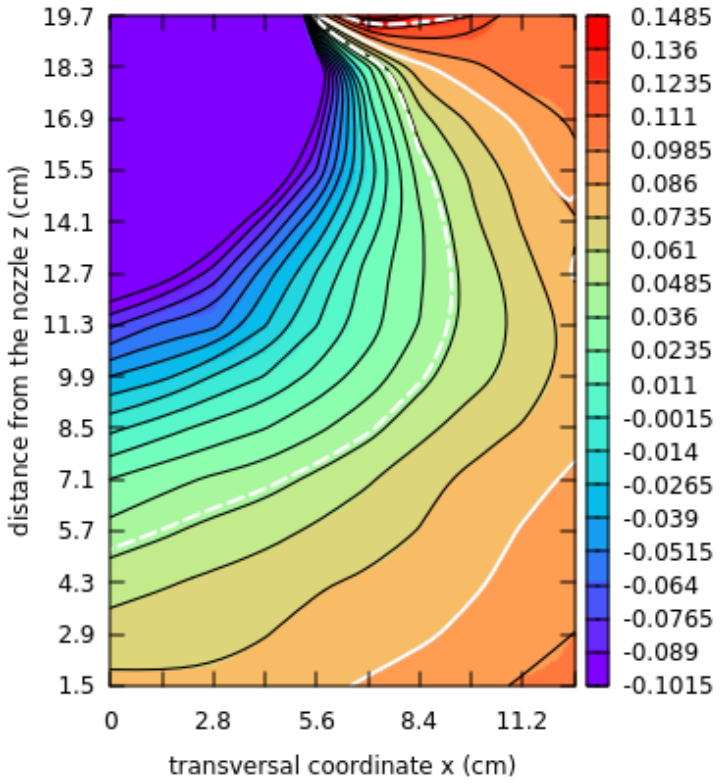

Fig. 5.10 Negative error field (scale in m/s) for Testo vane anemometer (propeller frame diameter 10.7 cm) in the wind tunnel of PTB, x-z plane, 5 m/s (Sup2 code: PT-T-5x). Test section open boundary (prolonged nozzle wall) at x = 16 cm; the most upstream point of the anemometer at z = 20.3 cm.

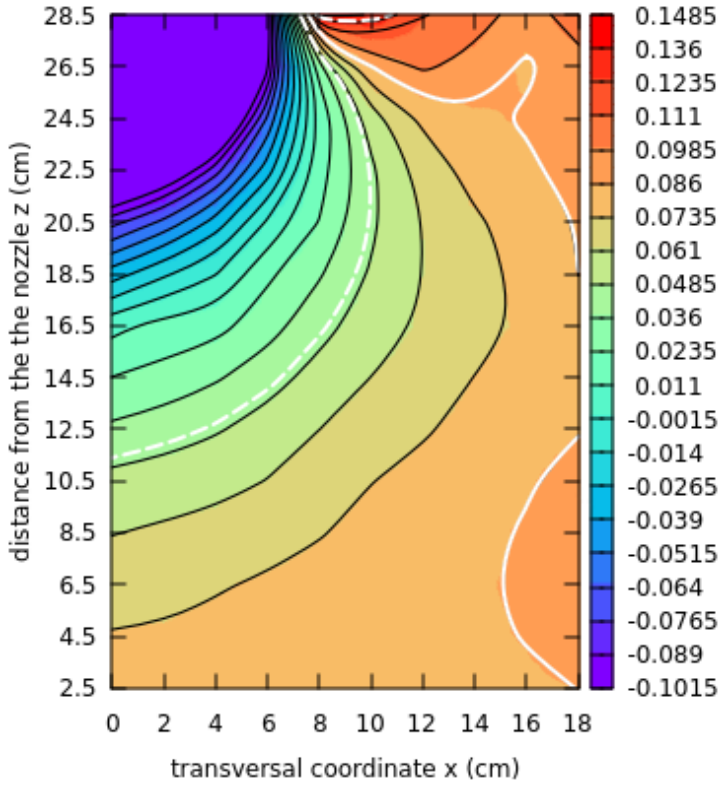

Fig. 5.11 Negative error field (scale in m/s) for Testo vane anemometer (propeller frame diameter 10.7 cm) in the wind tunnel of CMI, x-z plane, 5 m/s (Sup2 code: CM-T-5x). Test section open boundary (prolonged nozzle wall) at x = 22.5 cm; the most upstream point of the anemometer at z = 29.3 cm.

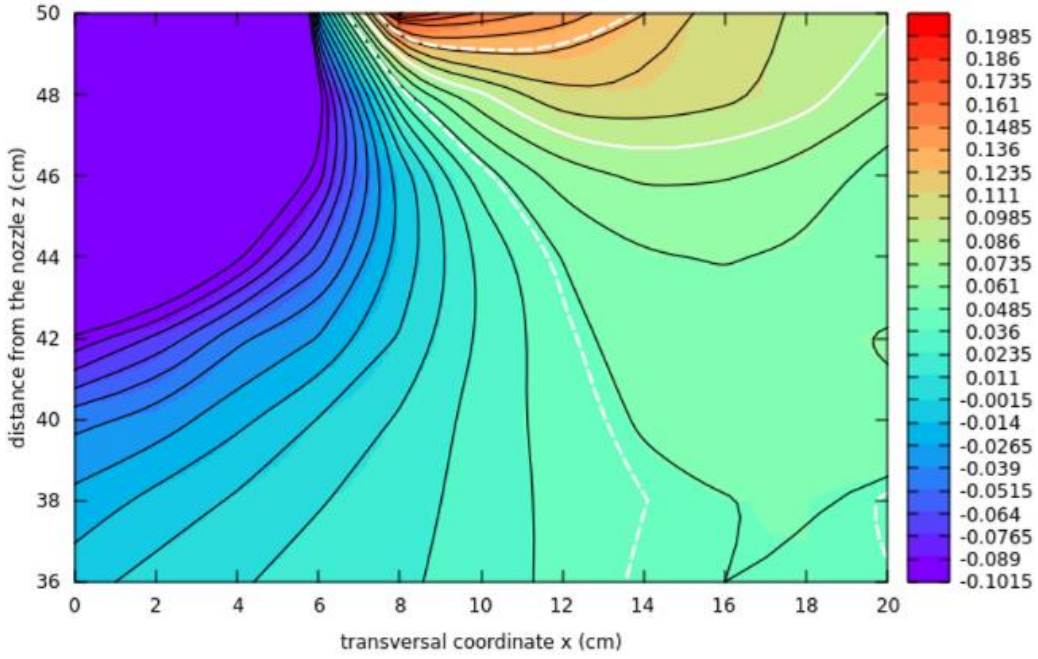

Fig. 5.12 Negative error field (scale in m/s) for Testo vane anemometer (propeller frame diameter 10.7 cm) in the wind tunnel of CETIAT, x-z plane, 5 m/s (Sup2 code: CE-T-5x). Test section boundary (solid wall) at x = 26.5 to 27 cm; the most upstream point of the anemometer at z = 52 cm.

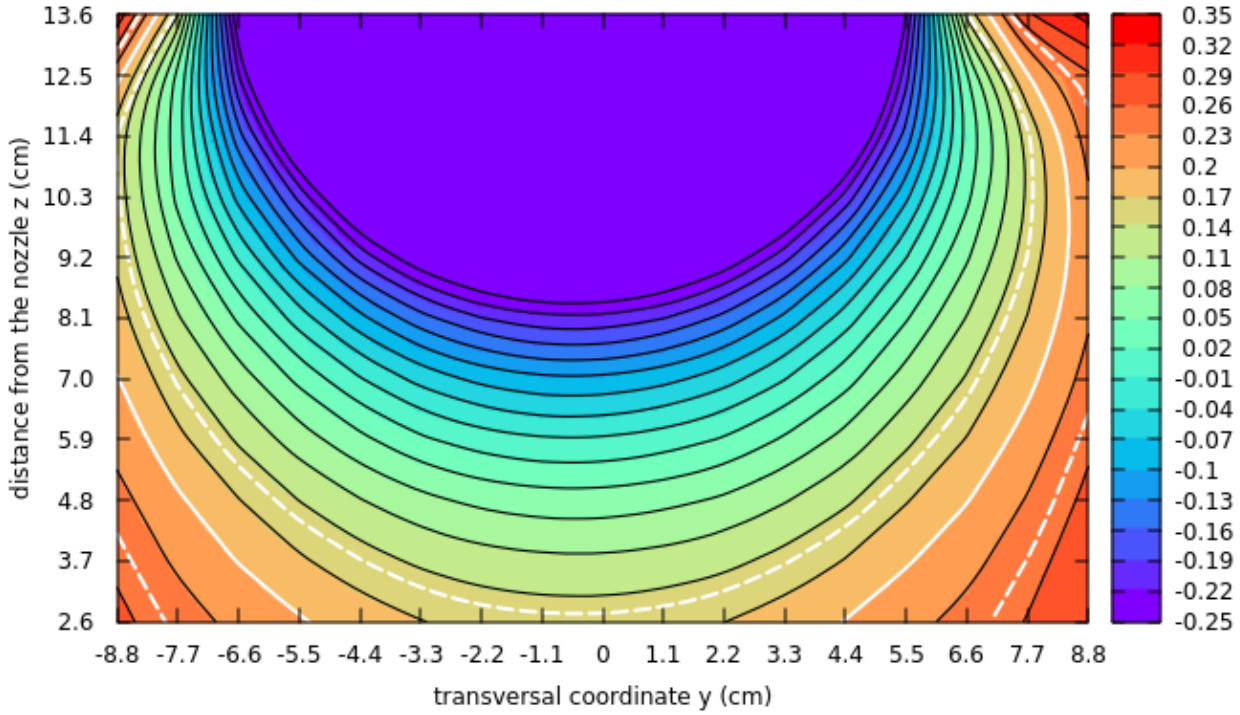

Fig. 5.13 Negative error field (scale in m/s) for Testo vane anemometer (propeller frame diameter 10.7 cm) in the wind tunnel of BEV/E+E, y-z plane, 12 m/s (Sup2 code: EE-T-12y). Test section open boundary (prolonged nozzle wall) at y = ±12.75 cm; the most upstream point of the anemometer at z = 15.3 cm.

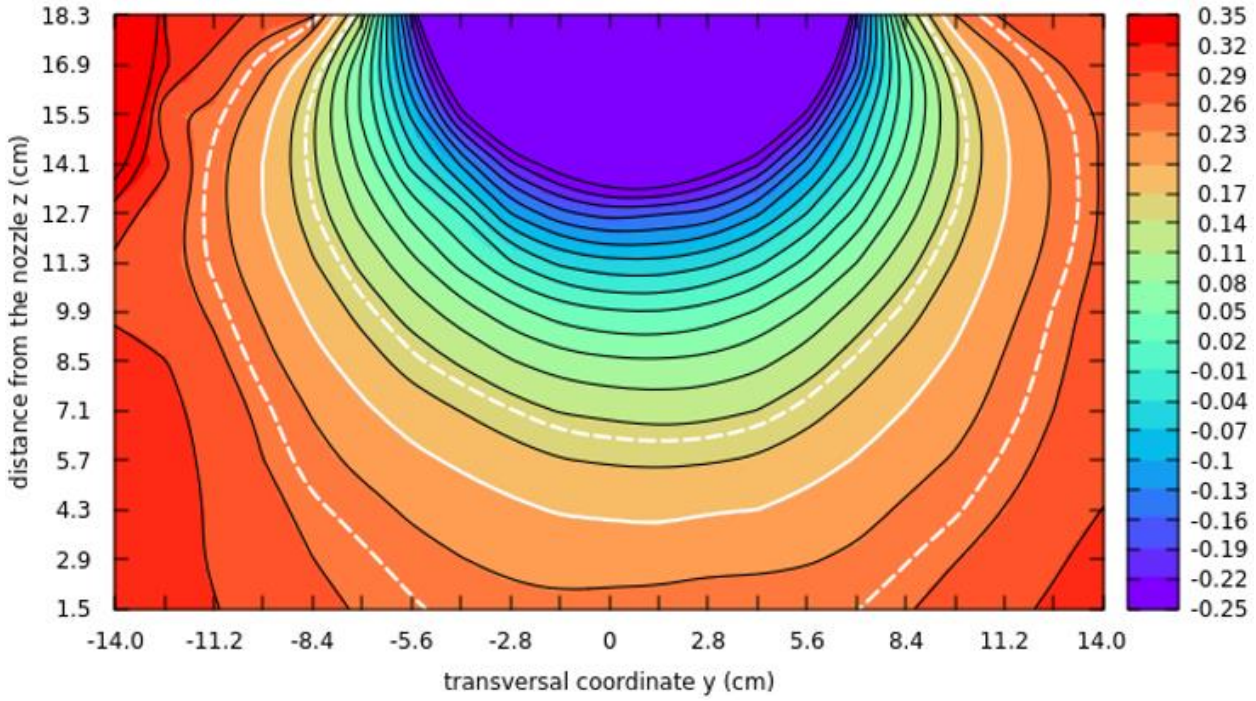

Fig. 5.14 Negative error field (scale in m/s) for Testo vane anemometer (propeller frame diameter 10.7 cm) in the wind tunnel of PTB, y-z plane, 12 m/s (Sup2 code: PT-T-12y). Test section open boundary (prolonged nozzle wall) at y = ±16 cm; the most upstream point of the anemometer at z = 20.3 cm.

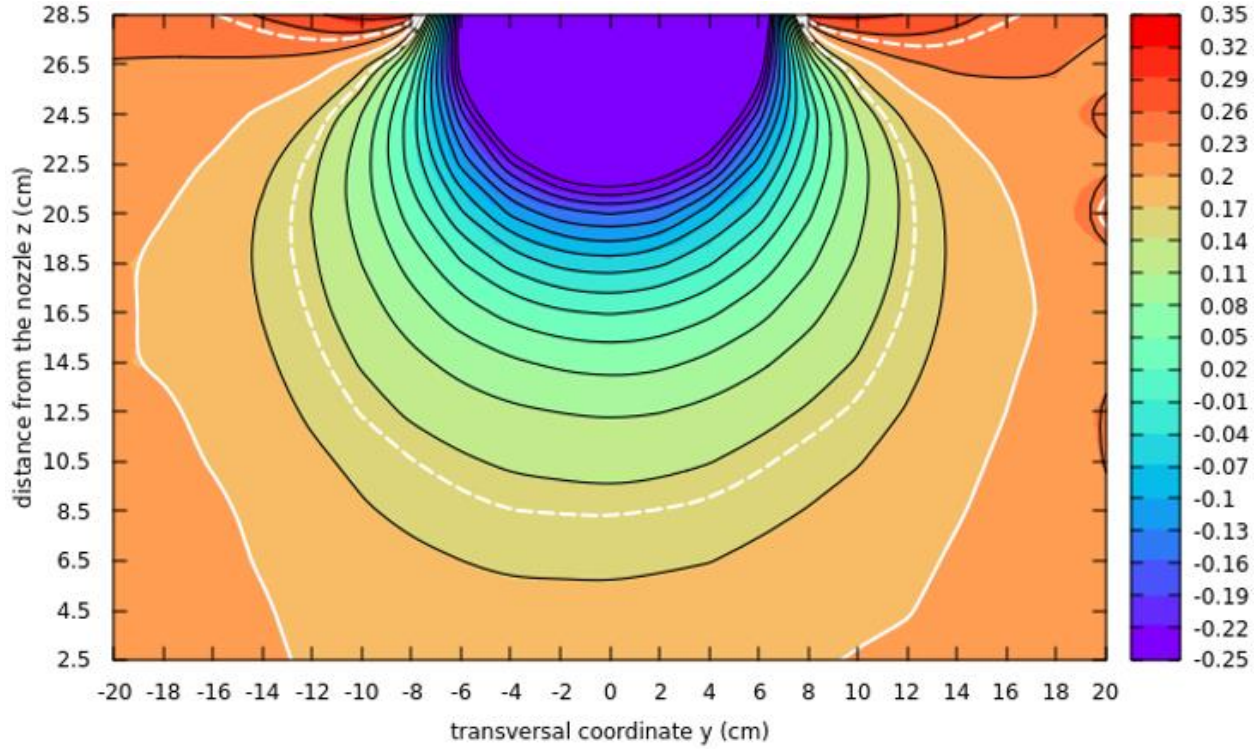

Fig. 5.15 Negative error field (scale in m/s) for Testo vane anemometer (propeller frame diameter 10.7 cm) in the wind tunnel of CMI, y-z plane, 12 m/s (Sup2 code: CM-T-12y). Test section open boundary (prolonged nozzle wall) at y = ±22.5 cm; the most upstream point of the anemometer at z = 29.3 cm.

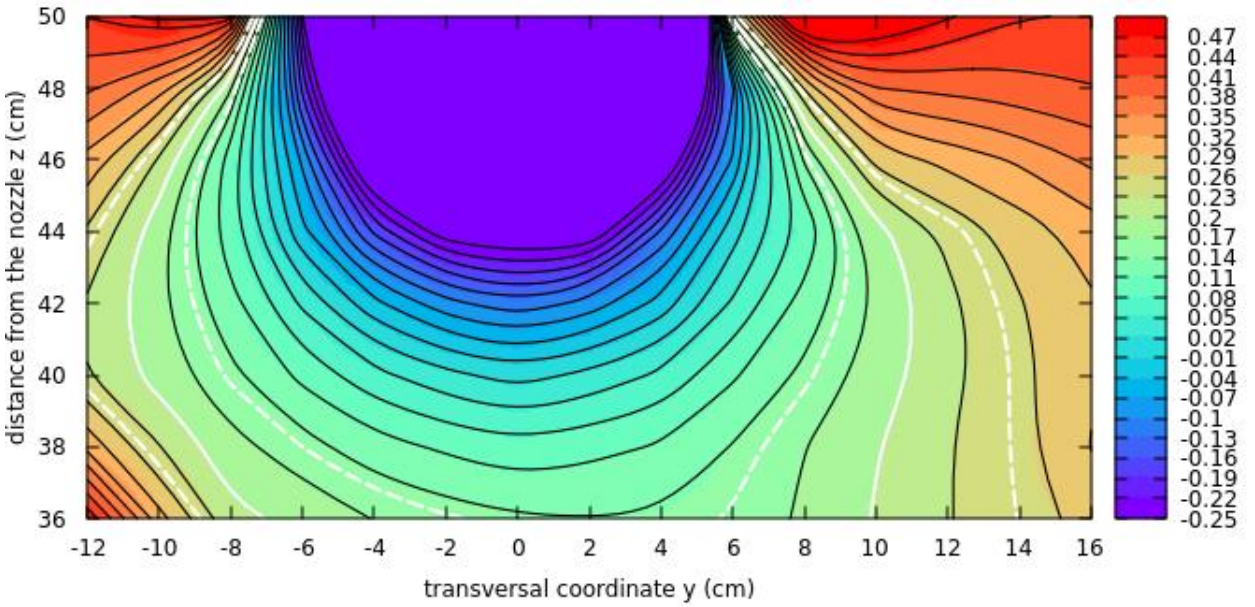

Fig. 5.16 Negative error field (scale in m/s) for Testo vane anemometer (propeller frame diameter 10.7 cm) in the wind tunnel of CETIAT, y-z plane, 12 m/s (Sup2 code: CE-T-12y). Test section boundary (solid wall) at y = ±25.5 cm; the most upstream point of the anemometer at z = 52 cm.

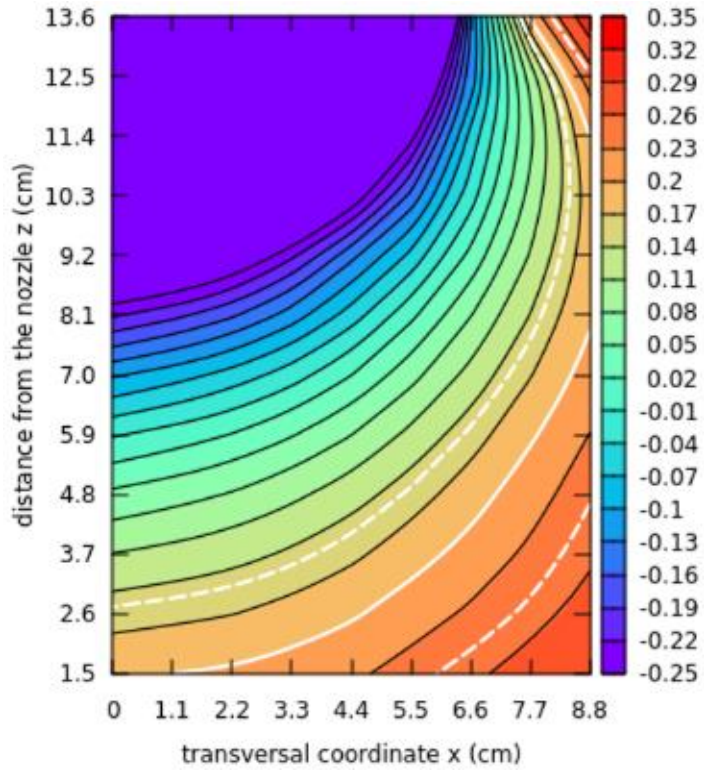

Fig. 5.17 Negative error field (scale in m/s) for Testo vane anemometer (propeller frame diameter 10.7 cm) in the wind tunnel of BEV/E+E, x-z plane, 12 m/s (Sup2 code: EE-T-12x). Test section open boundary (prolonged nozzle wall) at x = 12.75 cm; the most upstream point of the anemometer at z = 15.3 cm.

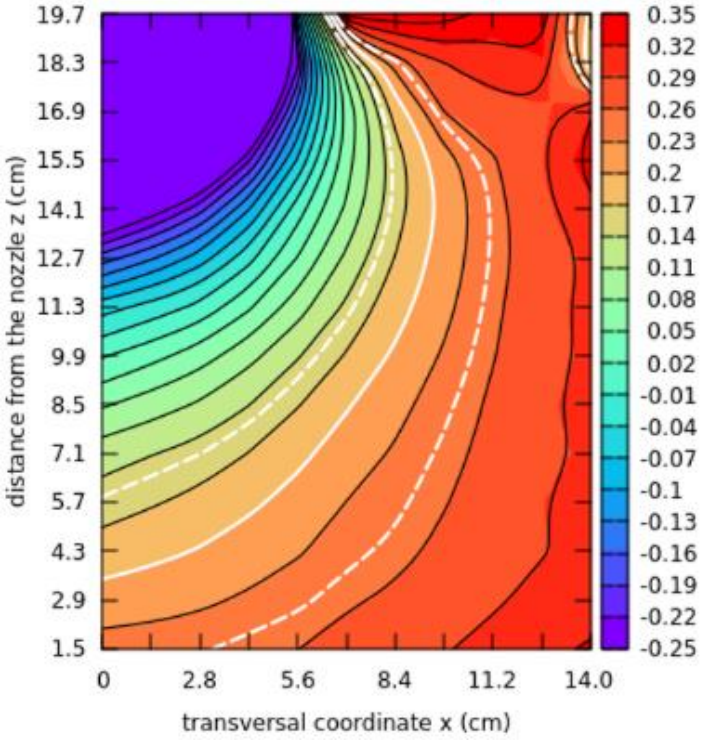

Fig. 5.18 Negative error field (scale in m/s) for Testo vane anemometer (propeller frame diameter 10.7 cm) in the wind tunnel of PTB, x-z plane, 12 m/s (Sup2 code: PT-T-12x). Test section open boundary (prolonged nozzle wall) at x = 16 cm; the most upstream point of the anemometer at z = 20.3 cm.

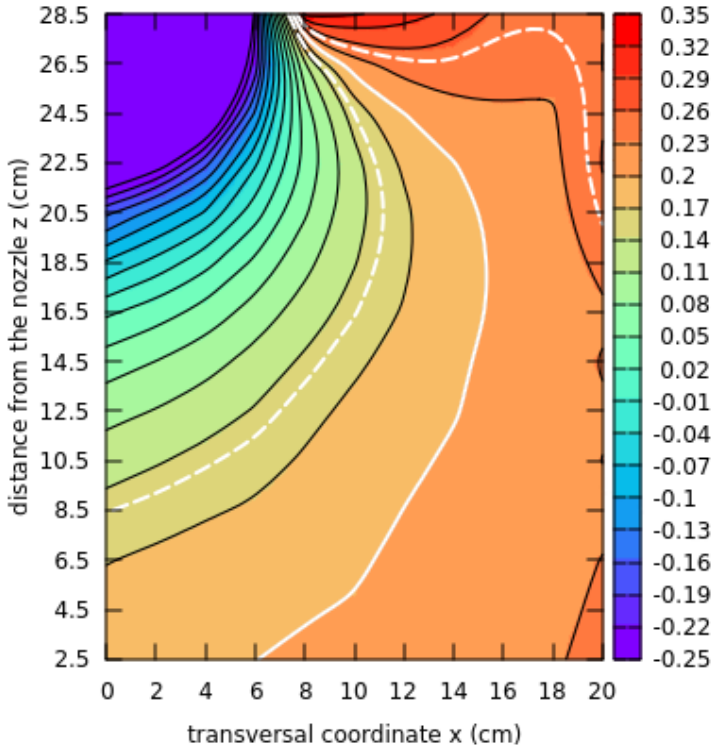

Fig. 5.19 Negative error field (scale in m/s) for Testo vane anemometer (propeller frame diameter 10.7 cm) in the wind tunnel of CMI, x-z plane, 12 m/s (Sup2 code: CM-T-12x). Test section open boundary (prolonged nozzle wall) at x = 22.5 cm; the most upstream point of the anemometer at z = 29.3 cm.

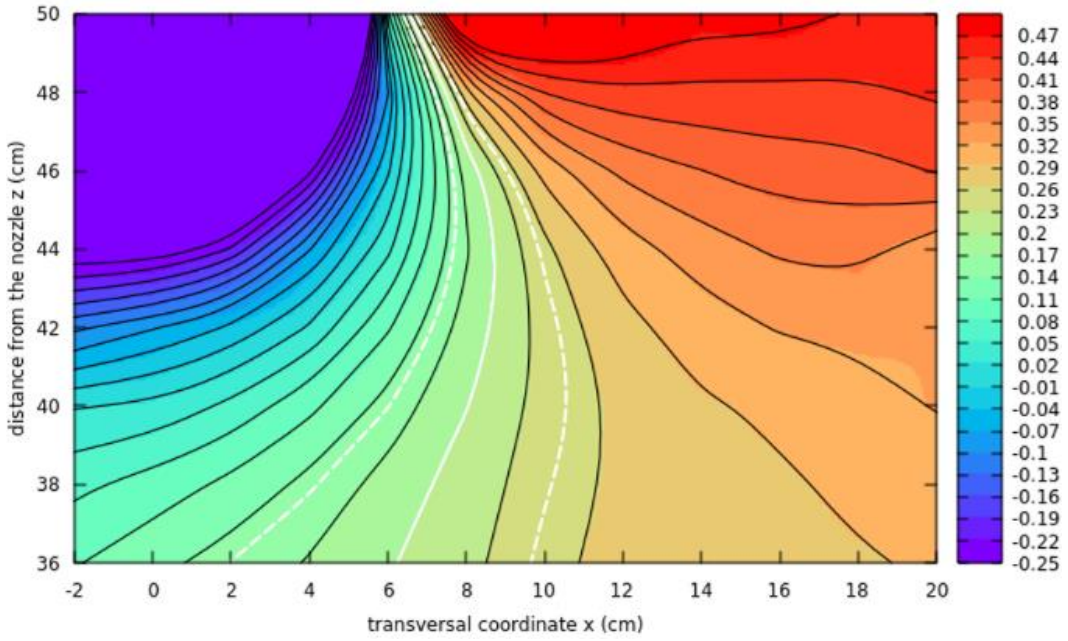

Fig. 5.20 Negative error field (scale in m/s) for Testo vane anemometer (propeller frame diameter 10.7 cm) in the wind tunnel of CETIAT, x-z plane, 12 m/s (Sup2 code: CE-T-12x). Test section boundary (solid wall) at x = 26.5 to 27 cm; the most upstream point of the anemometer at z = 52 cm.

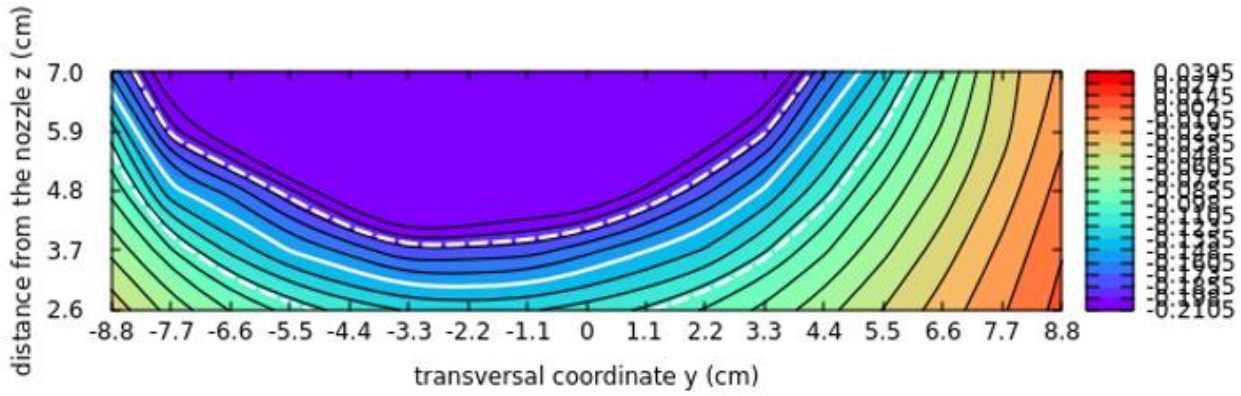

Fig. 5.21 Negative error field (scale in m/s) for Vaisala WAA151 cup anemometer (rotor diameter 18.2 cm) in the wind tunnel of BEV/E+E, y-z plane, 5 m/s (Sup2 code: EE-V-5y). Test section open boundary (prolonged nozzle wall) at y = ±12.75 cm; the most upstream point of the rotor at z = 8.4 cm.

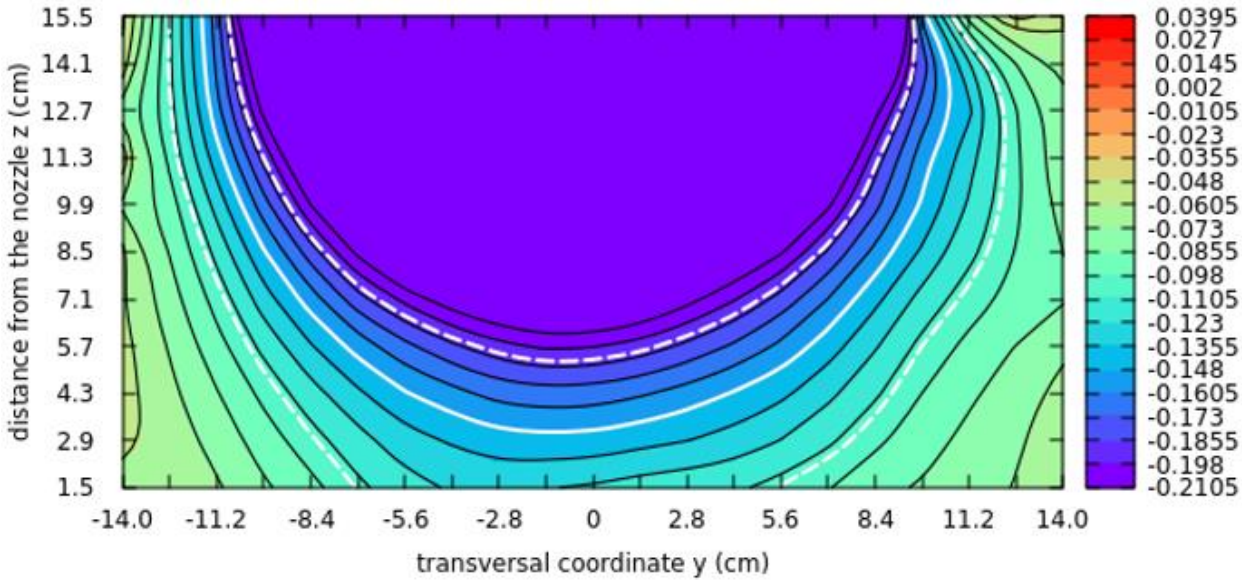

Fig. 5.22 Negative error field (scale in m/s) for Vaisala WAA151 cup anemometer (rotor diameter 18.2 cm) in the wind tunnel of PTB, y-z plane, 5 m/s (Sup2 code: PT-V-5y). Test section open boundary (prolonged nozzle wall) at y = ±16 cm; the most upstream point of the rotor at z = 13.4 cm.

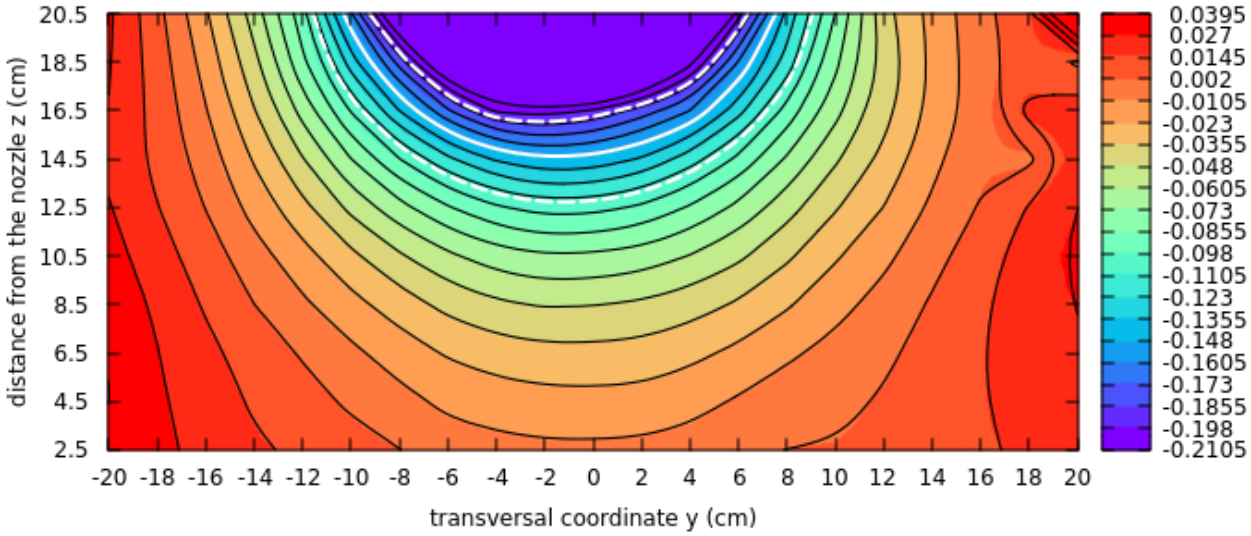

Fig. 5.23 Negative error field (scale in m/s) for Vaisala WAA151 cup anemometer (rotor diameter 18.2 cm) in the wind tunnel of CMI, y-z plane, 5 m/s (Sup2 code: CM-V-5y). Test section open boundary (prolonged nozzle wall) at y = ±22.5 cm; the most upstream point of the rotor at z = 22.4 cm.

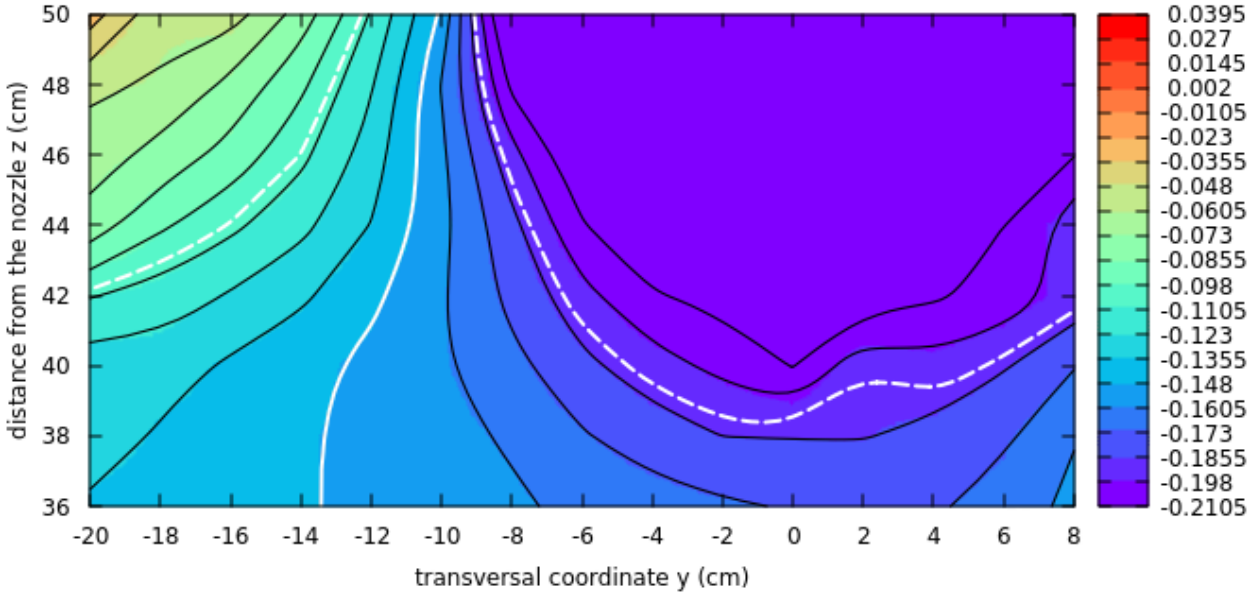

Fig. 5.24 Negative error field (scale in m/s) for Vaisala WAA151 cup anemometer (rotor diameter 18.2 cm) in the wind tunnel of CETIAT, y-z plane, 5 m/s (Sup2 code: CE-V-5y). Test section boundary (solid wall) at y = ± (26.5 to 27) cm; the most upstream point of the rotor at z = 52 cm.

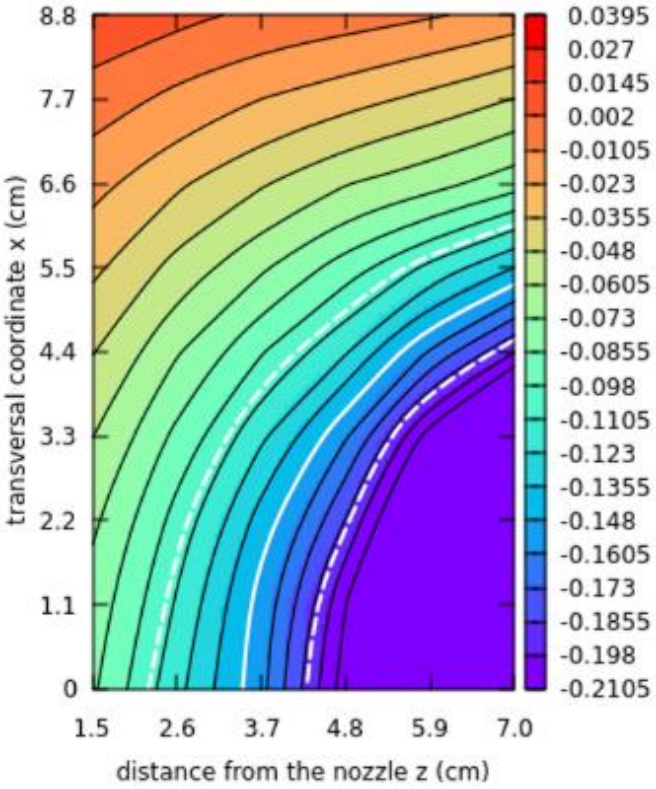

Fig. 5.25 Negative error field (scale in m/s) for Vaisala WAA151 cup anemometer (rotor diameter 18.2 cm) in the wind tunnel of BEV/E+E, x-z plane, 5 m/s (Sup2 code: EE-V-5x). Test section open boundary (prolonged nozzle wall) at x = 12.75 cm; the most upstream point of the rotor at z = 8.4 cm.

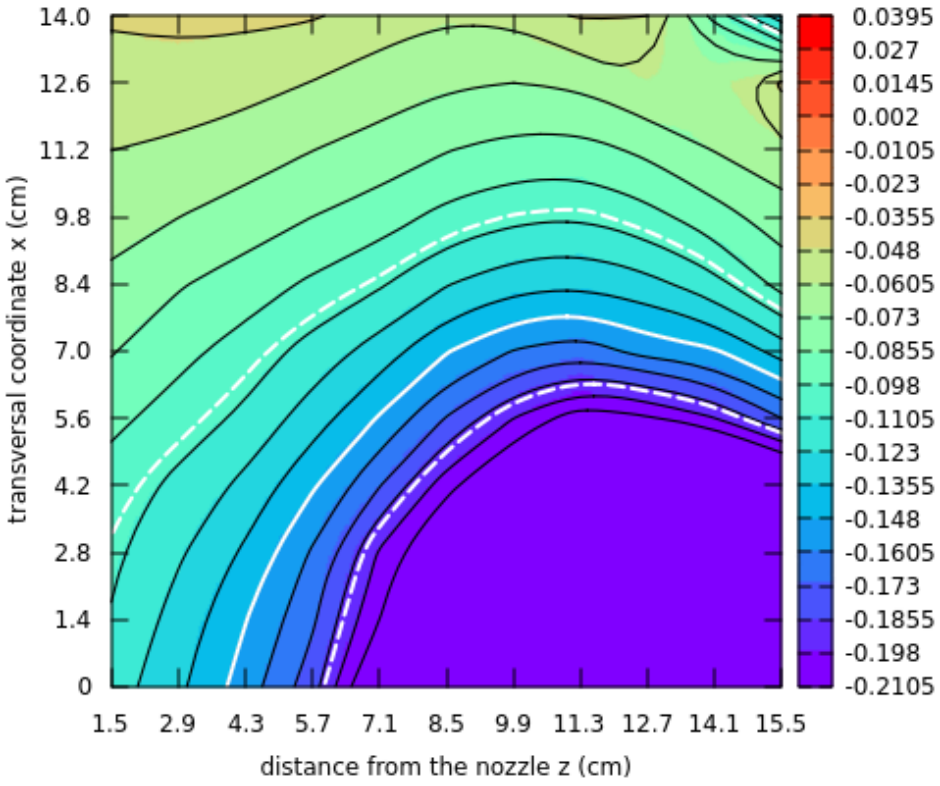

Fig. 5.26 Negative error field (scale in m/s) for Vaisala WAA151 cup anemometer (rotor diameter 18.2 cm) in the wind tunnel of PTB, x-z plane, 5 m/s (Sup2 code: PT-V-5x). Test section open boundary (prolonged nozzle wall) at x = 16 cm; the most upstream point of the rotor at z = 13.4 cm.

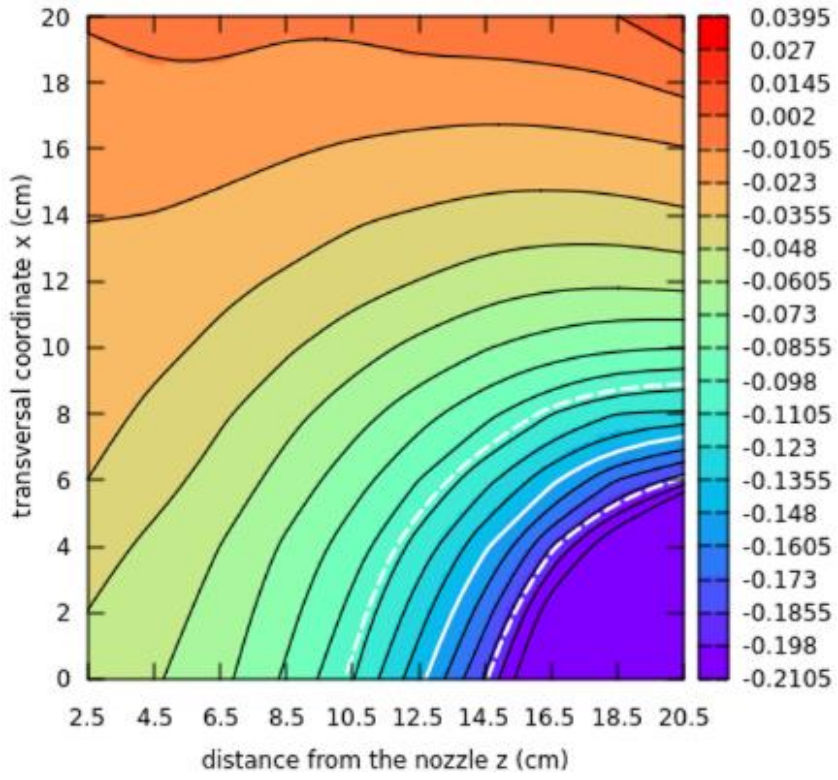

Fig. 5.27 Negative error field (scale in m/s) for Vaisala WAA151 cup anemometer (rotor diameter 18.2 cm) in the wind tunnel of CMI, x-z plane, 5 m/s (Sup2 code: CM-V-5x). Test section open boundary (prolonged nozzle wall) at x = 22.5 cm; the most upstream point of the rotor at z = 22.4 cm.

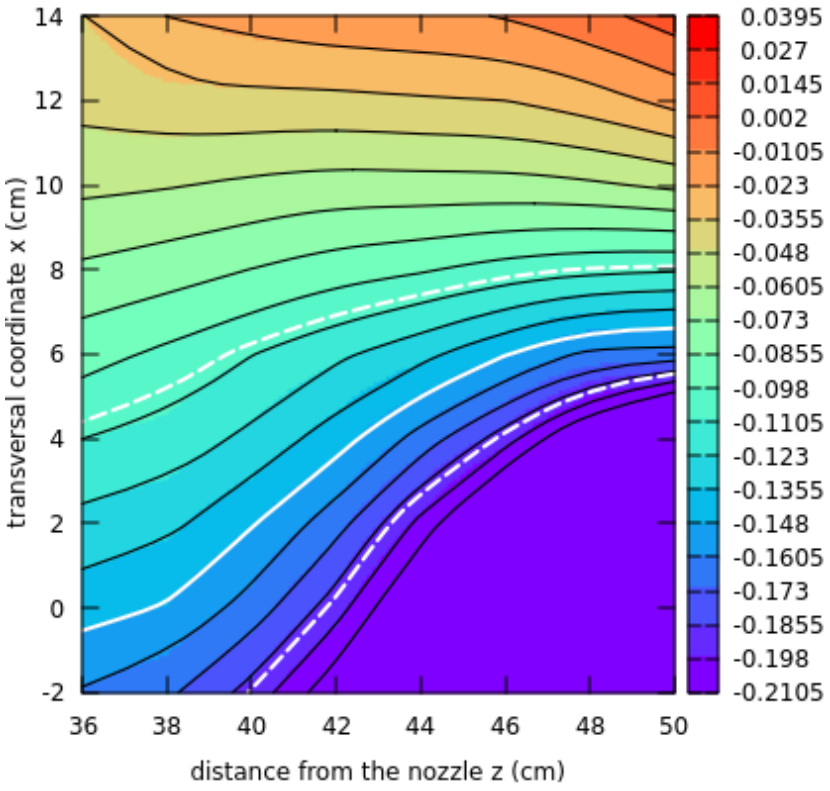

Fig. 5.28 Negative error field (scale in m/s) for Vaisala WAA151 cup anemometer (rotor diameter 18.2 cm) in the wind tunnel of CETIAT, x-z plane, 5 m/s (Sup2 code: CE-V-5x). Test section boundary (solid wall) at x = 25.5 cm; the most upstream point of the rotor at z = 52 cm.

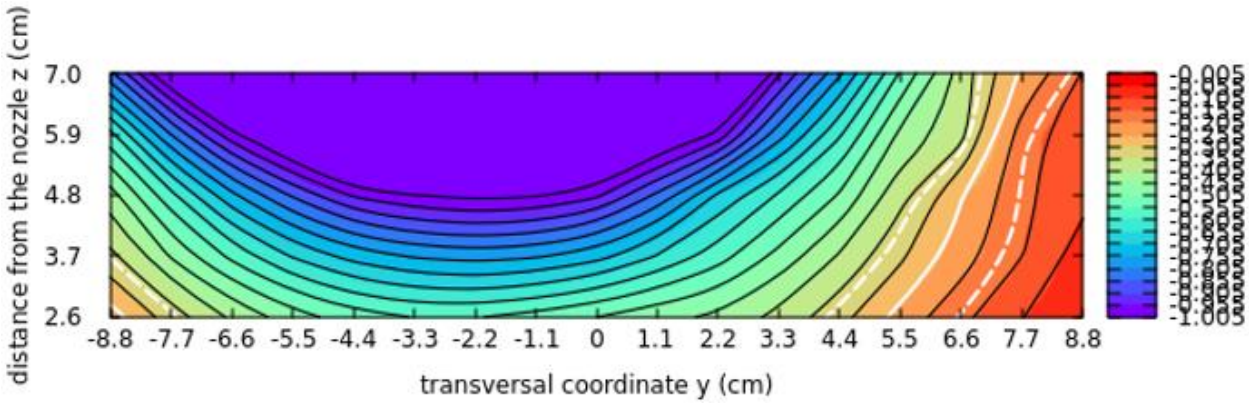

Fig. 5.29 Negative error field (scale in m/s) for Vaisala WAA151 cup anemometer (rotor diameter 18.2 cm) in the wind tunnel of BEV/E+E, y-z plane, 20 m/s (Sup2 code: EE-V-20y). Test section open boundary (prolonged nozzle wall) at y = ±12.75 cm; the most upstream point of the rotor at z = 8.4 cm.

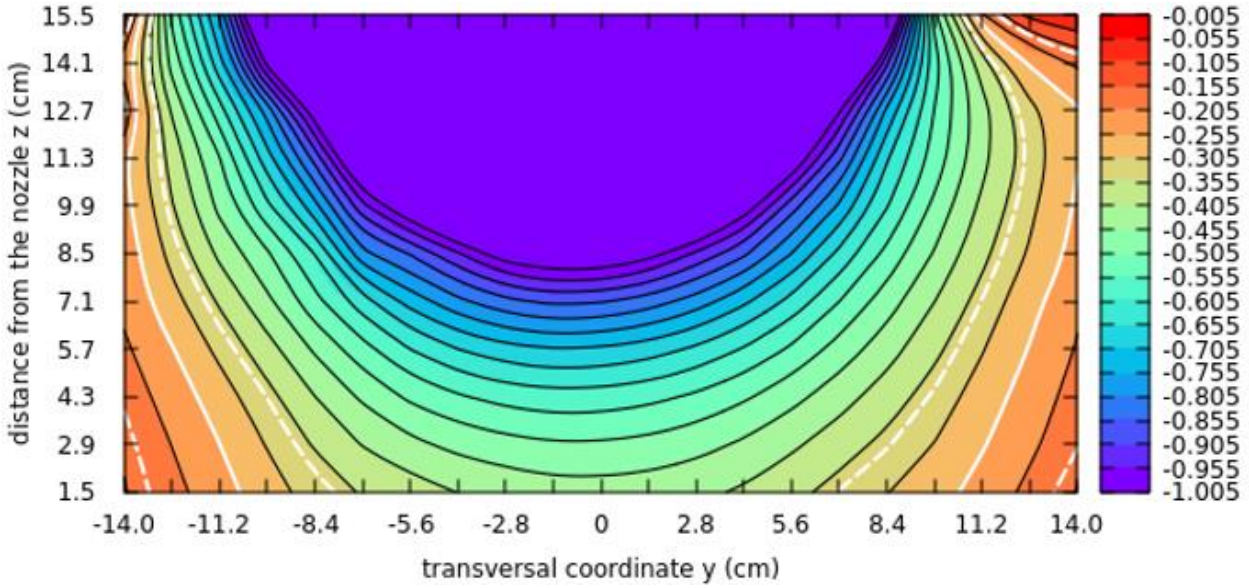

Fig. 5.30 Negative error field (scale in m/s) for Vaisala WAA151 cup anemometer (rotor diameter 18.2 cm) in the wind tunnel of PTB, y-z plane, 20 m/s (Sup2 code: PT-V-20y). Test section open boundary (prolonged nozzle wall) at y = ±16 cm; the most upstream point of the rotor at z = 13.4 cm.

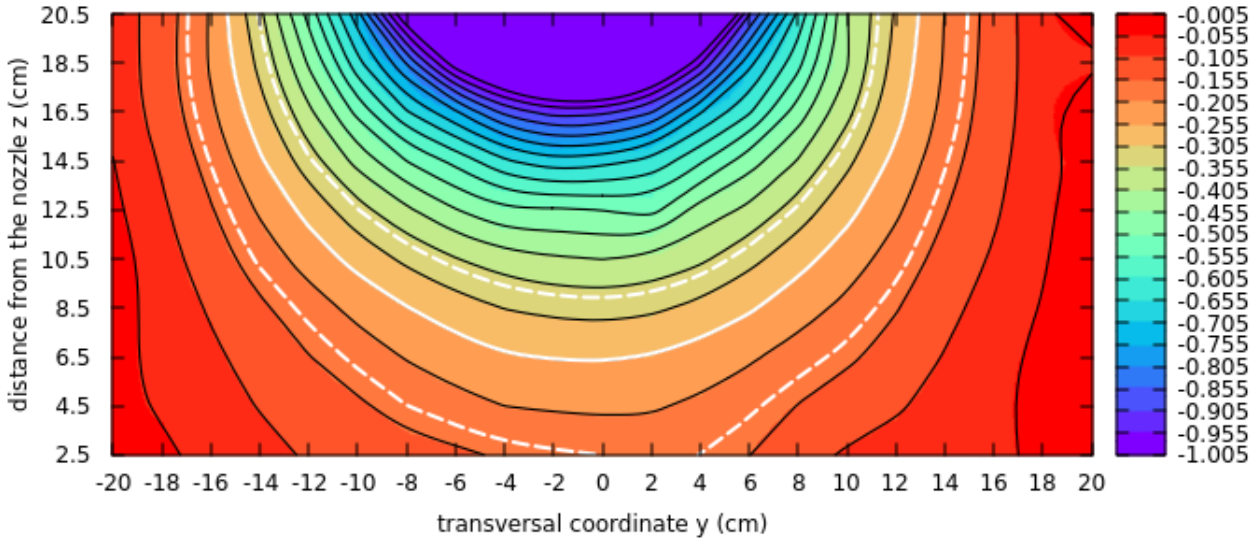

Fig. 5.31 Negative error field (scale in m/s) for Vaisala WAA151 cup anemometer (rotor diameter 18.2 cm) in the wind tunnel of CMI, y-z plane, 20 m/s (Sup2 code: CM-V-20y). Test section open boundary (prolonged nozzle wall) at y = ±22.5 cm; the most upstream point of the rotor at z = 22.4 cm.

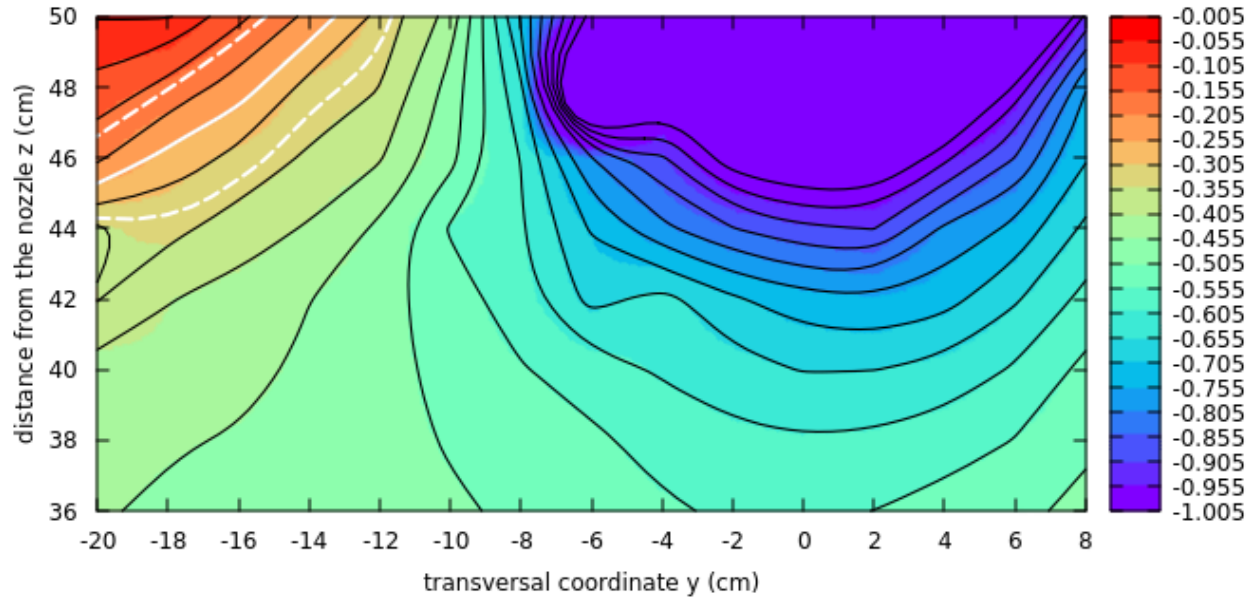

Fig. 5.32 Negative error field (scale in m/s) for Vaisala WAA151 cup anemometer (rotor diameter 18.2 cm) in the wind tunnel of CETIAT, y-z plane, 20 m/s (Sup2 code: CE-V-20y). Test section boundary (solid wall) at y = ± (26.5 to 27) cm; the most upstream point of the rotor at z = 52 cm.

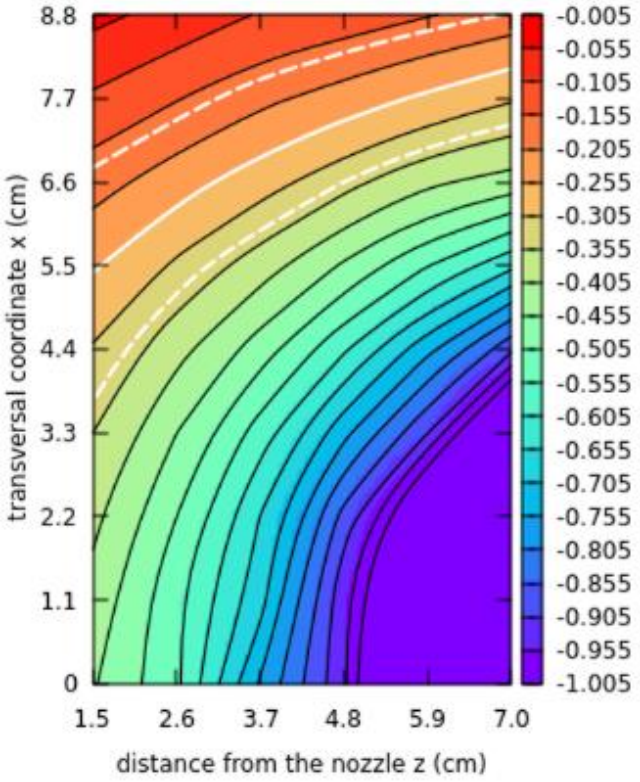

Fig. 5.33 Negative error field (scale in m/s) for Vaisala WAA151 cup anemometer (rotor diameter 18.2 cm) in the wind tunnel of BEV/E+E, x-z plane, 20 m/s (Sup2 code: EE-V-20x). Test section open boundary (prolonged nozzle wall) at x = 12.75 cm; the most upstream point of the rotor at z = 8.4 cm.

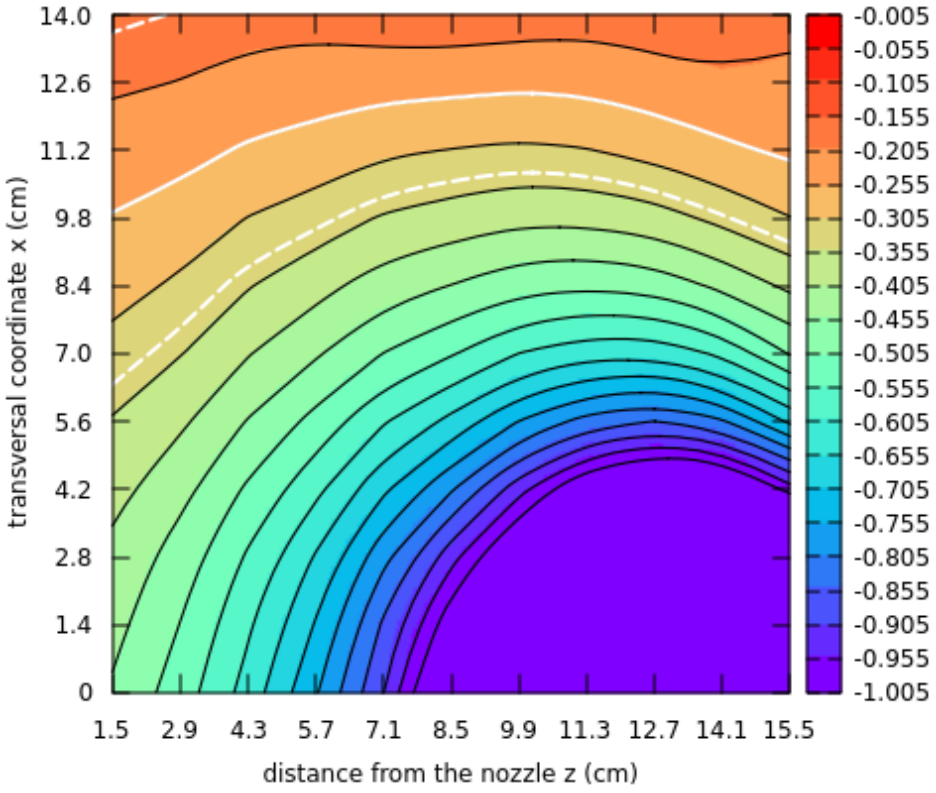

Fig. 5.34 Negative error field (scale in m/s) for Vaisala WAA151 cup anemometer (rotor diameter 18.2 cm) in the wind tunnel of PTB, x-z plane, 20 m/s (Sup2 code: PT-V-20x). Test section open boundary (prolonged nozzle wall) at x = 16 cm; the most upstream point of the rotor at z = 13.4 cm.

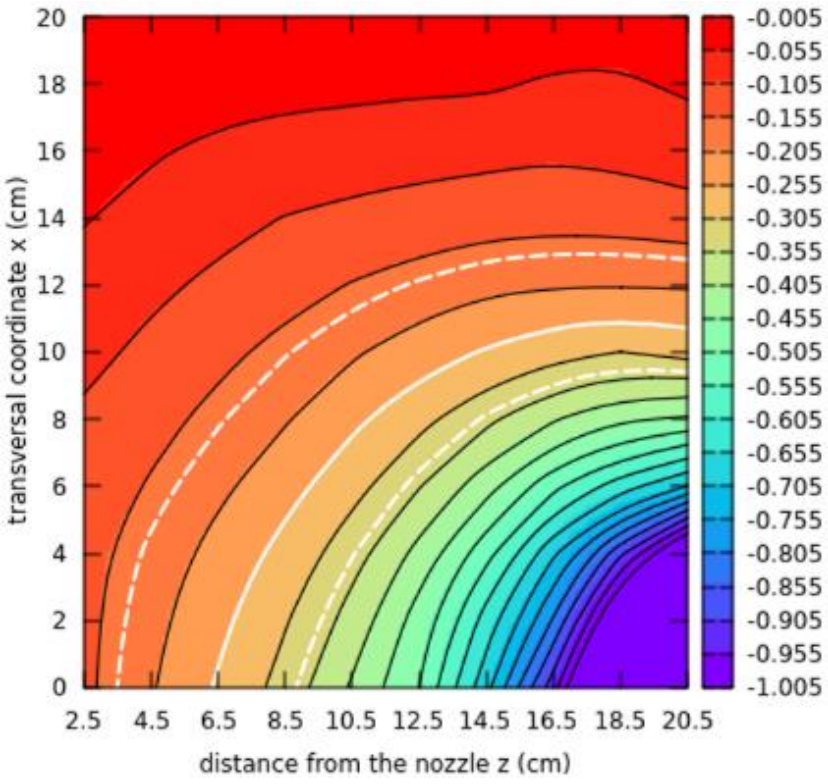

Fig. 5.35 Negative error field (scale in m/s) for Vaisala WAA151 cup anemometer (rotor diameter 18.2 cm) in the wind tunnel of CMI, x-z plane, 20 m/s (Sup2 code: CM-V-20x). Test section open boundary (prolonged nozzle wall) at x = 22.5 cm; the most upstream point of the rotor at z = 22.4 cm.

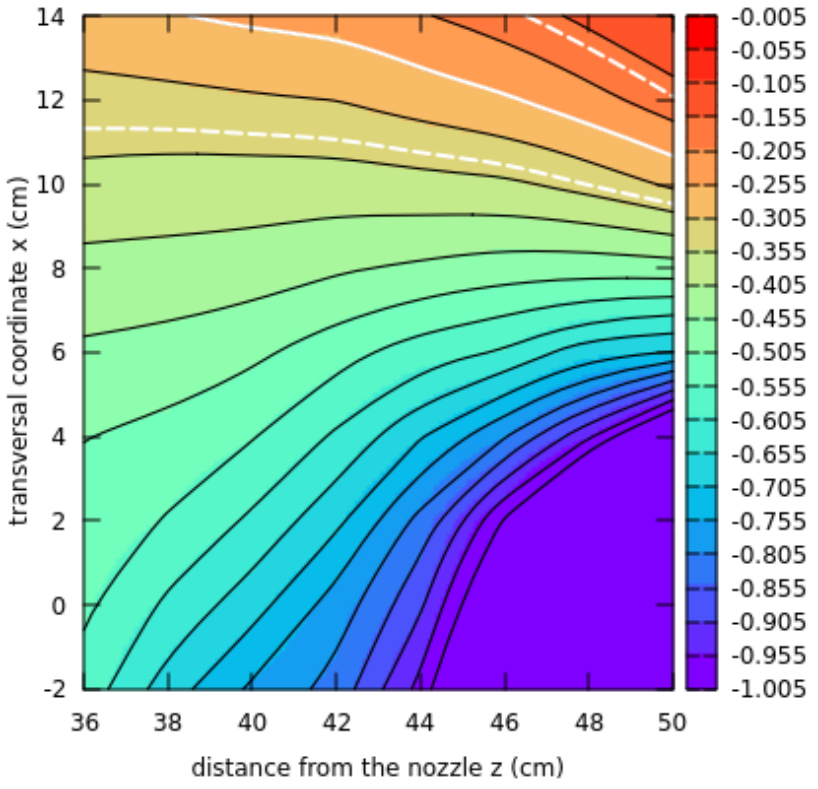

Fig. 5.36 Negative error field (scale in m/s) for Vaisala WAA151 cup anemometer (rotor diameter 18.2 cm) in the wind tunnel of CETIAT, x-z plane, 20 m/s (Sup2 code: CE-V-20x). Test section boundary (solid wall) at x = 25.5 cm; the most upstream point of the rotor at z = 52 cm.

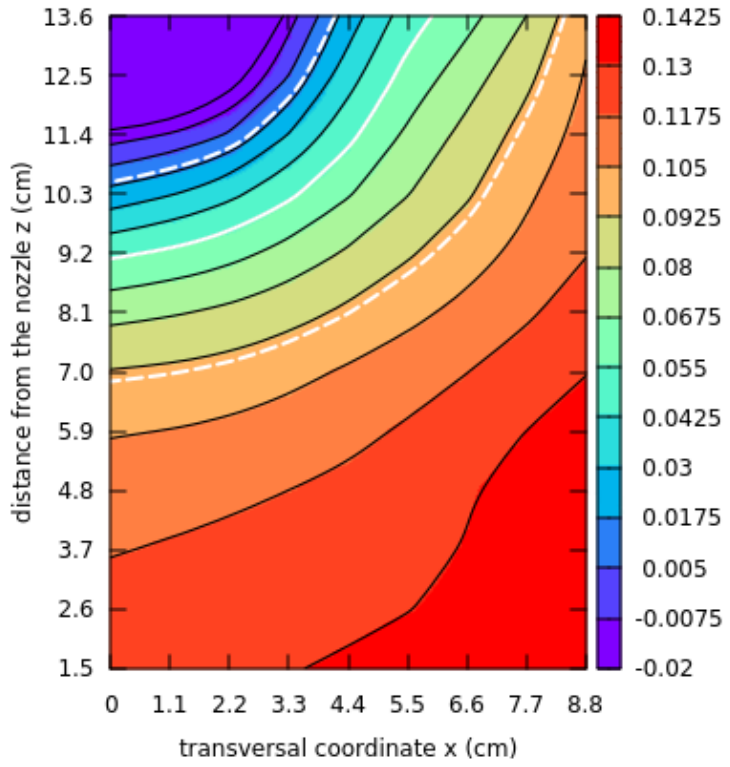

Fig. 5.37 Negative error field (scale in m/s) for RM Young Gill Propeller vane anemometer (propeller diameter 20 cm) in the wind tunnel of BEV/E+E, 5 m/s (Sup2 code: EE-Y-5). Test section open boundary (prolonged nozzle wall) at x = 12.75 cm; the most upstream point of the propeller at z = 16 cm.

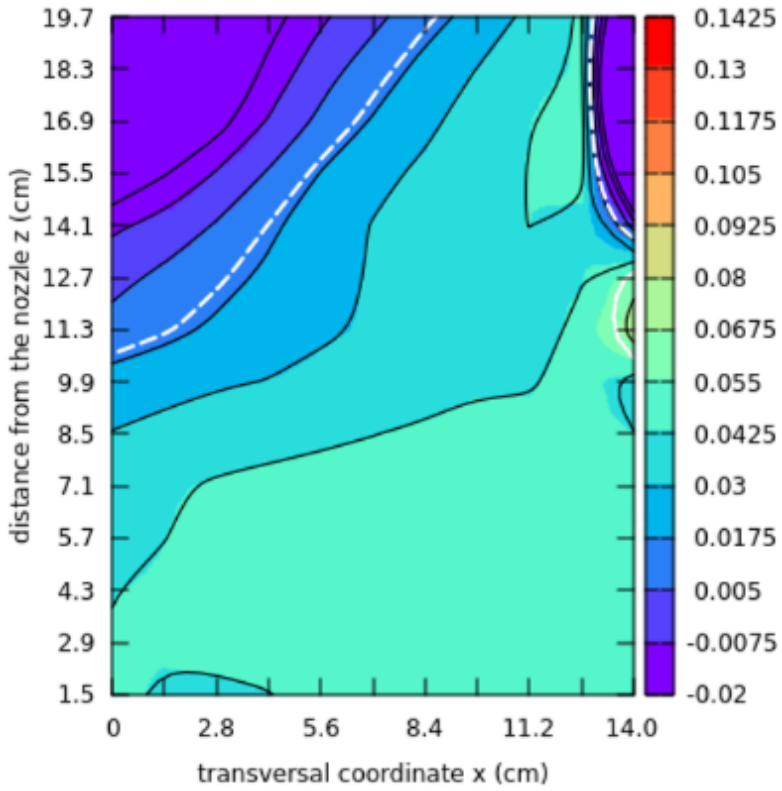

Fig. 5.38 Negative error field (scale in m/s) for RM Young Gill Propeller vane anemometer (propeller diameter 20 cm) in the wind tunnel of PTB, 5 m/s (Sup2 code: PT-Y-5). Test section open boundary (prolonged nozzle wall) at x = 16 cm; the most upstream point of the propeller at z = 21 cm.

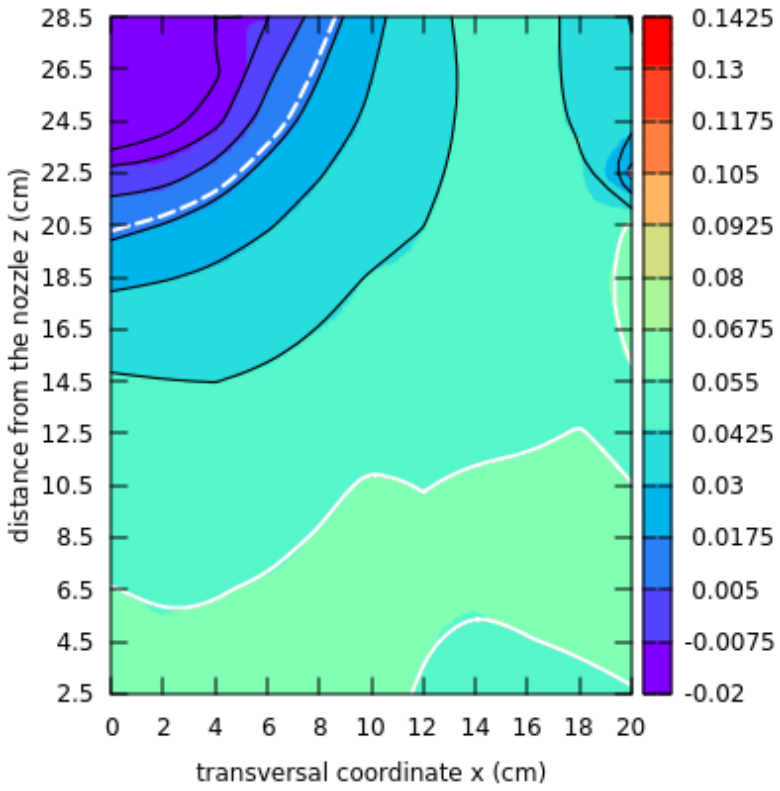

Fig. 5.39 Negative error field (scale in m/s) for RM Young Gill Propeller vane anemometer (propeller diameter 20 cm) in the wind tunnel of CMI, 5 m/s (Sup2 code: CM-Y-5). Test section open boundary (prolonged nozzle wall) at x = 22.5 cm; the most upstream point of the propeller at z = 30 cm.

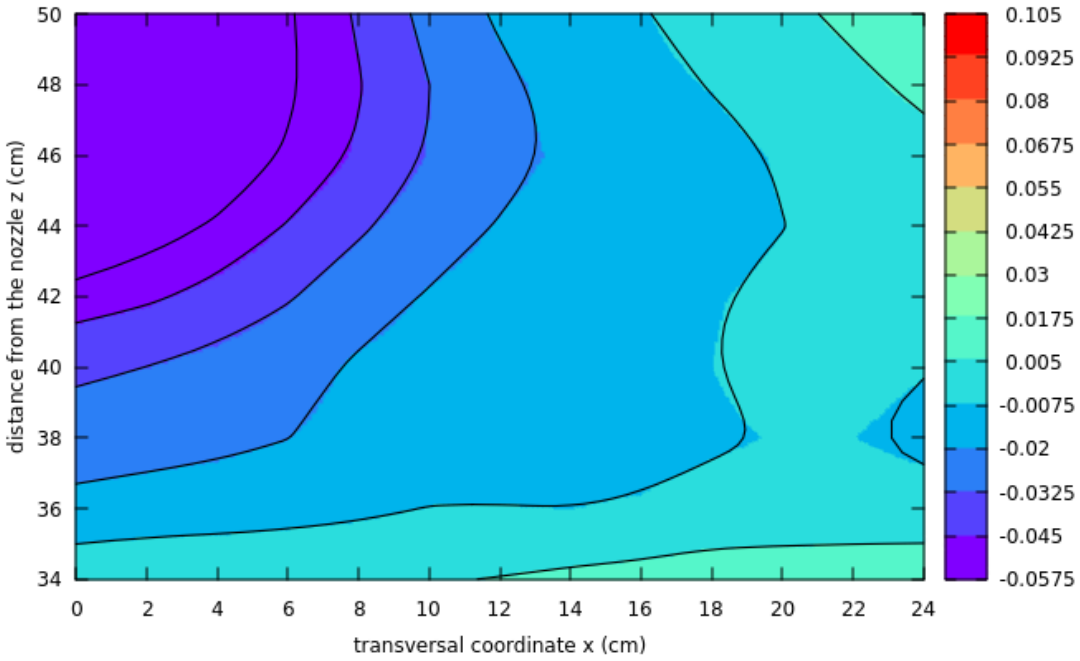

Fig. 5.40 Negative error field (scale in m/s) for RM Young Gill Propeller vane anemometer (propeller diameter 20 cm) in the wind tunnel of CETIAT, 5 m/s (Sup2 code: CE-Y-5). Test section boundary (solid wall) at x = 26.5 to 27 cm; the most upstream point of the propeller at z = 52 cm.

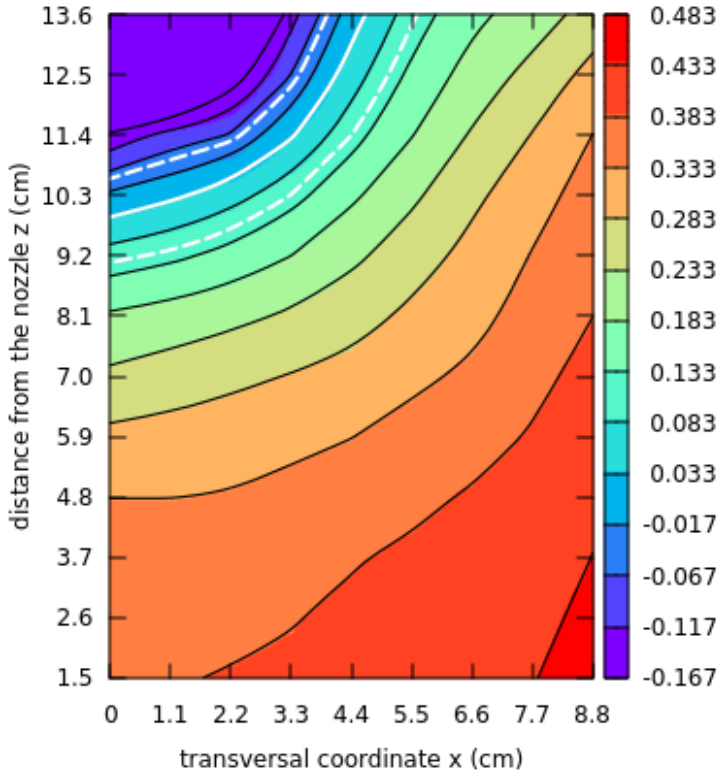

Fig. 5.41 Negative error field (scale in m/s) for RM Young Gill Propeller vane anemometer (propeller diameter 20 cm) in the wind tunnel of BEV/E+E, 20 m/s (Sup2 code: EE-Y-20). Test section open boundary (prolonged nozzle wall) at x = 12.75 cm; the most upstream point of the propeller at z = 16 cm.

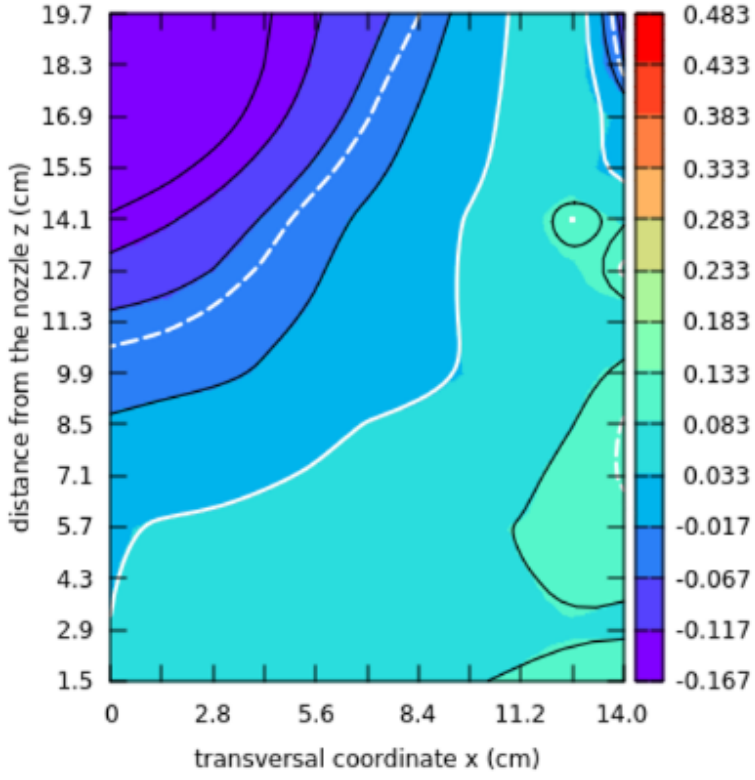

Fig. 5.42 Negative error field (scale in m/s) for RM Young Gill Propeller vane anemometer (propeller diameter 20 cm) in the wind tunnel of PTB, 20 m/s (Sup2 code: PT-Y-20). Test section open boundary (prolonged nozzle wall) at x = 16 cm; the most upstream point of the propeller at z = 21 cm.

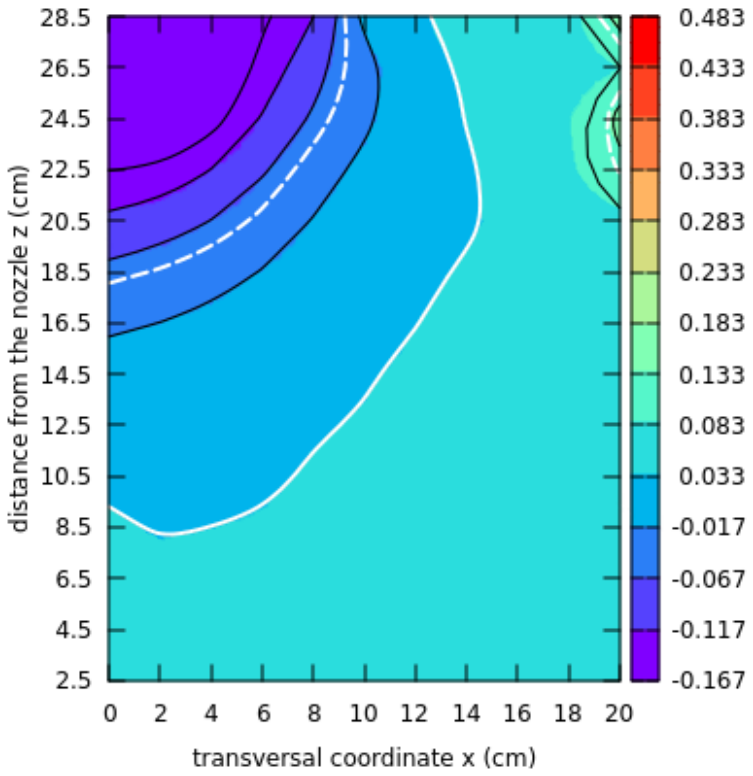

Fig. 5.43 Negative error field (scale in m/s) for RM Young Gill Propeller vane anemometer (propeller diameter 20 cm) in the wind tunnel of CMI, 20 m/s (Sup2 code: CM-Y-20). Test section open boundary (prolonged nozzle wall) at x = 22.5 cm; the most upstream point of the propeller at z = 30 cm.

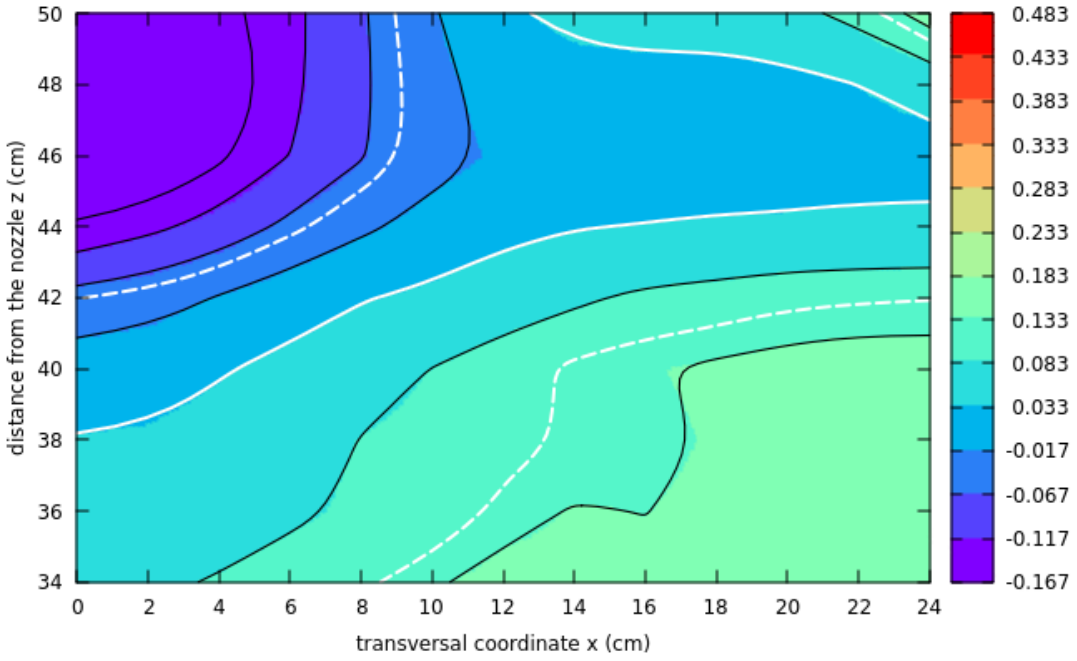

Fig. 5.44 Negative error field (scale in m/s) for RM Young Gill Propeller vane anemometer (propeller diameter 20 cm) in the wind tunnel of CETIAT, 20 m/s (Sup2 code: CE-Y-20). Test section boundary (solid wall) at x = 26.5 to 27 cm; the most upstream point of the propeller at z = 52 cm.

5.3.3 Reproducibility of the tested anemometers

Each of the tested anemometers has been calibrated repeatedly in the wind tunnel of CMI during the lifetime of the project. The measurement errors from the repeated calibrations are shown in the plots Fig. 5.45 to 5.47 below. Span of the measurement errors E_{max}-E_{min} and the standard uncertainty u_{drift} are summarised in Tab. 5.6. For the Testo and Vaisala anemometers where a larger number of repetitions is available, the uncertainty u_{drift} was calculated as a standard deviation. For RM Young Gill Propeller with two repetitions only, the formula (5) was used. We see excellent reproducibility for the anemometer Testo as well as for the RM Young Gill Propeller (in this case, however, the statistics of 2 repetitions is not so robust). For the Vaisala anemometer the reproducibility is worse, especially for 5 m/s, which should be taken into account when interpreting the plots in the previous section (see, e.g., the last paragraph in the next section 5.4). Note, that the two deviated calibrations for Vaisala at 5 m/s are from 2025 and 2026, thus, the related uncertainty more likely affects a comparison of the DWG calibration (2025) with the error fields from different wind tunnels obtained in 2022-2023, rather than a comparison between the error fields themselves.

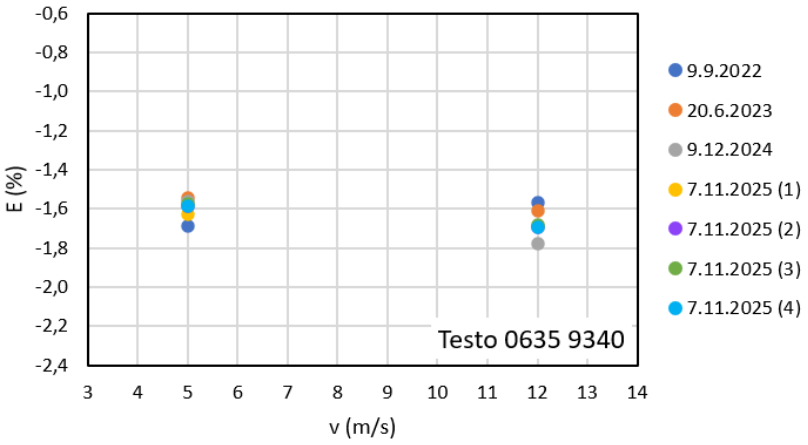

Fig. 5.45 Measurement errors from repeated calibrations of the anemometer Testo 0635 9340

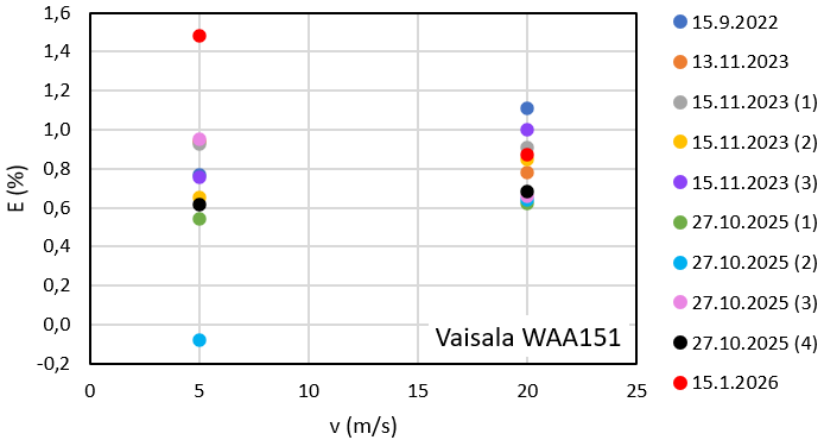

Fig. 5.46 Measurement errors from repeated calibrations of the anemometer Vaisala WAA151

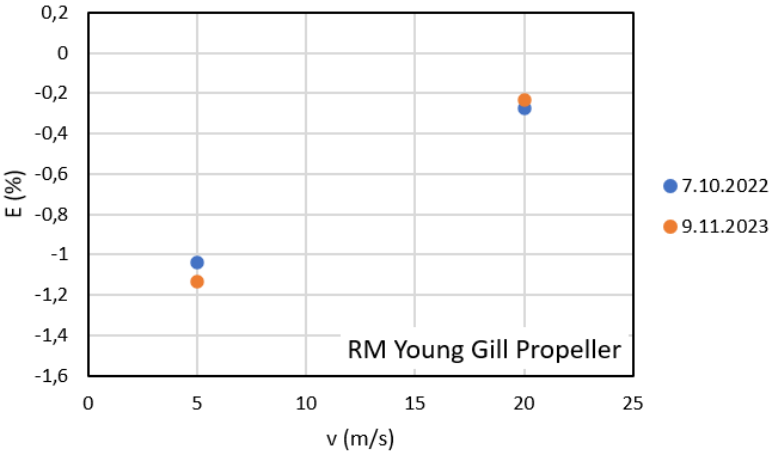

Fig. 5.47 Measurement errors from repeated calibrations of the anemometer RM Young Gill Propeller

	nominal air speed:	5 m/s		12 m/s		20 m/s	
	no. repetitions	span (%)	u_drift (%)	span (%)	u_drift (%)	span (%)	u_drift (%)
Testo 0635 9340	7	0.14	0.05	0.21	0.07		
Vaisala WAA151	10	1.56	0.39			0.49	0.17
RM Young Gill Prop.	2	0.09	0.03			0.04	0.01

Tab. 5.6 Span E_{max}-E_{min} and standard uncertainty u_{drift} of repeated calibrations in the wind tunnel of CMI

5.4 Discussion of the results

The Testo 0635 9340 vane anemometer has a propeller embedded in a frame with outer diameter of 10.7 cm. It was shown that for all the participating wind tunnels a region for placing a reference LDA exists upstream this anemometer such that the resulting measurement error agrees with (is within the uncertainty interval of) the measurement error obtained in the large wind tunnel of DWG. Such region is there even if the blockage ratio of the anemometer in the participating wind tunnels ranges from 5.7 % (CMI) to 18 % (BEV/E+E) for open test sections and it is 3.5 % for the closed test section of CETIAT. The larger is the wind tunnel the smaller is the velocity gradient in a neighbourhood of the wind tunnel nozzle (tested for open test sections only) and the larger is the region suitable for LDA placing. In a plane going through the central axis of a test section (= rotation axis of the anemometer propeller) the region forms a C-shaped band with its narrowing ends approaching the outer sides of the propeller frame and the opposite side of the band going through the nozzle neighbourhood at its centre. The smaller is the wind tunnel the narrower is the band.

The RM Young Gill Propeller vane anemometer has a propeller with diameter of 20 cm with no surrounding frame. The velocity gradients upstream this anemometer are smaller than for the Testo anemometer even if the propeller diameter and the blockage ratios are larger (7.9 % to 25 % for open test sections, 4.8 % for the closed test section). This is due to the missing propeller frame which, in case of the Testo anemometer, has negligible contribution to the blockage ratio but has significant effect to flow velocity reduction in the vicinity of the probe. It shows that blockage ratio is not the only parameter relevant for the blockage effect but also construction of the anemometer must be taken into account.
For the wind tunnels of PTB and CMI (open test section, blockage ratio 15.6 % and 7.9 %) placing the reference LDA anywhere upstream the tested anemometer further than approximately 10 cm from its propeller tip (avoiding a mixing layer at the test section boundary) leads to a measurement error which agrees with (is within the uncertainty interval of) the measurement error obtained in the large wind tunnel of DWG. In case of BEV/E+E the propeller occupies nearly entire cross section of the wind tunnel (2.75 cm between the end of the blades and the open test section boundary), the negative error field is shifted to larger values and the region of the reference LDA positions leading to agreement with DWG shrinks to a narrow band near the propeller tip where usually the LDA would not be placed. For CETIAT the region of agreement starts approximately 10 cm from the propeller tip upstream the tested anemometer for 20 m/s, however, for 5 m/s it is in a larger upstream distance where the velocity field measurement was not performed.

The cup anemometer Vaisala WAA151 has a rotor with diameter of 18.2 cm and cups with diameter of 5.3 cm corresponding to blockage ratios in the participating wind tunnels ranging from 8.9 % (CMI) to 18 % (BEV/E+E) for the open test sections and 5.4 % (CETIAT) for the closed test section. For the larger wind tunnels of CMI and CETIAT the wide bottom part of the anemometer housing enters the air stream whereas for the smaller wind tunnels of BEV/E+E and PTB it does not. The observed velocity gradients upstream this anemometer are the largest. This is expected due to the rotor motion which, on one side, goes against the air stream. Also for this anemometer a region for placing a reference LDA exists for each wind tunnel such that the resulting measurement error is within the uncertainty interval obtained in DWG, however, position of the region differs for various air speeds and various wind tunnels and the regions are narrower compared, e.g., to the Testo anemometer due to the larger velocity gradients. Therefore, it is difficult to draw any general recommendation for LDA placement. Also, unexpectedly, for 5 m/s the larger size of the test section of CMI does not give an advantage compared to the smaller test sections of PTB and

BEV/E+E. A possible effect of the large housing at the bottom part of the anemometer, which enters the CMI test section entirely whereas it is completely outside in case of PTB and BEV/E+E, was tested in the wind tunnel of CMI. However, it was shown that shifting the Vaisala anemometer downwards, such that the top of the housing is just at the test section boundary, leads to an increase in the anemometer measurement error by 0.5 % only for 5 m/s and almost no change for 20 m/s. The not so good reproducibility of the anemometer at 5 m/s can also play a role.

In the negative error plots in section 5.3.2 we used the uncertainty interval $-E_{DWG} \pm U_{DWG}$ of the calibration in DWG to draw a band of LDA positions where an agreement with the large wind tunnel of DWG is obtained. However, if we ask for which LDA positions an interlaboratory comparison with DWG would be successful in terms of the equivalence degree (6) not exceeding unity, a wider band given by an interval

$$-E_{DWG} \pm \sqrt{U_{DWG}^2 + U_{lab\,X}^2 + 2(2u_{\mathrm{drift}})^2}$$

would be applied with $U_{lab\,X}$ being an uncertainty of the anemometer calibration in the laboratory with a smaller wind tunnel (BEV/E+E, PTB, CMI or CETIAT).

5.5 Conclusions to section 5

A calibration wind tunnel with a reference LDA can be considered large enough if, within a required accuracy, the result of calibration is not sensitive to LDA positioning in a neighbourhood of the wind tunnel nozzle outlet and also it is not sensitive to further enlarging of the wind tunnel test section. In this case, an anemometer can be calibrated accurately without a reference to another larger wind tunnel. On the other hand, for wind tunnels which are not large enough, the accurate calibration is possible too, but an additional information is needed, either a region of optimal positioning of the reference LDA or correction factors, which can be reliably determined by comparison with a larger wind tunnel only.

In this report, we provide the additional information on optimal LDA positioning for several types of anemometers in several wind tunnels of different dimensions, which can be used as a guidance for mitigation of the blockage effect for all wind tunnels and anemometers with similar construction, geometry and dimensions.

In the presented plots of the negative error field, a wind tunnel proofs to be large enough if the band of the calibration interval obtained in the very large wind tunnel of DWG is wide and covering most of the region in a neighbourhood of the wind tunnel nozzle outlet. This property very much depends on a construction of the calibrated anemometer, not only on its size. Blockage ratio is not the only parameter which plays a role. For some types of anemometers, a wind tunnel is large enough even for blockage ratio exceeding 10 %, e.g., for the RM Young Gill Propeller in the wind tunnel with blockage ratio of 15.6 % (PTB), and in some cases a wind tunnel is not large enough even for blockage ratio below 10 %, e.g., for the Vaisala WAA151 in the wind tunnel with blockage ratio of 8.9 % (CMI) at 5 m/s. For the Testo 0635 9340 probe, the wind tunnel with blockage ratio of 5.7 % (CMI) is large enough and with 11 % (PTB) it is transitional. Therefore, a simple universal criterion for a wind tunnel being large enough cannot be formulated based on the blockage ratio only but the overall construction and its impact to air speed reduction upstream the anemometer should be taken into account.

Appendix A – Photos and schemes of the wind tunnels

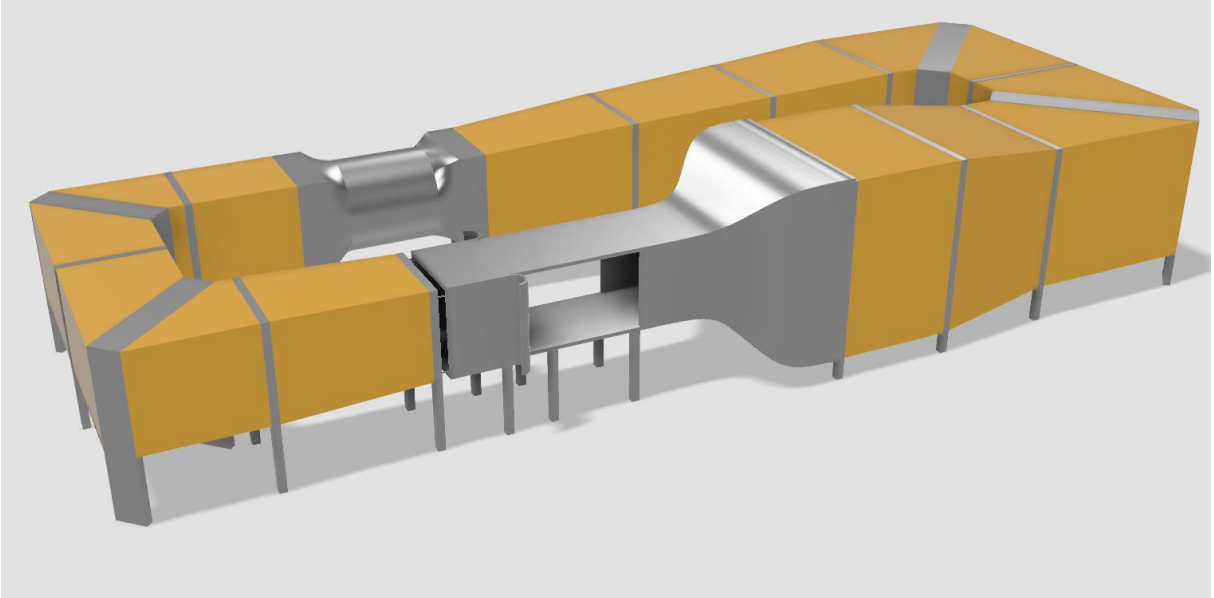

Fig. A.1a Wind tunnel of DWG

Fig. A.1b Wind tunnel of DWG – test section detail

Fig. A.2 Wind tunnel of CMI

Fig. A.3a Wind tunnel of LEI – general view

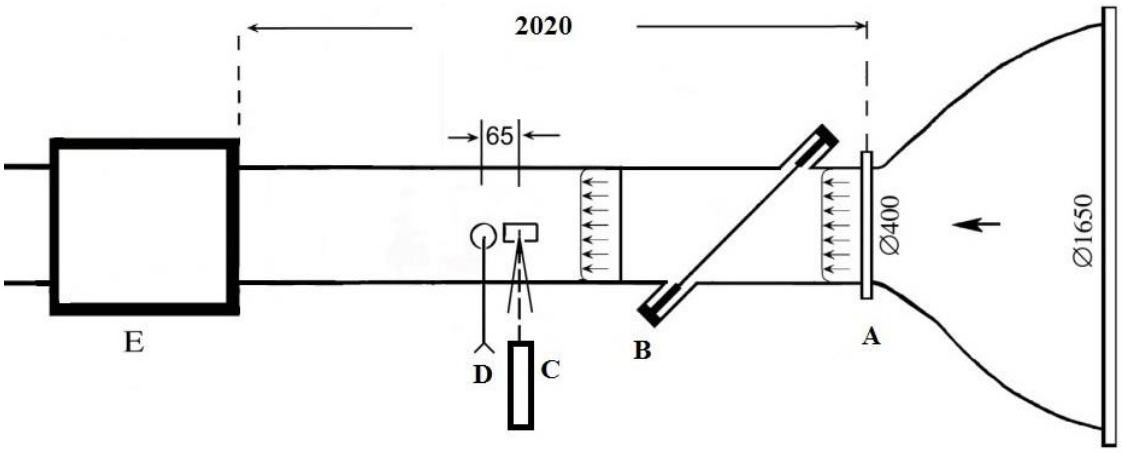

Fig. A.3b Wind tunnel of LEI – test section detail: A – test channel inlet; B – ultrasonic anemometer; C – LDA; E – test chamber for MUT (kept open for the insertion depth tests)

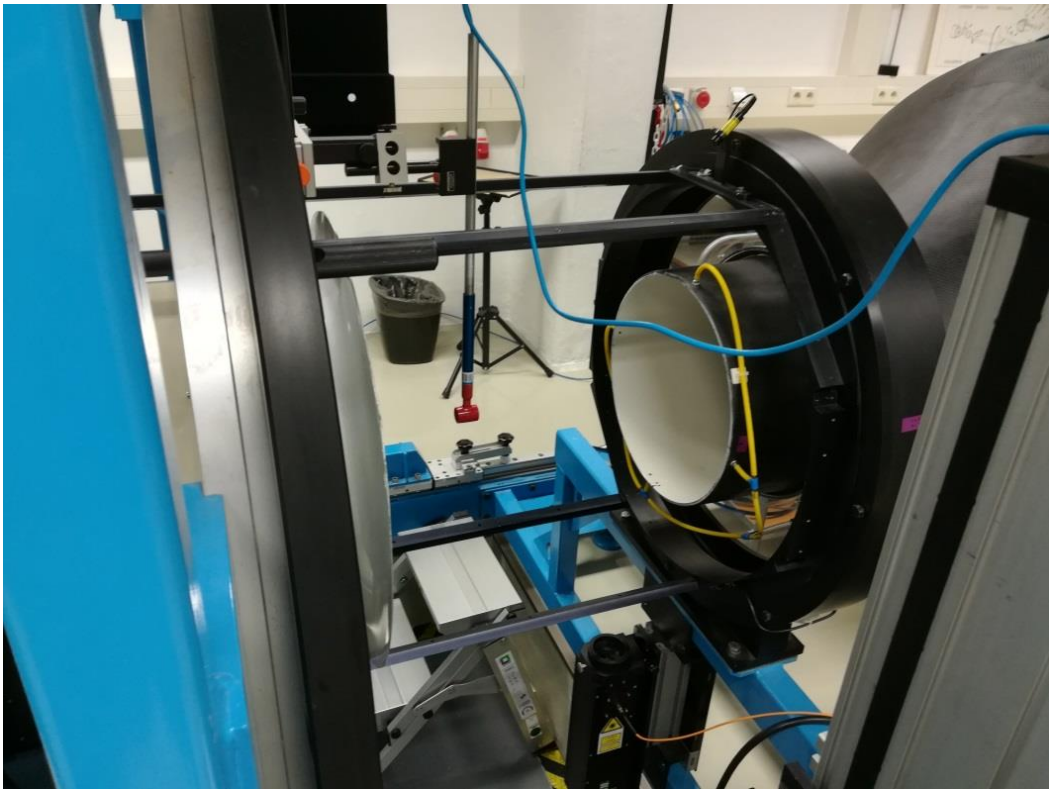

Fig. A.4 Wind tunnel of PTB – test section detail

Fig. A.5 Wind tunnel of BEV/E+E

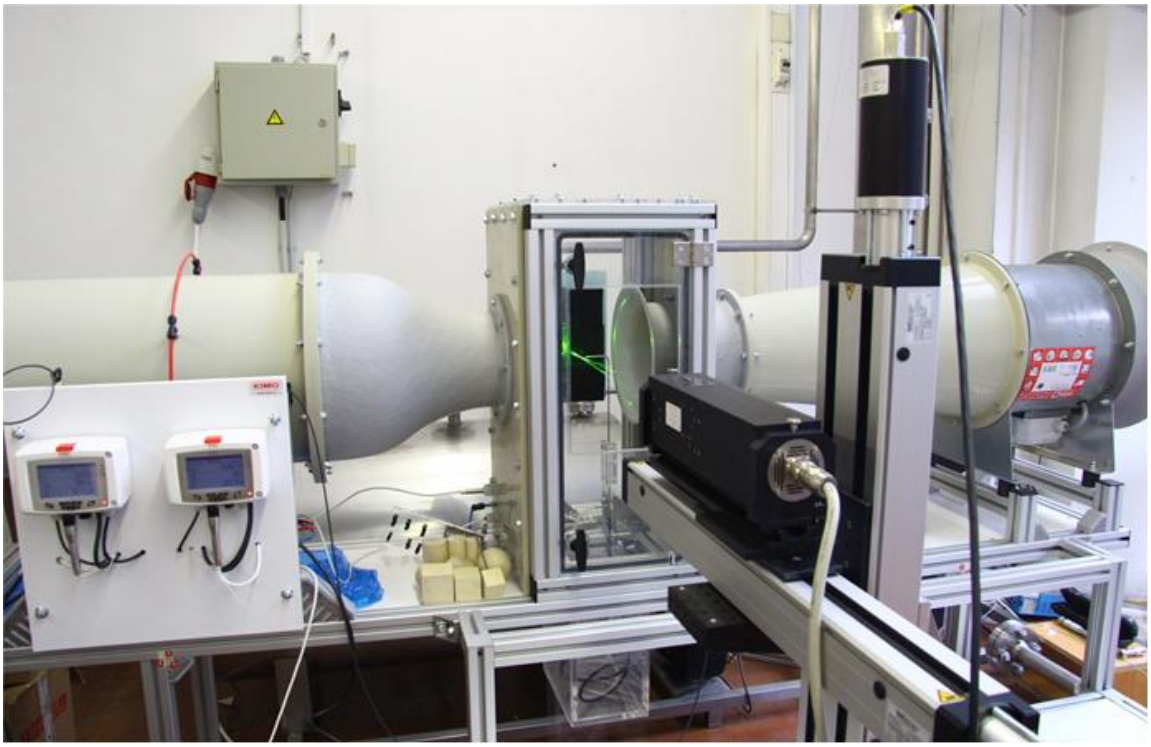

Fig. A.6 Wind tunnel of UL-LMPS

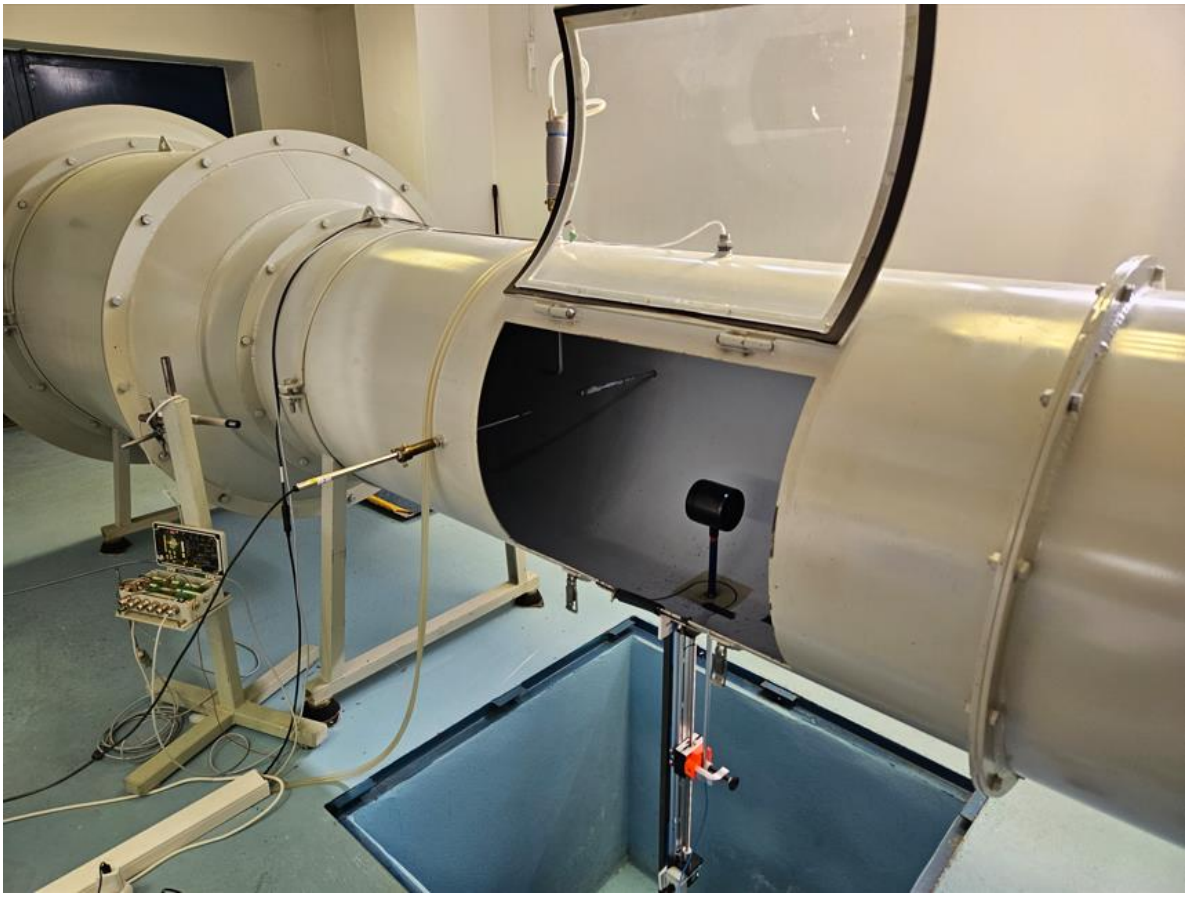

Fig. A.7 Wind tunnel of SHMU

Fig. A.8 Wind tunnel of CETIAT

Fig. A.9 Wind tunnel of DTI

Appendix B – Angular sensitivity of the small Testo 0635 9540 probe

Dependence of a velocity indication of the small vane anemometer Testo 0635 9540 on a rotation angle was measured in the wind tunnel of CMI. The anemometer was installed on a rotary actuator and rotated around the axis of its mounting rod (Fig. B.1). The dimple on the probe was facing upstream. The rotation from negative to positive angles was counter-clockwise when looking from the top. For the angle 0° the propeller axis was aligned with the air flow direction as accurately as possible. An uncertainty of the alignment at 0° should be about 1°. The dependency of the anemometer reading on the rotation angle was measured for several air speeds. Relative deviations (in %) of the velocity reading at various rotation angles compared to the reading at 0° are shown in Fig. B.2. We see that the probe is highly sensitive to the rotation especially for the lower air speeds 2 m/s and 5 m/s.

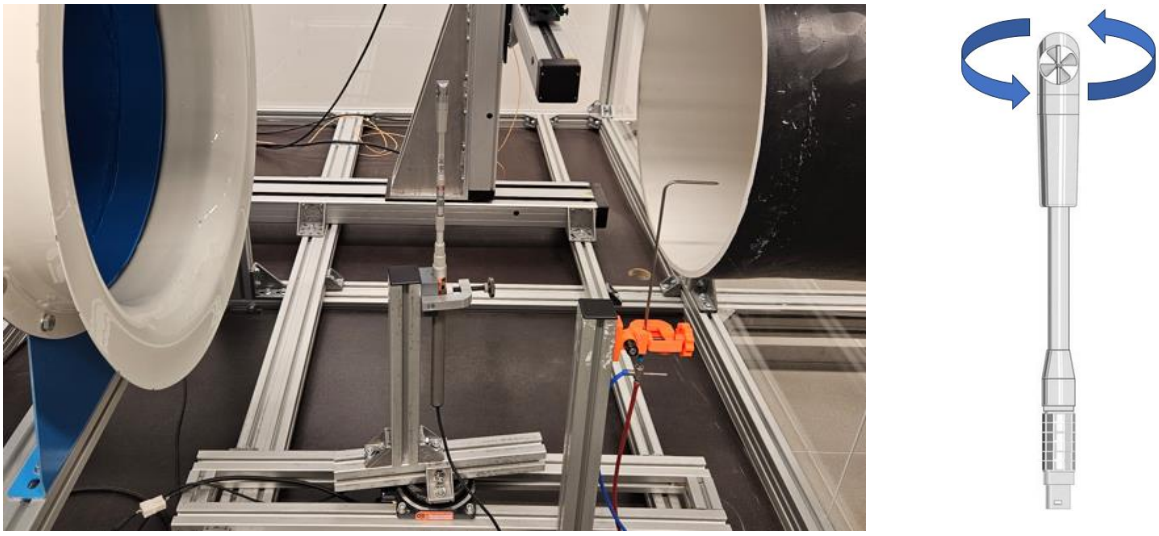

Fig. B.1 Installation of the anemometer Testo 0635 9540 for the angular dependency test (left); rotation direction of the anemometer during the test (right).

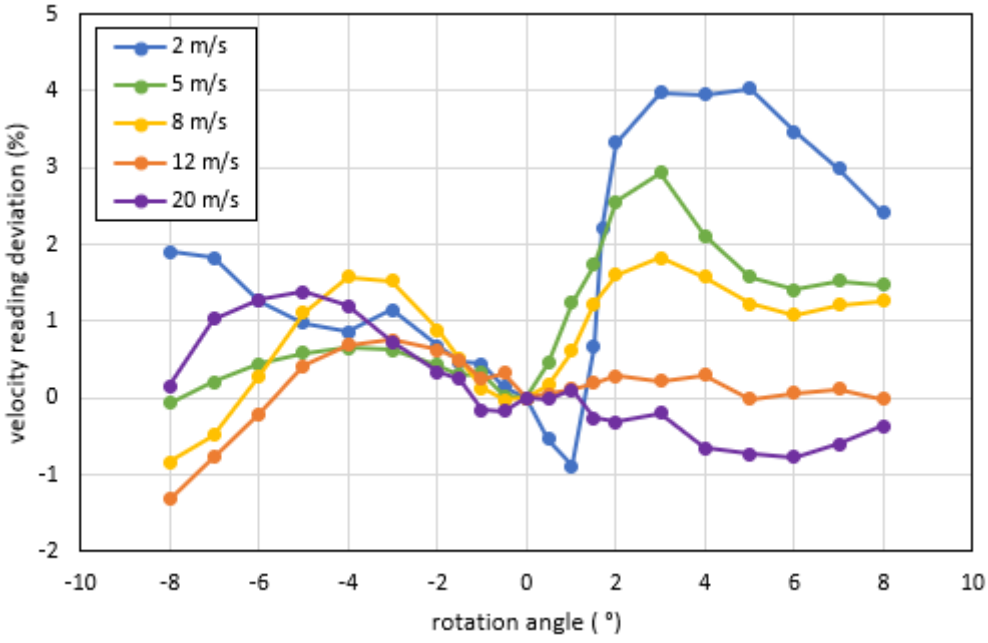

Fig. B.2 Percentual deviation of a velocity reading of the anemometer Testo 0635 9540 at various rotation angles compared to the reading at 0°.